CONTROL STRATEGIES FOR PERMANENT MAGNET SYNCHRONOUS MOTOR APPLICATIONS

Teză destinată obţinerii
titlului ştiinţific de doctor inginer
la
Universitatea Politehnica Timişoara
în domeniul INGINERIA SISTEMELOR
de către

ing. Cristina-Elena Coman

Conducător ştiinţific: prof.univ.dr.ing. Gheorghe-Daniel Andreescu
Referenţi ştiinţifici: prof.univ.dr.ing. Clement Feştilă
prof.univ.dr.ing. Ioan Naşcu
prof.univ.dr.ing. Toma-Leonida Dragomir

Ziua susţinerii tezei: 27.02.2014

Seriile Teze de doctorat ale UPT sunt:

1. Automatică
2. Chimie
3. Energetică
4. Ingineria Chimică
5. Inginerie Civilă
6. Inginerie Electrică
7. Inginerie Electronică şi Telecomunicaţii
8. Inginerie Industrială
9. Inginerie Mecanică
10. Ştiinţa Calculatoarelor
11. Ştiinţa şi Ingineria Materialelor
12. Ingineria sistemelor
13. Inginerie energetică
14. Calculatoare şi tehnologia informaţiei
15. Ingineria materialelor
16. Inginerie şi Management

Universitatea Politehnica Timişoara a iniţiat seriile de mai sus în scopul diseminării expertizei, cunoştinţelor şi rezultatelor cercetărilor întreprinse în cadrul Şcolii doctorale a universităţii. Seriile conţin, potrivit H.B.Ex.S Nr. 14 / 14.07.2006, tezele de doctorat susţinute în universitate începând cu 1 octombrie 2006.

România, 300159 Timişoara, Bd. Republicii 9,
Tel./fax 0256 403823
e-mail: editura@edipol.upt.ro

Preface

This thesis is submitted to the Faculty of Automation and Computers, Department of Automation and Applied Informatics, at Politehnica University Timişoara in partial fulfillment of the requirements for the PhD degree in Control Systems Engineering.

This work was partially supported by the strategic grant POSDRU/107/1.5/S/77265 (2010) within the Sectoral Operational Program for Human Resources Development 2007-2013, Romania, co-financed by the European Social Fund - Investing in people.

The research study has been followed by my supervisor, Prof.Dr.Eng. *Gheorghe-Daniel ANDREESCU*, between October 2010 and February 2014.

During my research study I have published 4 papers in collaboration with Prof. Dr. Eng. *Gheorghe-Daniel ANDREESCU*, Dr. *Sorin-Cristian AGARLIŢĂ*, Prof. Dr. Eng. *Ion BOLDEA* and Dr. *Ana MOLDOVAN (POPA)*, whom I would like to thank for their help that contributed to finalizing the PhD thesis.

I also want to express my gratitude to the members of the PhD evaluation committee, Prof. Dr. Eng. *Clement FEŞTILĂ*, from the Department of Automation at Technical University of Cluj-Napoca, Prof. Dr. Eng. *Ioan NAŞCU*, from the Department of Automation at Technical University of Cluj-Napoca, and Prof. Dr. Eng. *Toma-Leonida DRAGOMIR*, from the Department of Automation and Applied Informatics at Politehnica University Timişoara, for accepting to be part of this committee and for reviewing the PhD thesis.

Nevertheless I would like to show appreciation to my close colleagues and friends for their patience, help and encouragement during my research study: Eugen Horaţiu GURBAN, Ana Maria DAN, Pal-Ştefan MURVAY and, definitely not the last, Bogdan GROZA. I have at least one wonderful moment with them. Many thanks go to Ovidiu PELAN, Emil GURAN, Alexandru CODREAN and Alexandra STÎNEAN, for the many discussions we had.

Finally, I would like to express my deepest gratitude to the people that mean the most to me, Vlad, my sister Alina and my wonderful parents Dumitru and Tinca. There is nothing I can write that can express what I feel for them. Thank you for your endless love and support.

Timişoara, February 2014 Cristina-Elena COMAN

Coman, Cristina-Elena

Control Strategies for Permanent Magnet Synchronous Motor Applications

Teze de doctorat ale UPT, Seria 12, Nr. 13, Editura Politehnica, 2014, 114 pagini, 62 figuri, 10 tabele.

ISSN: 2068-7990

ISBN: 978-606-554-800-8

Cuvinte cheie:
control strategies, PMSM, Observers, ISA, sensorless control, V/f control

Rezumat:
The *direction* of the research study presented in this thesis is the control of PMSM drives; mainly sensorless control for applications where low cost requirements are mandatory, and ISA control for automotive industry were the demand for high efficiency and low cost production is continuously growing. In Chapter 3 are presented three categories of observers for sensorless control PMSM drives, Chapter 4 continues with sensorless control by developing the V/f control with two stabilizing feedback corrections and Chapter 5 is an introduction to automotive industry by developing an ISA control structure used in HEV topology.
The *multidisciplinary research study* of the thesis includes: control system engineering, electric drives, power electronics, electrical engineering and mechanical engineering. The arguments for including the thesis in the control system engineering field of study are presented as follows:

- Modeling of PMSM, with parameters identification;
- Development of an nonlinear state and disturbance observer;
- Implementing and developing sensorless control systems, i.e., V/f control with two stabilizing feedback corrections;
- Proposing an ISA control structure;
- Real-time implementation;
- Comparative simulation results.

Table of Contents

List of Figures

List of Tables

Nomenclature

Abbreviations

AC	Alternating Current
AF	Active Flux
AFO	Active Flux Observer
BLDCM	Brushless DC Machine
CSFC	Constant Stator Flux Control
CTAC	Constant Torque Angle Control
DC	Direct Current
DTC	Direct Torque Control
DTFC	Direct Torque and Flux Control
emf	Electromotive force
EV	Electric Vehicles
FOC	Field Oriented Control
FWC	Flux Weakening Control
HEV	Hybrid Electric Vehicles
HPF	High Pass Filter
HVAC	Heating, Ventilation and Air Conditioning
HW	Hardware
ICE	Internal Combustion Engine
IPMSM	Interior Permanent Magnet Synchronous Machine
ISA	Integrated Starter-Alternator
LPF	Low Pass Filter
MRAS	Model Reference Adaptive System
MTPA	Maximum Torque per Ampere
MTPV	Maximum Torque per Voltage
NSDO	Nonlinear State and Disturbance Observer
PI	Proportional Integral
PMSM	Permanent Magnet Synchronous Machine
PT1	First Order Controller
PWM	Pulse Width Modulation
SPMSM	Surface Permanent Magnet Synchronous Machine

SVM	Space Vector Modulation
SW	Software
UPFC	Unity Power Factor Control
V/f	Voltage per frequency
VFD	Variable Frequency Drive
VSI	Voltage Source Inverter

Symbols

abc	Stator reference frame given by the supply three-phases
B	Viscous friction coefficient
dq	Rotor reference frame
i_d	*d* axis stator current
i_q	*q* axis stator current
i_s	Stator current
i_α	α axis stator current
i_β	β axis stator current
J	Moment of inertia
L_0	Stator self inductance
L_d	*d* axis inductance
L_M	Mutual inductance between stator phases
L_q	*q* axis inductance
L_s	Stator inductance
L_σ	Leakage inductance
P	Active power
p	Number of pole pairs
Q	Reactive power
R_s	Stator resistance
T_e	Electromagnetic torque
T_L	Load torque
v_d	*d* axis stator voltage
V_{DC}	Inverter DC-link voltage
v_q	*q* axis stator voltage

v_s	Stator voltage
v_α	α axis stator voltage
v_β	β axis stator voltage
$\alpha\beta$	Stator reference frame
θ_r	Rotor position
λ_{act}	Active flux
λ_{PM}	PM flux linkage
λ_s	Stator flux
φ	Power factor angle
ω_m	Mechanical rotor speed
ω_r	Electrical rotor speed

Superscripts

*	Reference quantity
^	Estimated quantity

1 Introduction

Permanent magnet synchronous motors (PMSM) have gained more ground due to their advantages; i.e., high air gap flux density, high power/weight ratio, large torque/inertia ratio, low speed smooth torque operation, high speed operation, high efficiency, high power factor, compact design [Vas1998], etc. The simple low cost implementation control techniques are more in demand. The PMSMs are commonly used in applications like: pumps, fans, blowers, compressors, centrifuges, machine tools, servo drives, robots, HVAC systems, automotive industry and many others [Gie2010].

The need for high efficiency, high dynamic response and high torque/power to weight ratio has lead to PMSM use in high performance electric drives [Sul2011].

The PMSM control can be performed by using scalar or vector control techniques. Scalar control, i.e., V/f control, is mostly used for applications where high performance is not required and computational effort is limited; on the other hand vector control is the better choice for high performance drives.

The main requirement for vector control is the rotor position information. This is done by using an encoder mounted on the shaft of the motor. In applications where the size of the drive is limited, high speed applications where the use of an encoder is costly and not reliable or in case of faulty encoder, the PMSM control is done using sensorless control strategies.

Sensorless techniques are based on estimating rotor position/speed by measuring electrical quantities, like stator phase currents and/or inverter DC-link voltage/current [Com2013].

1.1. Thesis Directions

The main purpose of this thesis is to develop new control strategies for PMSM applications. At the beginning of the research study various observer topologies were studied, i.e., for PMSM sensorless control strategies. The contribution for this study is the developed nonlinear state and disturbance observer (NSDO), used mainly for rotor position estimation.

After the studied observer topologies, the research was directed to scalar control. Unlike vector control, scalar control inherently has no need for coordinate transform because the reference command is the electric frequency of the stator voltage. The principle of V/f control is to maintain the ratio between the magnitude and the frequency of the stator voltage constant. Usually, the V/f control is performed in open loop, but in order to maintain synchronism conditions (for sudden loading torque) and to improve systems performance, a sensorless stable V/f control is introduced in [Per2003]. The proposed V/f control introduces stability aspects for sensorless scalar control with two stabilizing feedback corrections, a voltage vector speed correction and a voltage amplitude correction. The contributions brought to this field are published in [And2012], [Aga2013] and [Com2013].

A new direction of research was considered for PMSMs use in the automotive industry, namely integrated starter-alternator (ISA) control. The recent studies for ISA control prove the need for further research in this field. The proposed ISA control system considers the following: motor to generator modes selection, the

battery model and simulations considering real life scenarios. The contribution for this study is published in [And2013].

1.2. Thesis Objectives

The proposed objectives during the research study are presented in what follows, considering the outline of the thesis.

1) The significant cost decrease of motion sensorless control strategies leads to *rotor position observers* study. Various recent topologies of observers are studied and simulated in order to compare their performance and implementation complexity.

2) The need to reduce computation effort and to improve stability leads to the study and development of sensorless stable *V/f control with two stabilizing feedback corrections.*

3) The decrease of PM prices determined the automotive industry to show an increased interest into using PM machines. This is the main reason that leads to *integrated starter-alternator (ISA) control system* study in the last part of the thesis.

1.3. Thesis Outline

After the introduction to the field of study, in Chapter 2 are presented the PMSM model and the control strategies. The classification of PM machines is done for a better comprehension of where the PMSM is situated. The PMSM equation model, with the experimental determination of the *dq* inductances and the iron loss resistance modeling, is presented.

The studied topologies for position observers are detailed in Chapter 3 along with simulation results. The following observers are taken into account: i) *Modified Equivalent Integrators for Stator Flux Estimation* using Active Flux Concept, ii) *MRAS* based observer, and iii) *Nonlinear State and Disturbance Observer*.

The comprehensive description of the proposed stable V/f control study is done in Chapter 4. Here the performances for the proposed V/f control with two stabilizing loops are presented along with simulation and experimental results to prove the proposed method novelty. Extensive comparative simulation and experimental results are shown for the proposed V/f control, first, with field oriented control (FOC), and next with sensorless vector control based on active flux.

Chapter 5 illustrates the introduction of the thesis to automotive industry. An ISA control system is developed, supported by extensive simulation results.

The experimental test stand is presented in Chapter 6, along with the hardware and the software implementation.

The final conclusions and contributions of the thesis are drawn in Chapter 7.

2 Permanent Magnet Synchronous Machines

A synchronous machine (SM) is an electric machine composed of a stator and a rotor. The SM stator has three-phase supplied windings in which a rotating magnetic field is produced. The SM rotor, with DC excited winding or permanent magnets (PMs), rotates with the same frequency as the stator's rotating magnetic field. This particularity of SMs is called synchronization.

2.1. Classification of PM Machines

Depending on the type of excitation PM machines can be classified as DC or AC excitation machines, i.e., PMDC machines and PMAC machines. The PMDC machines are similar to conventional DC commutator machines, the difference being that they contain PMs instead of field windings. The PMAC machines are SMs with PMs generating the field flux. They are the most attractive machine type among the PM machines thanks to their simple structure [Moh2000], [Hug2006].

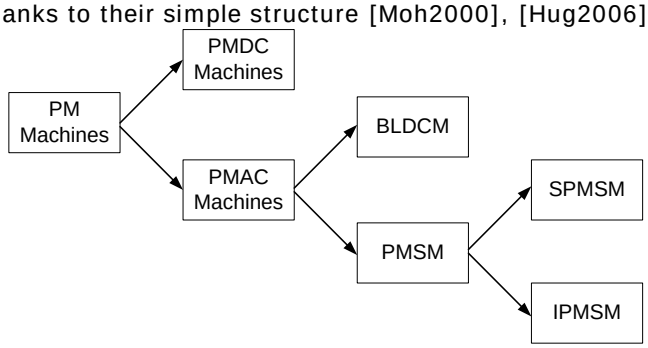

Fig. 2.1. PM machines classification [Per2002]

PMAC machines are further classified based on their back-emf, which can be trapezoidal and sinusoidal. The trapezoidal back-emf type are called brushless DC machine (BLDCM) and the sinusoidal back-emf type are called PMSM.

The difference between a BLDC and a DC brush commutator machine can be seen in Fig. 2.2.

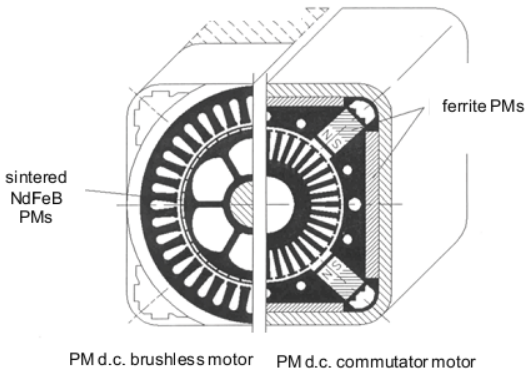

Fig. 2.2. Comparison between BLDC and a DC brush commutator machine [Gie2010]

Depending on the rotor PM location, the PMSM can be surface PM machine or interior PM machine.

In the case of surface PMSM (SPMSM) the PMs are mounted on the surface of the rotor, having the advantage of easy building and lower cogging torque. This topology cannot be used for high speed operations because the friction forces can make PMs fly apart. For SPMSM the *dq* inductances are equal, i.e., $L_d=L_q$.

Interior PMSMs (IPMSMs) have PMs mounted inside the rotor and can operate at high speed. This type of machine has saliency with *q* axis inductance greater than *d* axis inductance, i.e., $L_d<L_q$.

2.2. PMSM Model

The electric rotor speed ω_r in [rad/s] has the expression

$$\omega_r = 2\pi f \tag{2.1}$$

where *f* is the supply frequency in [Hz]. The mechanical speed ω_m is given by

$$\omega_m = \frac{\omega_r}{p} \tag{2.2}$$

where *p* is the number of pole pairs.

The PMSM voltage equations can be written in different reference frames. There are two stator reference frames, fixed to the stator, i.e., *abc* and *αβ*, and one rotor reference frame, fixed to the rotor, i.e., *dq*.

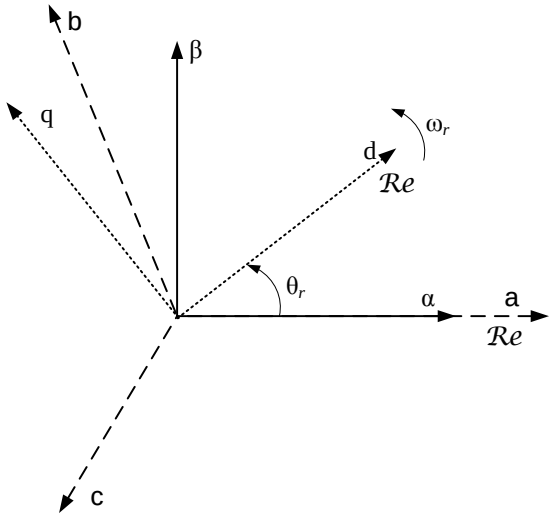

Fig. 2.3. Coordinate correspondence between stator and rotor reference frames

The *abc* reference frame is given by the supply three-phase system, with the real *a* axis along the *a* phase flux linkage. The *αβ* reference frame uses a Clarke transform to reduce the number of equations to two (biphasic model). The *α* axis is the same as *a* axis.

The ***αβ*** stator voltage vector equation is expressed as

$$\begin{aligned} \bar{v}_s &= R_s \bar{i}_s + \frac{d\bar{\lambda}_s}{dt}, \quad \bar{\lambda}_s(0) = \bar{\lambda}_{s0} \\ \bar{v}_s &= v_\alpha + jv_\beta, \ \bar{i}_s = i_\alpha + ji_\beta, \ \bar{\lambda}_s = \lambda_\alpha + j\lambda_\beta \end{aligned} \tag{2.3}$$

where R_s is the stator phase resistance, $\bar{i}_S(i_\alpha, i_\beta)$ is the stator phase current vector, and $\bar{\lambda}_S(\lambda_\alpha, \lambda_\beta)$ is the stator phase flux vector.

The stator flux vector is given in [Per2002] as

$$\bar{\lambda}_s = \left(L_\sigma + \frac{3}{2}L_0\right)\bar{i}_s + \frac{3}{2}L_M \bar{i}_s^{\,*} e^{j2\theta_r} + \lambda_{PM} e^{j\theta_r} \tag{2.4}$$

where L_σ is the leakage inductance, L_0 is the stator self inductance, L_M is the mutual inductance between stator phases, λ_{PM} is the PM flux linkage and θ_r is the electric rotor position.

The $a\beta$ components of the stator flux are expressed as

$$\lambda_\alpha = \left[L_\sigma + \frac{3}{2}L_0 + \frac{3}{2}L_M \cos(2\theta_r)\right] i_\alpha + \frac{3}{2}L_M \sin(2\theta_r) i_\beta + \lambda_{PM}\cos(\theta_r)$$

$$\lambda_\beta = \left[L_\sigma + \frac{3}{2}L_0 - \frac{3}{2}L_M \cos(2\theta_r)\right] i_\beta + \frac{3}{2}L_M \sin(2\theta_r) i_\alpha + \lambda_{PM}\sin(\theta_r)$$

$$L_0 = \frac{L_{md} + L_{mq}}{3}$$

$$L_M = \frac{L_{md} - L_{mq}}{3}$$

where L_{md} and L_{mq} are the magnetizing inductances [Per2002].

The dq inductance components L_d and L_q are defined as

$$L_d = L_\sigma + L_{md}$$

$$L_q = L_\sigma + L_{mq}$$

In particular, the stator flux vector (2.4) for SPMSM has the expression

$$\bar{\lambda}_s = L_s \bar{i}_s + \lambda_{PM} e^{j\theta_r} \tag{2.5}$$

where L_s is the stator phase inductance (L_d=L_q=L_s).

The dq reference frame has the real d axis along the PM flux linkage λ_{PM}. In order to change from stator reference to rotor reference, a Park transform is needed. The Park transform is θ_r dependent, see Appendix A.

The stator voltage vector equation (2.3) written in ***dq*** rotor reference frame [Bol2006a] has the expression

$$\bar{v}_S = R_S \bar{i}_S + \frac{d\bar{\lambda}_S}{dt} + j\omega_r \bar{\lambda}_S \tag{2.6}$$

The stator voltage vector components are defined as

$$\begin{aligned} v_d &= R_S i_d + \frac{d\lambda_d}{dt} - \omega_r \lambda_q \\ v_q &= R_S i_q + \frac{d\lambda_q}{dt} + \omega_r \lambda_d \end{aligned} \tag{2.7}$$

The stator flux linkage vector $\bar{\lambda}_S = \lambda_d + j\lambda_q$ has the dq components

$$\begin{aligned} \lambda_d &= L_d i_d + \lambda_{PM} \\ \lambda_q &= L_q i_q \end{aligned} \tag{2.8}$$

2.2.1. Experimental Identification of *dq* Inductances

For a better modeling of the PMSM experimental test stand (see Chapter 6), the *dq* axis inductances were experimentally determined after performing the DC current decay test presented in [Com2013]. With the machine at standstill, direct current is passed through two phases with the rotor aligned along the *d* axis and along the *q* axis, respectively.

The electrical configuration of the test is illustrated in Fig. 2.4. Phases B and C are energized by the DC voltage V_{DC} through the IGBT path. When the IGBT is opened, the current decay on phases B and C is conducted through diode D thanks to the electromagnetic induction phenomenon. The current decay can be observed in phases *B* and *C* (connected in series) until the diode D opens, while in phase *A* a different value of constant current (i_{cc}) is injected.

The calculated *dq* inductances have the expression:

$$L_{d,q} = \left(2 \cdot R_S \cdot \int i dt + \int v_D(i)\, dt\right) \Big/ \left(2 \cdot I_{cont}\right) \qquad (2.9)$$

where: R_s - phase resistance; i - decay current, v_D(i)- diode voltage drop, I_{cont} - the DC current before the decay.

The dependencies (λ_d - λ_{PM}) $= L_d I_d$ and $\lambda_q = L_q I_q$ are illustrated in Fig. 2.4 *a*, *b*. The cross coupling is visible for both axis, but more pronounced for the *q* axis.

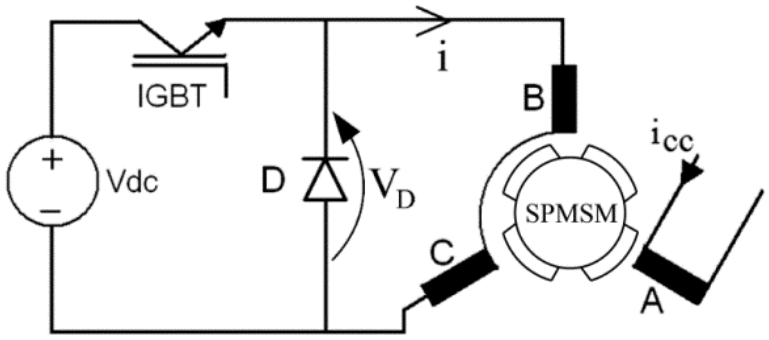

Fig. 2.4. DC current decay test at standstill for *dq* inductances identification

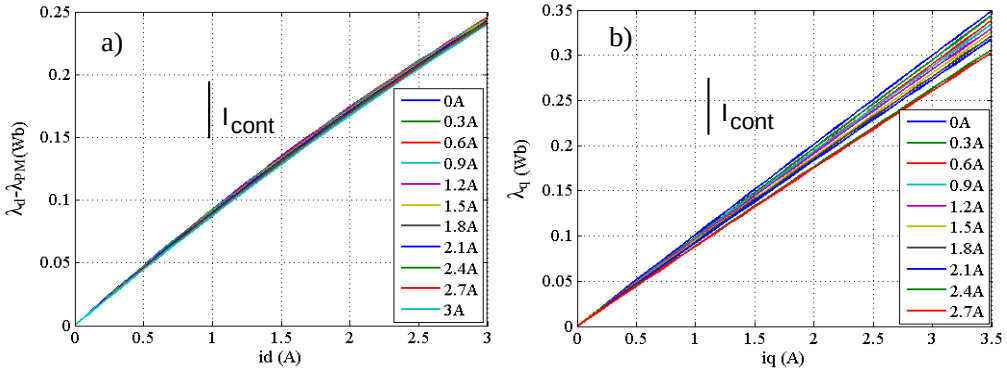

Fig. 2.5. Experimentally determined (λ_d - λ_{PM})(i_d) and λ_q(i_q) dependencies

2.2.2. PMSM Iron Loss Resistance Estimation

The real PMSM model is further enhanced by taking into consideration the core losses. A traditional approach is used, which considers only two components: hysteresis losses and eddy current losses

$$P_{iron} = k_h f \lambda_s^2 + k_e f^2 \lambda_s^2 \quad (2.10)$$

where P_{iron} are the core losses, k_h and k_e are the hysteresis and the eddy currents coefficients, f is the frequency and λ_s is the stator flux amplitude.

The iron losses are usually modeled as a resistance connected in parallel with the induced emf. The resistance can be calculated based on:

$$R_{iron} = \frac{3}{2}\frac{\omega^2 \lambda_s^2}{P_{iron}} \quad (2.11)$$

By introducing (2.10) in (2.11) the following is obtained:

$$R_{iron} = \frac{6\pi^2}{k_e + k_h / f} \quad (2.12)$$

For a given λ_s=constant, k_h and k_e can be identified by linear fitting having at least two measurements. In this case k_h=0.47 and k_e=0.005.

This approach will be used in Section 4.2, where experimental and simulation results are compared. The results prove that the real model is well identified.

The PMSM parameters are specified in Table 2.1.

Table 2.1. PMSM Parameters

Rated mechanical speed (ω_{rn})	1500 rpm
Rated power (P_n)	400 W
Rated phase voltage (V)	220 V
Rated current (I)	0.8 A
Number of pole pairs (p)	2
Stator resistance (R_s)	16.5 Ω
Stator phase inductance (L_s)	0.09 H
Permanent magnet flux (λ_{PM})	0.75 Wb
Motor inertia (J)	0.0025 kgm^2
Viscous friction coefficient (B)	0.003 Nms/rad

2.3. PMSM Control Strategies

The speed of the PMSM is determined by the stator frequency and the number of poles because of the constant rotor excitation [Leo1997].

There are two types of variable frequency drive (VFD) control methods:

- Scalar control;
- Vector control.

On the other hand, there are control strategies employing sensor information (motion sensors, current sensors, voltage sensors) and control strategies without motion sensors (sensorless control).

2.3.1. Scalar Control

The scalar control method, i.e., V/f control, is based on the principle of varying the frequency and the voltage magnitude by mainly maintaining V/f ratio constant.

The simplest control method is *open-loop V/f control* (without motion sensors) for PMSMs designed with damper windings. The solution to eliminate this big disadvantage is to use *closed-loop V/f control* with stabilizing loops instead.

2.3.2. Vector Control

The vector control method has several different approaches:

- Field Oriented Control (FOC);
- Direct Torque Control (DTC);
- Active Flux Based Vector Control;
- Flux Weakening Control (FWC).

The **Field Oriented Control (FOC)** is a closed loop control method that uses the position of the rotor as a feedback. FOC is classified into two categories depending on the chosen reference frame: i) *dq* rotor reference frame oriented along the PM flux, and ii) stator reference frame oriented along the stator flux vector.

This is an indirect control because, beside the speed loop, it has two current loops that indirectly control the electromagnetic torque. It is suitable for low speed applications and high speed drives. The advantages of using FOC are: accurate speed control, fast torque response (1-3 ms time response), full load at zero speed. The disadvantages are the high computation effort and the need for a modulation technique [Per2002]. FOC strategy in *dq* reference frame will be used in sections 3.1, 4.3 and 4.1.

The **Direct Torque Control (DTC)** is a control method used to control the torque (eventually generated by motion controller) and stator flux by selecting the appropriate voltage vector from a predefined switching table to maintain the torque and stator flux within their hysteresis bands [Xu2007]. The advantages of using DTC are: fast torque response equivalent to FOC, no need for modulation techniques, low complexity/processing requirements. The main disadvantage is the presence of current, toque and speed ripples, especially for low speed operation [Pac2005].

The **Active Flux (AF)** concept refers to the torque producing flux from the electromagnetic torque formula of AC machines in *dq* reference frame [Bol2008]. The active flux expression is given by

$$T_e = \frac{3}{2} p \, \lambda_{act} \, i_q$$

$$\lambda_{act} = \lambda_{PM} \qquad \text{for SPMSM}$$

$$\lambda_{act} = \lambda_{PM} + \left(L_d - L_q\right) i_d \qquad \text{for IPMSM}$$

$$\theta_{\lambda_{act}} = \theta_r$$

The active flux vector is aligned along the rotor *d* axis for SMs, making the rotor position and speed observer more amenable to a wide speed range sensorless drives [Bol2011].

The **Flux Weakening Control (FWC)** is based on a set of current and voltage constrains intended to generate the maximum torque in very large speed ranges [Sul2011].

Depending on the control strategy used, different control properties are imposed for an effective control. These control properties are as follows [Per2002]:

- ➔ *Constant Torque Angle Control* (CTAC), also called i_d=0 control: the torque angle is kept constant at 90°;
- ➔ *Maximum Torque per Ampere Control* (MTPAC): the minimum stator current needed for a required electromagnetic torque, in order to achieve minimum copper losses;
- ➔ *Unity Power Factor Control* (UPFC): in order to increase efficiency, reactive power can be reduced by maintaining the power factor angle to zero (φ=0);
- ➔ *Constant Stator Flux Control* (CSFC): the stator voltage is kept low by limiting the stator flux linkage magnitude.

2.3.3. Sensorless Control

The term 'sensorless' used in drive control refers to the absence of motion sensors; usually other types of sensors are used in the drive system, e.g. current sensors, voltage sensors [Vas1998].

Position or speed sensors are mounted directly on the rotor shaft of the machine. Some advantages achieved by eliminating these sensors are:

- reduction of cost, mass and volume of the drive;
- achievement of noise immunity;
- reduction of hardware complexity of the drive;
- elimination of disturbance induced by vibrations at very high speed and sensor failures;
- removal of accurate mounting and calibration needed for mechanical sensors;
- removal of wires from the sensor to the controller.

Sensorless methods are divided into three classes [Sul2011], [And2012]:

(i) Methods based on the fundamental machine model (emf estimation), with model parameter dependence, working at speed greater than nx10 rpm;

(ii) Injection methods, which inject additional sinusoidal or square wave voltages with high frequency, exploiting machine anisotropies, with

robustness to parameter variations. They are recommended at low speed including zero speed;

(iii) Hybrid methods for wide speed ranges, that combine the advantage of the (i) and (ii) methods.

Because the knowledge of the rotor position is very important in control strategies, e.g. for coordinate transforms, estimation techniques are introduced. The rotor position/speed can be estimated using different strategies that employ the use of measured values, e.g. stator voltages/currents.

Some observer topologies for position/speed estimation are discussed in the following chapter.

3 Observer Topologies for PMSM Sensorless Control

This chapter presents a review of the observers studied as part of the research done for this thesis, in order to highlight the advantages and disadvantages of different topologies. As a result, a novel structure, validated through simulation results, is developed.

PMSM vector control strategies, such as Field Oriented Control (FOC) or Direct Torque and Flux Control (DTFC), need the rotor position of the rotor in order to perform coordinate transforms and the rotor speed for speed control.

The observers are mainly employed for:

- ✓ Sensorless control structures (without motion sensors);
- ✓ Fault tolerant systems that usually use sensored control and switch to sensorless control mode and reverse in case of faulty sensors.

In both cases, the rotor position and rotor speed must be estimated.

The estimation of the needed measure can be done using two kinds of estimators [And1999]:

- *Estimators without feedback* (**Estimators**), in open loop;
- *Estimators with feedback* (**Observers**), in closed loop.

In what follows, three types of observers for rotor position and speed estimation, without motion sensors, will be analyzed: *Modified Equivalent Integrators for Stator Flux Estimation* using Active Flux Concept, *MRAS based observer* and *Nonlinear State and Disturbance Observer*. Next, simulation results are presented in order to highlight the advantages and disadvantages of the studied observers and eventually to enhance the observer structure to reduce the disadvantages.

3.1. Modified Equivalent Integrators for Stator Flux Estimation

The PMSM stator voltage model in $\alpha\beta$ stator reference frame is given by

$$\dot{\bar{\lambda}}_S = \bar{v}_S - R_S \bar{i}_S = \bar{e} \tag{3.1}$$

$$\bar{\lambda}_S = \lambda_\alpha + j\lambda_\beta,\ \bar{v}_S = v_\alpha + jv_\beta,\ \bar{i}_S = i_\alpha + ji_\beta \tag{3.2}$$

where $\bar{\lambda}_S$ (λ_α , λ_β) is the stator flux vector; $\bar{v}_S$ (v_α , v_β) is the stator voltage vector; $\bar{i}_S$ (i_α , i_β) is the stator current vector, R_s is the stator resistance; $\bar{e}$ (e_α , e_β) is the back emf;.

To estimate the stator flux $\hat{\bar{\lambda}}_S$ from (3.1), a pure integrator is employed:

$$\hat{\bar{\lambda}}_S = \int_{t_0}^{t} \bar{e}\, dt + \hat{\bar{\lambda}}_S(t_0) \tag{3.3}$$

where $\hat{\bar{\lambda}}_S(t_0)$ is the initial stator flux vector at time t_0.

The ideal integrator (3.5) can induce serious problems in terms of determining the initial conditions and compensating the DC offset from the stator current measurement chain. Because the DC offset input can lead to integrator saturation, the use of a pure integrator is not possible in real applications.

In order to avoid the pure integrator disadvantages, a simple solution is to replace the integrator with a 1st order LPF. The disadvantages of using LPF are the amplitude and phase errors which depend on the input frequency, mostly for frequencies around the cutoff frequency. For this reason LPFs are used for medium to high speed ranges, $\omega \geq 3\text{-}5\omega_c$.

An improvement for integrators and LPFs is to use feedback corrections. A general case is presented below [Hu1998], [And1999], [Zha2008]

$$\bar{\lambda}_S = \frac{1}{s+\omega_c}\bar{e} + \frac{\omega_c}{s+\omega_c}\bar{z} \tag{3.4}$$

where ω_c is the cutoff frequency, $\bar{e} = \bar{v}_S - R_S\bar{i}_S$ is the emf, $\bar{z}$ is the feedback.

Note that, if $\bar{z} = \bar{\lambda}_S$ then $\bar{\lambda}_S = \bar{e}/s$, i.e., ideal integrator, and if $z=0$ then (3.4) is a LPF with the cutoff frequency ω_c that approximates the integrator.

Three modified integrators which use different methods of obtaining the feedback z are presented in the following sections along with comparative simulation results.

3.1.1. Modified Integrator with Stator Flux Amplitude Limiter

The first modified integrator topology is based on the stator flux amplitude limiter (Fig. 3.1) in order to eliminate the pure integrator disadvantages. This structure is based on (3.4) and uses two coordinate transforms, from Cartesian to Polar and from Polar to Cartesian, and an amplitude limiter for $\hat{\lambda}_S$ [Hu1998].

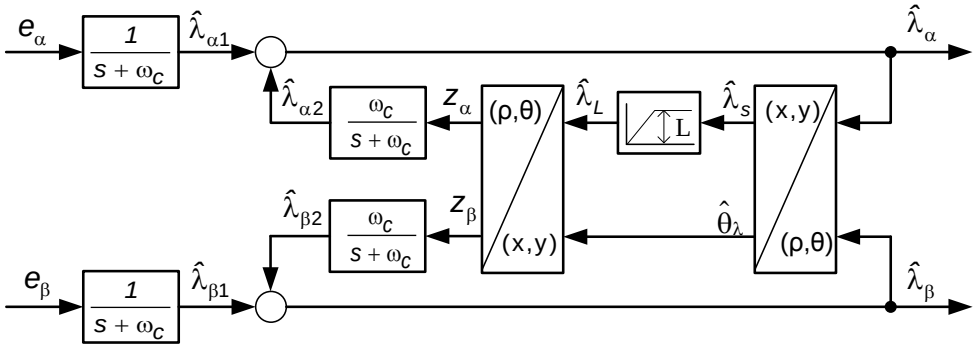

Fig. 3.1. Modified integrator with stator flux amplitude limiter in $\alpha\beta$ reference frame

$$\hat{\bar{\lambda}}_S = \hat{\lambda}_S \cdot e^{j\hat{\theta}},\ \hat{\bar{\lambda}}_L = \hat{\lambda}_L \cdot e^{j\hat{\theta}},\ \hat{\lambda}_S = \sqrt{\hat{\lambda}_\beta^2 + \hat{\lambda}_\alpha^2} \tag{3.5}$$

$$\sin\hat{\theta}_\lambda = \frac{\hat{\lambda}_\beta}{\hat{\lambda}_S},\ \cos\hat{\theta}_\lambda = \frac{\hat{\lambda}_\alpha}{\hat{\lambda}_S} \tag{3.6}$$

The *cos* and *sin* functions from (3.6) are needed for Polar to Cartesian transform, with the note that θ_λ is the stator flux angle and not the rotor position θ_r. The rotor position θ_r is estimated using active flux (AF), presented in section 3.1.4.

The *advantage* of using this method is that the feedback corrections $\hat{\bar{\lambda}}_2\left(\hat{\lambda}_{2\alpha}, \hat{\lambda}_{2\beta}\right)$ work to stabilize the λ_S amplitude to the real $\lambda_S^* = L$ amplitude and reduces the DC offset. This structure is equivalent with the ideal integrator in frequency domain.

The *disadvantage* of this method is that if the proper value of the *L* limit is not chosen correctly then a phase error for $\hat{\bar{\lambda}}_S$ is introduced [Zha2008].

This structure is recommended in control strategies that regulate the stator flux $\hat{\bar{\lambda}}_S$ =const., i.e., DTC, FOC, where stator flux feedback is used. In these cases $L = \lambda_S^*$ (stator flux reference).

3.1.2. Modified Integrator with Adaptive Correction based on emf and Stator Flux Orthogonality

This type of modified integrator is based on the fact that the stator flux is orthogonal to its emf (3.3). A quadrature detector is introduced to identify the orthogonality between the estimated stator flux and the emf [Hu1998], [And1999].

Fig. 3.2 depicts the connection between the stator flux vector and the emf vector, where Δθ is the angle between $\hat{\bar{\lambda}}_S$ and $\bar{e}$, γ is the error angle introduced by a DC offset or wrong initial conditions, $\bar{\lambda}_S$ is the correct stator flux vector and $\bar{\lambda}_S'$ is the modified stator flux vector after the γ angle is introduced.

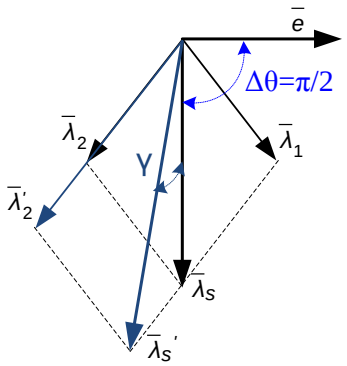

Fig. 3.2. Vector diagram of emf and stator flux [Hu1998]

$$\left.\begin{aligned}\bar{e} &= e\cdot e^{j\theta_e} = e_\alpha + je_\beta \\ \bar{\lambda}_S &= \lambda_{S\alpha} e^{j\theta_\lambda} = \lambda_\beta + j\lambda\end{aligned}\right| \quad \bar{e}\perp\bar{\lambda}_S \Rightarrow \theta_e - \theta_\lambda = \Delta\theta = \frac{\pi}{2} \quad (3.7)$$

$$\left(\bar{e}\cdot\bar{\lambda}_S^*\right) = e\lambda_{S\alpha} + e_\beta\lambda_{S\beta} + j\left(e_\beta\lambda_{S\alpha} - e_\alpha\lambda_{S\beta}\right) \quad (3.8)$$

$$Re\left(\bar{e}\cdot\bar{\lambda}_S^*\right) = e\lambda_{S\alpha} + e_\beta\lambda_{S\beta}$$

For small values of γ using the approximation $sin(\gamma)\approx\gamma$ in (3.8) the error angle expression is obtained

$$\gamma = -\frac{e\lambda_\alpha + e\lambda_\beta}{e\lambda_s} \tag{3.9}$$

For an adaptive compensation of λ_s amplitude a PI compensator is introduced, with the expression

$$H_{PI}(s) = k_p + \frac{k_i}{s} \tag{3.10}$$

where k_p is the proportional constant and k_i is the integral constant of the PI compensator.

As can be seen, $\bar{\lambda}_s$ is composed of two vectors: the feedforward vector $\bar{\lambda}_1$, the output of the LPFs, and the feedback vector $\bar{\lambda}_2$. If the angle $\Delta\theta$ is 90° then the output of (3.9) is zero. When the error angle γ is introduced, the vector $\bar{\lambda}_s$ increases to $\bar{\lambda}_s'$ and the output of the PI regulator (3.10) is negative.

The modified integrator with adaptive correction based on emf and stator flux orthogonality is presented in Fig. 3.3.

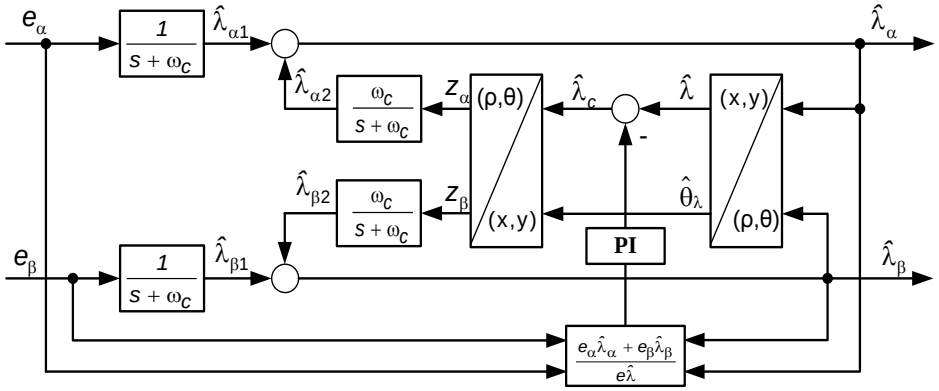

Fig. 3.3. Modified Integrator with Adaptive Correction based on emf and Stator Flux Orthogonality

3.1.3. Modified Integrator with Adaptive Correction based on Stator Flux Vector components Orthogonality

Another approach for the modified integrator presented in the previous paragraph is using adaptive correction based on stator flux vector components orthogonality. The idea comes from the assumption that when γ is zero the stator flux components $\bar{\lambda}_1$ and $\bar{\lambda}_2$ are orthogonal, having the same delay introduced by the feedforward and feedback LPFs on $\bar{e}$ and $\bar{\lambda}_s$ ways, respectively [And1999]. Because $\bar{e}\lambda\perp\bar{}_s$, it can be said that $\bar{\lambda}_1 \perp \bar{\lambda}_2$.

The adaptive correction is computed similar to (3.9)

$$\gamma = -\frac{\hat{\lambda}_{\alpha_1}\hat{\lambda}_{\alpha_2} + \hat{\lambda}_{\beta_1}\hat{\lambda}_{\beta_2}}{\hat{\lambda}_1\hat{\lambda}_2} \tag{3.11}$$

The observer structure is presented in Fig. 3.4, where the difference regarding Fig. 3.3 is the estimation of the orthogonality error.

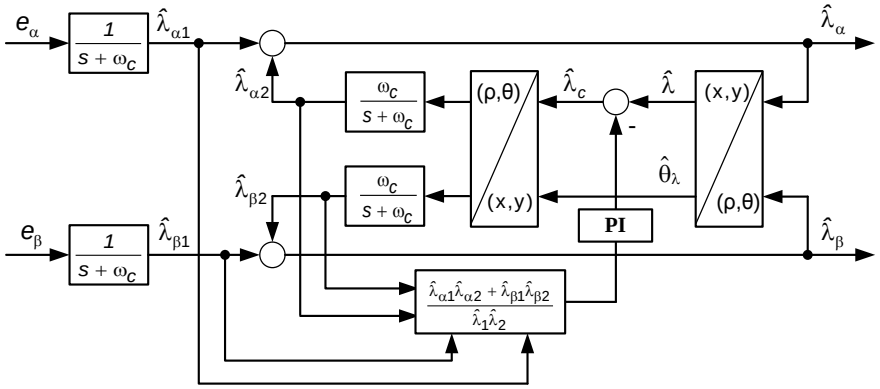

Fig. 3.4. Modified Integrator with Adaptive Correction based on Stator Flux Vector components Orthogonality

The *advantage* of both modified integrators with adaptive correction is the use of filtered components only, which attenuates the noise generated due to the inverter block switching. This method is recommended for variable stator flux amplitude [And1999].

3.1.4. Rotor Position Estimation using Active Flux

In order to estimate the rotor position, i.e., $\theta_\lambda \neq \theta_r$, the active flux (AF) is used. The AF concept, first introduced by [Bol2008], refers to the torque-producing flux aligned along the *d* axis, having the great *advantage* that the active flux angle is the same as the rotor position

$$\theta_{\lambda_{act}} = \theta_r \tag{3.12}$$

The connection between the stator flux vector and the AF vector, *for any reference frame*, is expressed as

$$\bar{\lambda}_{act} = \bar{\lambda}_S - L_q \bar{i}_S \tag{3.13}$$

where $\bar{\lambda}_S$ is the stator flux vector, L_q is the q axis inductance and $\bar{i}_S$ is the stator current vector.

The rotor position is computed employing the *atan2* function and the *αβ* AF vector components, i.e., the AF estimator equations, given by

$$\begin{aligned} \hat{\theta}_r &= atan2\left(\hat{\lambda}_{act\beta}, \hat{\lambda}_{act\alpha}\right) \\ \hat{\bar{\lambda}}_{act} &= \hat{\lambda}_{act\alpha} + j\hat{\lambda}_{act\beta} \end{aligned} \tag{3.14}$$

3.1.5. Simulation Results

The test system structure, presented in Fig. 3.5, is used to validate the modified integrators for rotor position estimation. A standard FOC strategy with $i_d^* = 0$ for PMSM control works aside the three modified integrators for stator flux estimation and active flux based estimator (3.12) for rotor position estimation.

The *objective* is to compare the measured stator flux components in *αβ* reference frame with the estimated ones using the three modified integrator structures presented above.

Simulations results are presented in order to compare the performance of the three modified integrators presented above, which are symbolized as:

- *1/s* - pure integrator;
- *method 1* - Modified Integrator with Stator Flux Amplitude Limiter;
- *method 2* – Modified Integrator with Adaptive Correction based on emf and Stator Flux Orthogonality;
- *method 3* – Modified Integrator with Adaptive Correction based on Stator Flux Vector components Orthogonality.

The simulation scenario is considered for a 15 rad/s speed, i.e., 10% of the rated speed (Table 3.1), and a 1.2 Nm load torque, i.e., 50% of the rated torque. A 0.1 V DC offset is introduced for *α* axis emf. A comparison between the 3 modified integrators and a pure integrator is performed in order to show the DC offset compensation performance of the modified integrators.

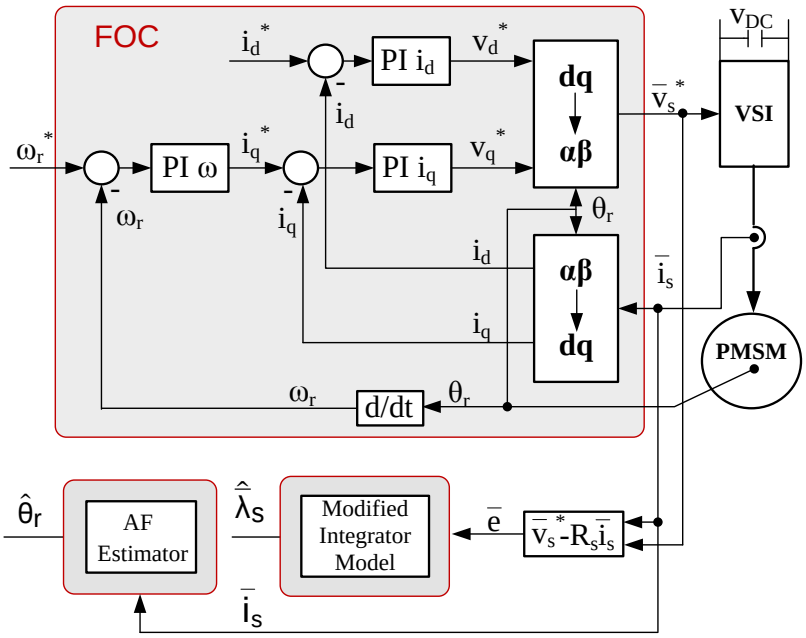

Fig. 3.5. Control structure for validating the modified integrators for rotor position estimation

Table 3.1. PMSM Parameters

Rated mechanical speed (n_{rn})	1500 rpm
Rated power (P_n)	400 W
Rated phase voltage (V)	220 V
Rated current (I)	0.8 A
Number of pole pairs (p)	2
Stator resistance (R_s)	16.5 Ω
Stator phase inductance (L_s)	0.09 H
Permanent magnet flux (λ_{PM})	0.75 Wb
Motor inertia (J)	0.0025 kgm^2
Viscous friction coefficient (B)	0.003 Nms/rad

Table 3.2. Modified Integrator Parameters

Cutoff frequency (ω_c)	10 rad/s
DC offset	0.1 V
Limit (L)	0.8 Wb
Proportional constant (k_p)	0.5
Integral constant (k_i)	0.1

As can be seen in Fig. 3.6*a*, the pure integrator drifts and leads the integrator to saturation limit while the modified integrators remain stable and eliminates the DC offset effects. The β axis flux illustrated in Fig. 3.6*b* is not disturbed by the DC offset, this being set only for the α axis.

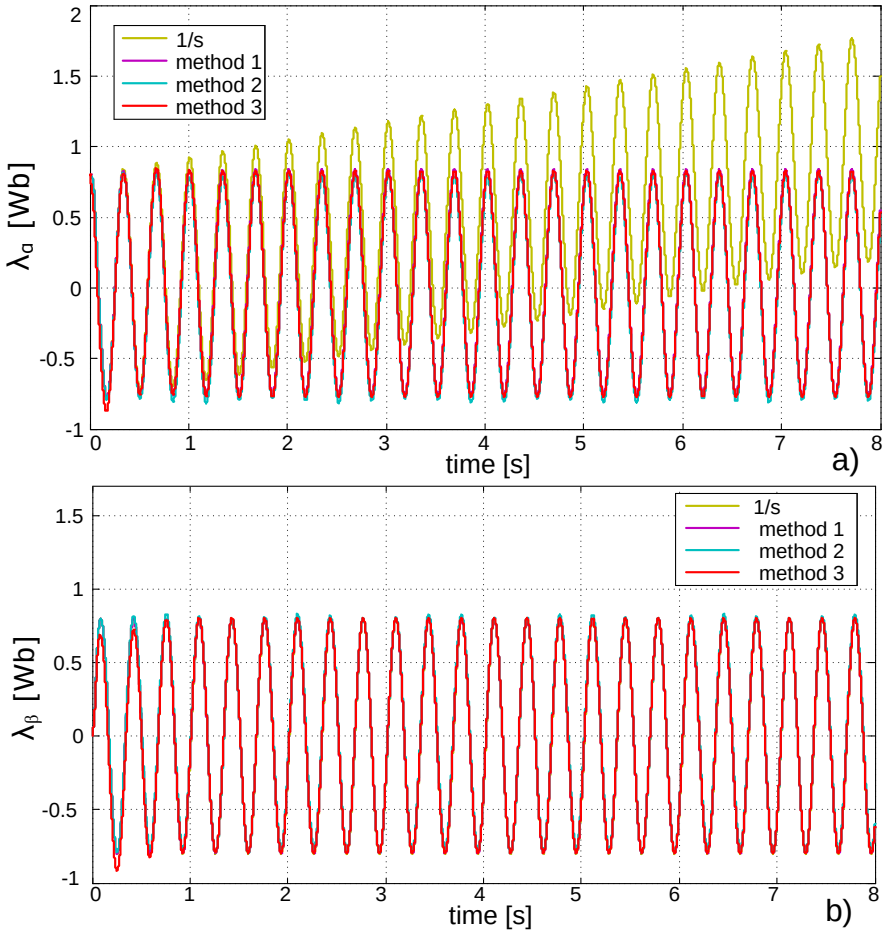

Fig. 3.6. Compared simulation results, at 15 rad/s electric speed and 1.2 Nm load, of the 3 modified integrators with the pure integrator: a) α axis flux, b) β axis flux

Next, for a better performance analysis of the 3 modified integrators, a comparison between the PMSM stator $\alpha\beta$ fluxes (obtained by coordinate transform from dq fluxes) and each modified integrator is performed. The simulation scenario remains the same. The rotor position is estimated using AF based estimator, with the remark that the AF angle is the same as the rotor position.

Method 1 (Fig. 3.7): the real *αβ* flux linkages in the machine and the estimated *αβ* flux linkages are compared in Fig. 3.7*a*. There is a small amplitude deviation, 0.02 Wb (2.5%), introduced by the DC offset.

The measured rotor position and the estimated rotor position are compared in Fig. 3.7*b*. A small position estimation error only occurs at startup. This method presents good results for the linkage flux estimation and good results for rotor position estimation.

Method 2 (Fig. 3.8): the real *αβ* flux linkages in the machine and the estimated *αβ* flux linkages are compared in Fig. 3.8*a* while Fig. 3.8*b* shows a comparison between the measured rotor position and the estimated rotor position.

This method has similar results as method 1, having a low deviation in the flux linkage amplitude and correct rotor position estimation.

Method 3 (Fig. 3.9): in Fig. 3.9*a* depicts a comparison between the real *αβ* flux linkages in the machine and the estimated *αβ* flux linkages. In this case, even though the same flux amplitude deviation is present, at startup both *αβ* fluxes are wrongfully estimated until a full period passes. This startup estimation error is observed in Fig. 3.9*b* in the estimated rotor position.

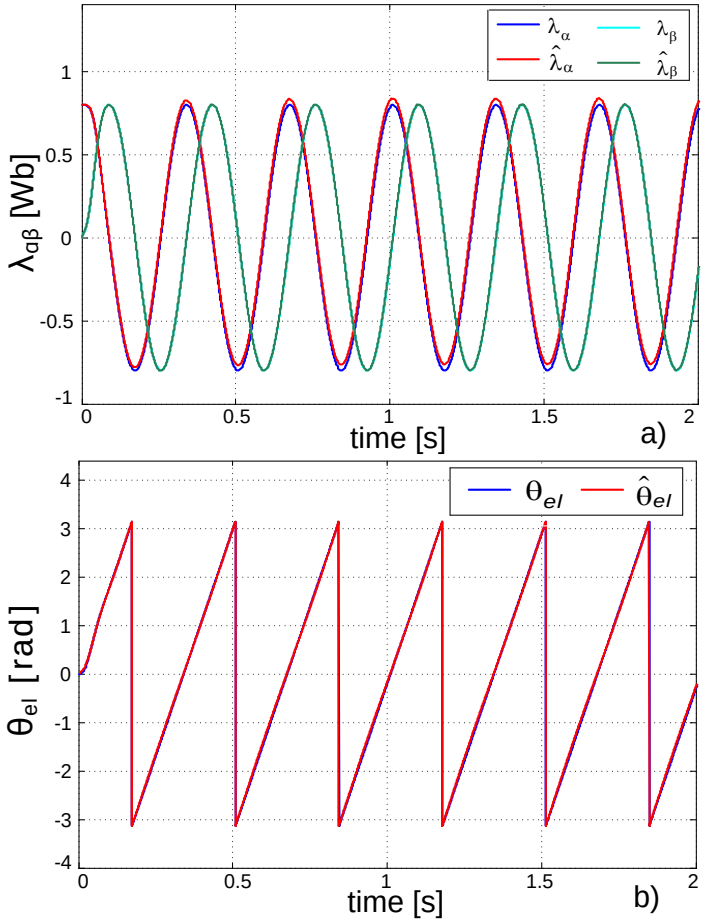

Fig. 3.7. Comparison between a) PMSM *αβ* fluxes and **method 1** estimated *αβ* fluxes, and b) measured rotor position and estimated rotor position

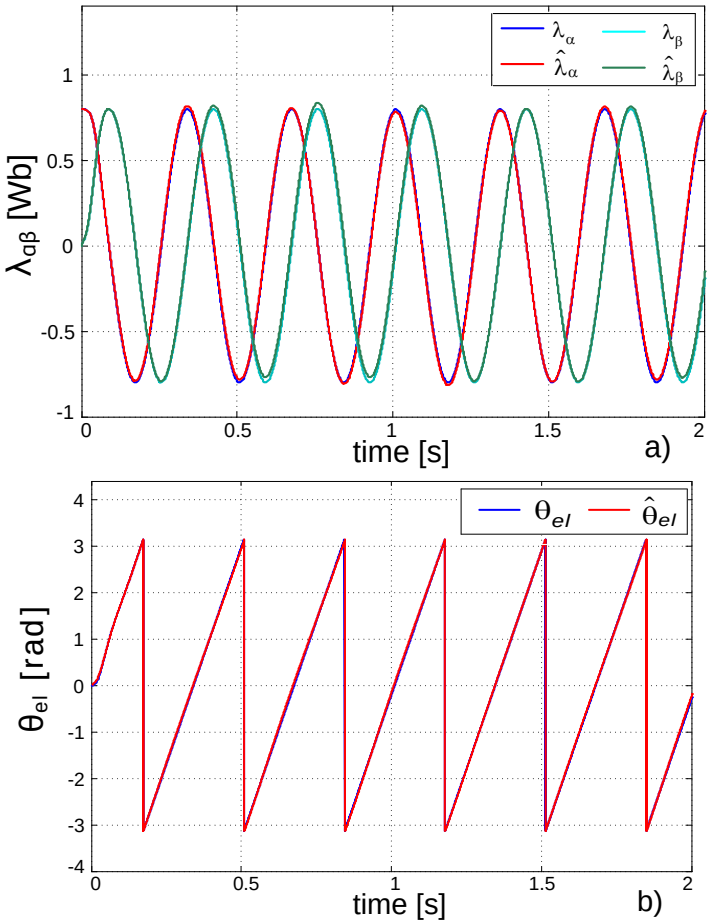

Fig. 3.8. Comparison between a) PMSM *αβ* fluxes and **method 2** estimated *αβ* fluxes, and b) measured rotor position and estimated rotor position

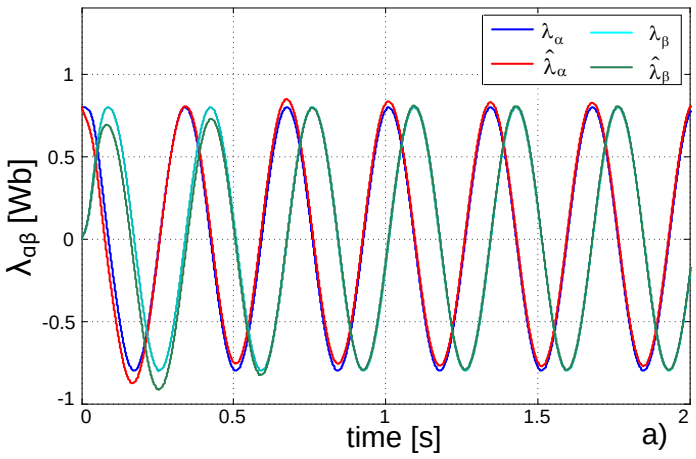

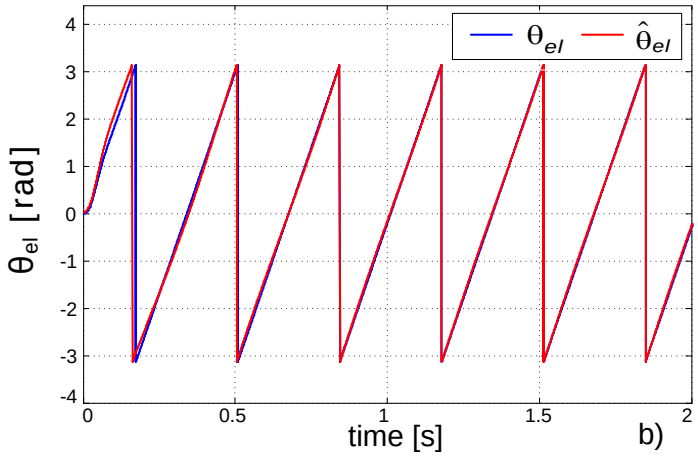

Fig. 3.9. Comparison between a) PMSM *αβ* fluxes and **method 3** estimated *αβ* fluxes, and b) measured rotor position and estimated rotor position

3.1.6. Conclusions

The 3 modified integrator methods presented resolve the pure integrator problem, i.e., the DC offset drift and initial condition of stator flux, as shown in the simulation results.

Method 1 reduces the DC offset and presents good results. Its disadvantage is that if limit *L* is not chosen correctly then a phase error is introduced for $\hat{\bar{\lambda}}_S$. This topology is suitable for constant flux linkage applications.

Method 2 presents also good results being a good candidate for sensorless drive control where the flux linkage may vary during operation.

Method 3 presents the advantage of using only filtered components, which attenuates the noise generated due to the inverter block switching, but the disadvantage is that it introduces a delay in estimating the flux and rotor position at startup. This method is also suitable for applications were the flux linkage is variable.

3.2. Model Reference Adaptive System based Observer

The basic concept for MRAS implies the use of two models: the reference model and the adaptive model [Miy1990]. The purpose of this approach is to adjust the parameters of the adaptive model so that the outputs of these models coincide [Kha2012], [Gad2013].

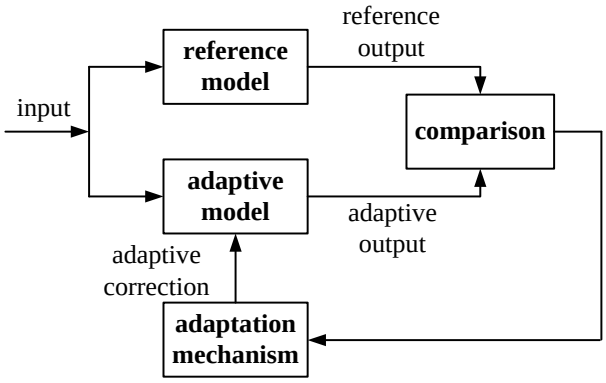

Fig. 3.10. Model Reference Adaptive System (MRAS) flowchart

The proposed MRAS based observer used in SPMSM control for the estimation of rotor position and speed is illustrated in Fig. 3.11 [And1999], employing sensorless $i_d^*=0$ FOC strategy. Only the stator currents are measured. The block components are discussed in what follows.

3.2.1. Back emf Estimator with adaptive LPF

Starting with the $a\beta$ equations (2.3)-(2.5) for SPMSM, the back emf $\bar{e}$ has the expression

$$\begin{aligned} \bar{e} &= \bar{v}_S - \left(R_S + sL_S\right)\bar{i}_S \\ \bar{e} &= \omega_r \lambda_{PM} e^{j\left(\theta_r + \pi/2\right)} \end{aligned} \tag{3.15}$$

with the $a\beta$ back emf components

$$\begin{aligned} e_\alpha &= -\omega_r \lambda_{PM}\, sin\left(\theta_r\right) \\ e_\beta &= \omega_r \lambda_{PM}\, cos\left(\theta_r\right) \end{aligned} \tag{3.16}$$

The importance of choosing the correct filter for the back emf estimation is explained in [And1999]. A first order LPF is used to estimate $\bar{e}$ in order to reduce disturbances introduced by the derivative function of $\bar{i}_S$ from (3.18), with the adaptive time constant τ. The transfer function in the frequency domain is

$$\begin{aligned} H_{LPF}\left(j\omega\right) &= \frac{1}{1+j\omega\tau} = A_f\ e^{-j\theta_f} \\ A_f &= \frac{1}{\sqrt{1+\left(\omega\tau\right)^2}},\ \theta_f = a\tan\left(\omega\tau\right) \end{aligned} \tag{3.17}$$

where A_f is the filter attenuation, θ_f is the phase and ω is the cutoff frequency.

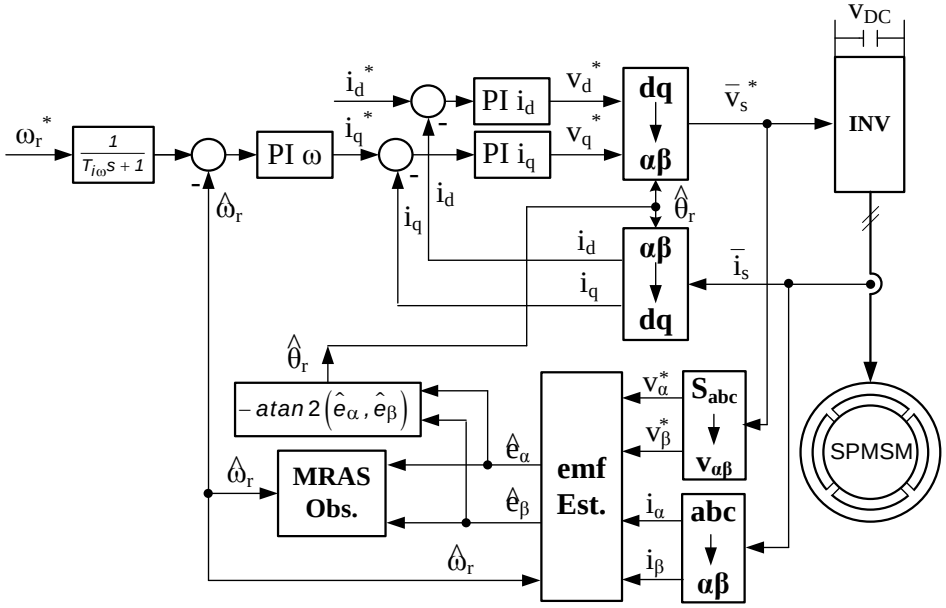

Fig. 3.11. MRAS based observer for SPMSM sensorless control

In conclusion, the back emf estimation uses the measured stator currents and the reference stator voltages with adaptive LPF

$$\hat{\bar{e}} = \frac{\bar{v}_s^* - (R_{so} + sL_{so})\bar{i}_s}{1 + s\tau}, \quad \tau = \frac{c}{|\hat{\omega}|} \tag{3.18}$$

where c is a positive constant, R_{so} and L_{so} are the SPMSM parameters used in emf estimator.

The implementation structure given in Fig. 3.12 is based on the equivalent expression:

$$\hat{\bar{e}} = \frac{\bar{v}_s^* + \left(-R_{so} + L_{so}/\tau\right)\bar{i}_s}{1 + s\tau} - \frac{L_{so}}{\tau}\bar{i}_s \tag{3.18'}$$

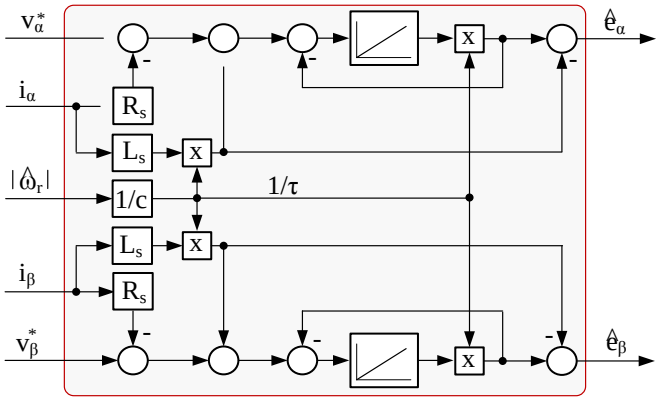

Fig. 3.12. Back emf estimation implementation block

Using an adaptive LPF the phase error delay, $\theta_f = atan(c)$, of the $\bar{e}$ estimation is constant.

The rotor position is estimated employing the *αβ* back emf components using the *atan2* function with the extended domain [-π,π), compatible with the *sin* and *cos* functions used in *dq* to *αβ* transforms

$$\hat{\theta}_r = -atan2\left(\hat{e}_\alpha, \hat{e}_\beta\right) \tag{3.19}$$

3.2.2. Rotor Speed MRAS Observer

The MRAS observer contains the $\bar{e}$ emf estimator (3.18') as reference model, and the adaptive model $\hat{\bar{e}}_m$ with the rotor speed as the adaptive correction. These components are described next.

The *Luenberger observer* is based on the speed adaptive harmonic oscillator $\hat{\bar{e}}_m$, and with back emf error as correction term

$$\dot{\hat{\bar{e}}}_m = j\hat{\omega}_m\hat{\bar{e}}_m + L\left(\hat{\bar{e}} - \hat{\bar{e}}_m\right) \tag{3.20}$$

having the dynamic error equation (3.21) and the adaptive parameter *L*

$$\dot{\varepsilon} = \left(j\hat{\omega}_r - L\right)\varepsilon + j\left(\hat{\omega}_r - \hat{\omega}_m\right)\hat{\bar{e}}_m \tag{3.21}$$

$$L = b\,|\,\hat{\omega}_r\,|$$

The *sliding mode based observer (SMO)* for speed estimation $\hat{\omega}_r$, uses position correction [And1999], [And2003]

$$\Delta\theta_r = \frac{1}{\left(\omega_r\lambda_{PM}\right)^2}\left(\hat{e}_\beta\hat{e}_{m\alpha} - \hat{e}_\alpha\hat{e}_{m\beta}\right) \tag{3.22}$$

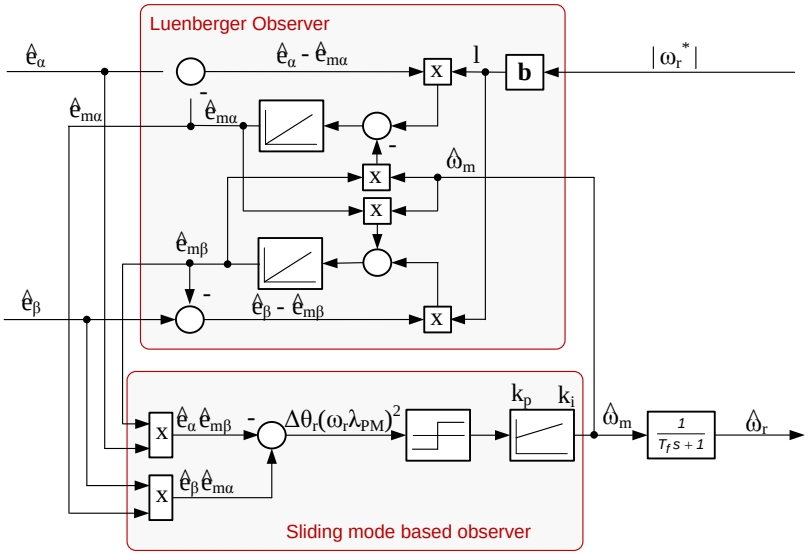

Fig. 3.13. Rotor Speed MRAS based Observer implementation

3.2.3. Simulation Results

The sensorless control for SPMSM with the MRAS observer and FOC strategy (Fig. 3.11) was implemented in MATLAB®/Simulink®, using a 100 μs sampling time.

The PMSM parameters are defined in Table 3.1. The observer parameters are b=2, c=240 and A_f=1.

The purpose of the simulations is to show the dynamic behavior of the studied sensorless SPMSM control. For this reason, extended simulations for low and high speed were made.

Fig. 3.14 presents the simulation results for **low speed**. ω_r^* is set to 10 rad/s and after 2.5 s is reversed to -10 rad/s. A torque load T_L^*=0.24 Nm is applied at 1 s and removed, after reversal, at 4 s.

The system has good performance for low speed operation. The comparison between measured rotor position and estimated rotor position is very good for startup or reversal, proving that the MRAS observer identifies the rotor speed sign automatically.

Fig. 3.15 depicts the simulation results for **high speed**. In this case ω_r^* is set to 314 rad/s and at 2.5 s is reversed to -314 rad/s. A torque load T_{L1}^*=1.5 Nm (60% of the rated torque) is applied at 1 s and T_{L2}^*=-0.5 Nm is applied at 4 s.

The system performances are improved for high speeds, as shown by the electric rotor speed variation. The rotor position estimation remains as good as in the first scenario, with an error estimation $\Delta\theta_r$ of approximate 0.6 degrees.

3.2.4. Conclusions

The presented MRAS based observer for estimations of rotor position and speed, used in sensorless control of SPMSM drives [And1999], contains the two main parts:

i) The back emf estimator based on the voltage model with adaptive LPF. This estimates the *rotor position* and requires only the measured stator currents.
ii) The MRAS observer for the *rotor speed* estimation. The adaptive model contains the following two components:
   - the Luenberger observer (based on the *harmonic oscillator model*) for sinusoidal emf estimation, with the *speed as adaptive correction* (phase correction) and the back emf error as correction term (amplitude correction);
   - the sliding mode observer for rotor speed estimation using the back emf angle error.

The error in estimating the rotor position, $\Delta\theta_r$, is approximately 0.6 degrees and depends only on the PMSM electric parameter variations, except λ_{PM}. The speed estimation is obtained independently of the PMSM parameter variations.

The MRAS based observer has no need for additional structure modifications of the rotor speed sign identification and is suited for low and high speed PMSM sensorless control applications.

The simulation results prove very good performance of the MRAS based observer in large speed ranges.

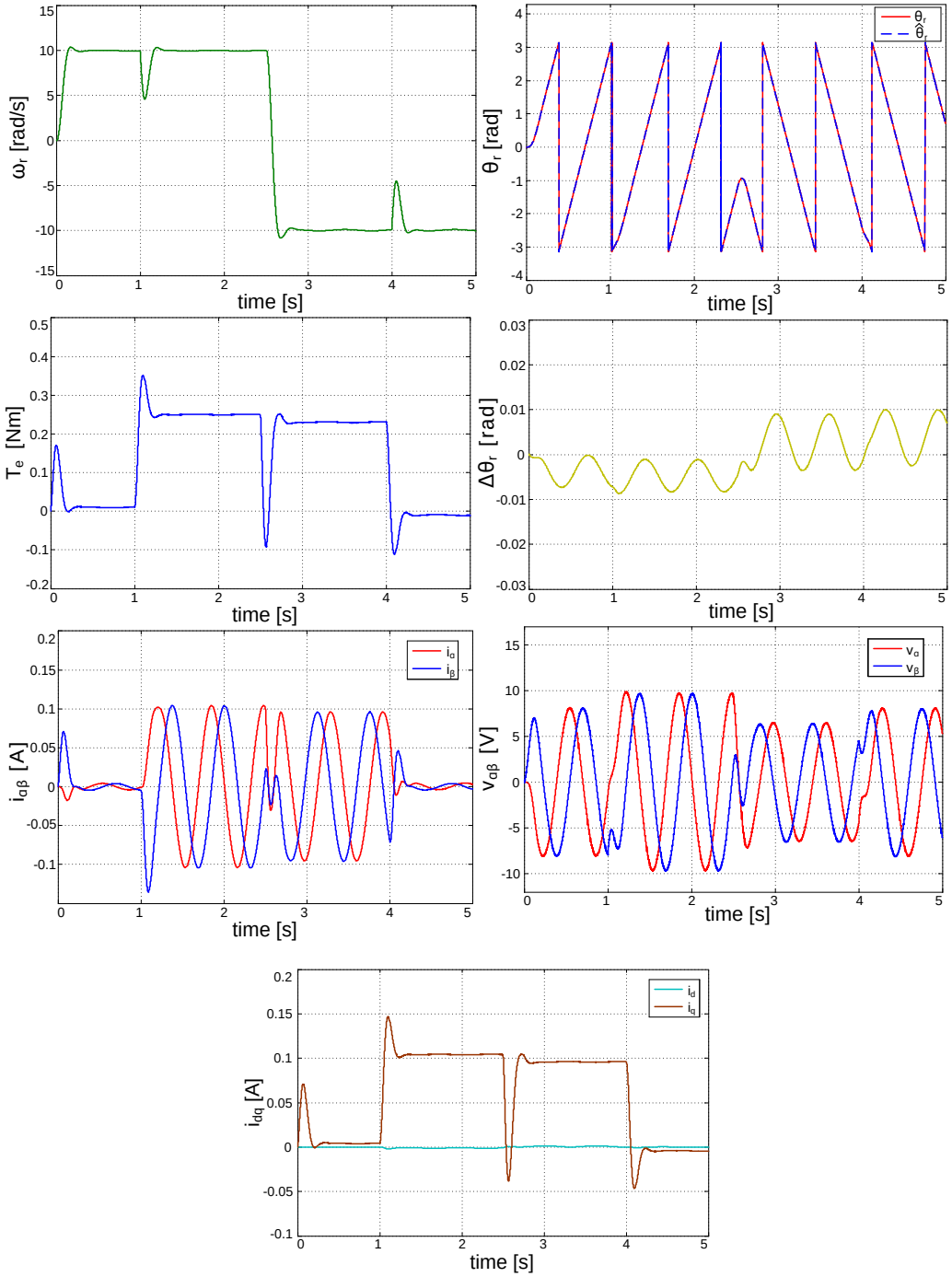

Fig. 3.14. Simulation results, at low speed, for electric rotor speed, electromagnetic torque, *aβ* currents, *aβ* voltages, rotor position, error between measured and estimated rotor position, *dq* currents.

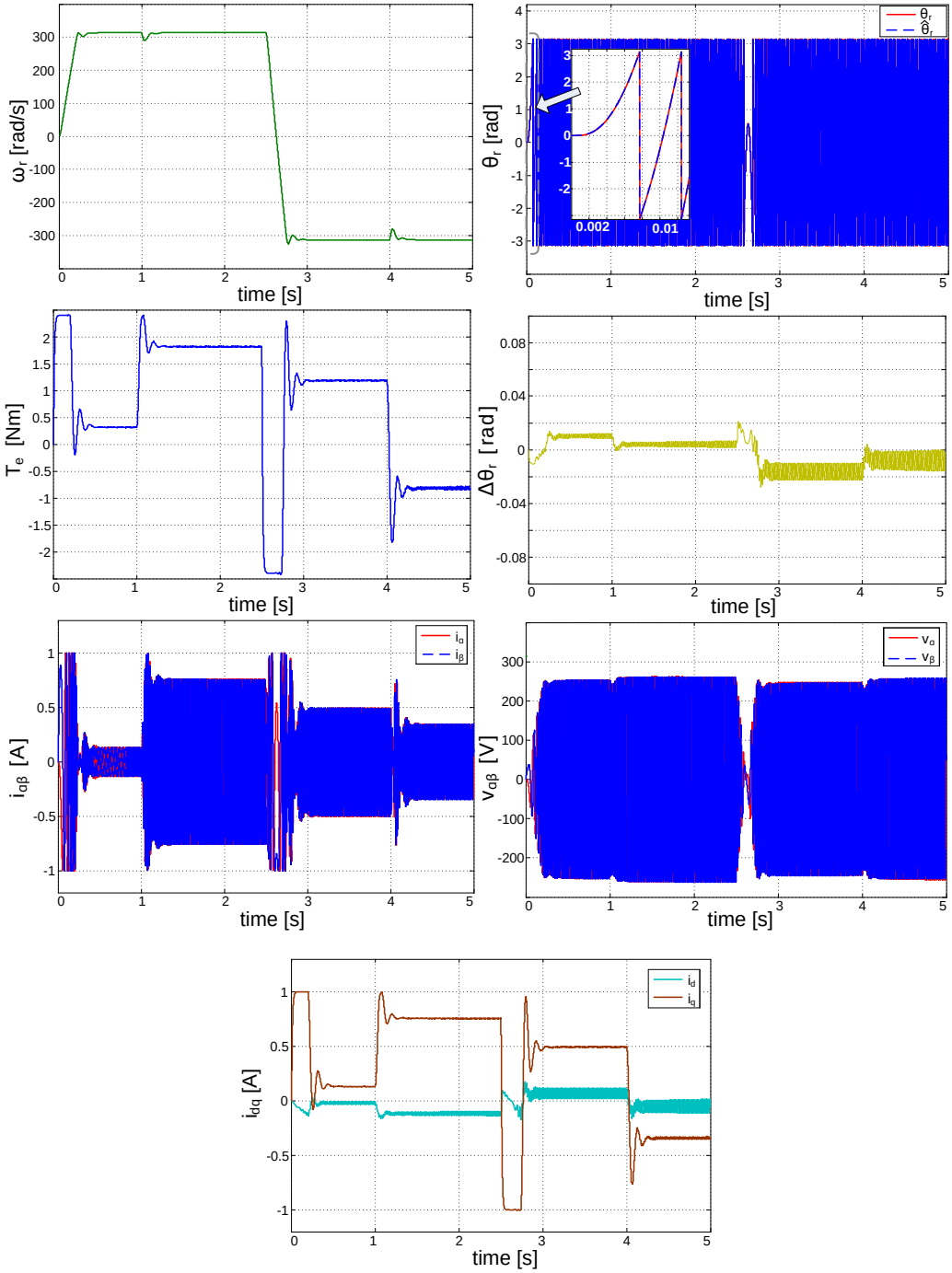

Fig. 3.15. Simulation results, at high speed, for electric rotor speed, electromagnetic torque, *αβ* currents, *αβ* voltages, rotor position, error between measured and estimated rotor position, *dq* currents.

3.3. Nonlinear State and Disturbance Observer

Starting from the notions introduced by [And1999] (pp. 66-75) and the study of [Lau2005], [Lin2007], [Yon2013], [Pii2007] and [Pii2008] a nonlinear state and disturbance observer (NSDO) structure is developed. NSDO estimates the rotor position θ_r, the rotor speed ω_r, the loading torque T_L and the q axis current i_q. The NSDO robustness to parameter variations is also studied.

3.3.1. Proposed Nonlinear State and Disturbance Observer

Starting from the PMSM equations in dq rotor reference frame

$$v_d = R_s i_d + L_d \dot{i}_d - \omega_r L_q i_q \tag{3.23}$$

$$v_q = R_s i_q + L_q \dot{i}_q + \omega_r \left(L_d i_d + \lambda_{PM}\right) \tag{3.24}$$

$$T_e = \frac{3}{2} p \left[\lambda_{PM} i_q + \left(L_d - L_q\right) i_q i_d\right] \tag{3.25}$$

$$\frac{J}{p}\dot{\omega}_r = T_e - T_L - \frac{B}{p}\omega_r \tag{3.26}$$

$$\dot{\theta}_r = \omega_r \tag{3.27}$$

where v_d, v_q are the stator voltage components; i_d, i_q are the stator current components; R_s is the stator resistance; L_d, L_q are dq axis inductances, ω_r, θ_r are the electrical rotor speed and position, λ_{PM} is the PM flux, T_e is the electromagnetic torque, T_L is the load torque, J is the motor inertia, B is the viscous friction coefficient and p is the number of pole pairs.

Substituting (3.25) in (3.26), the expression of speed dynamics is

$$\dot{\omega}_r = \frac{3}{2}\frac{p^2}{J}\lambda_{PM} i_q + \frac{3}{2}\frac{p^2}{J}\left(L_d - L_q\right) i_d i_q - \frac{p}{J} T_L - \frac{B}{J}\omega_r \tag{3.28}$$

Rearranging the equations (3.23)-(3.27) and considering an exogenous model for the disturbance T_L, results:

$$\dot{\theta}_r = \omega_r \tag{3.29}$$

$$\dot{\omega}_r = \frac{3}{2}\frac{p^2}{J}\lambda_{PM} i_q - \frac{B}{J}\omega_r + \frac{3}{2}\frac{p^2}{J}\left(L_d - L_q\right) i_d i_q - \frac{p}{J} T_L \tag{3.30}$$

$$\dot{i}_q = -\frac{R_s}{L_q} i_q - \frac{\lambda_{PM}}{L_q}\omega_r + \frac{1}{L_q} v_q - \frac{L_d}{L_q}\omega_r i_d \tag{3.31}$$

$$\dot{i}_d = -\frac{R_s}{L_d} i_d + \frac{1}{L_d} v_d + \frac{L_q}{L_d}\omega_r i_q \tag{3.32}$$

$$\dot{T}_L = 0 \tag{3.33}$$

The system (3.29)-(3.33) is rewritten as a state space model, without (3.32), as:

$$\begin{aligned} \dot{\bar{x}} &= A\bar{x} + g\left(\bar{x}\right)\bar{u} \\ \bar{y} &= C\bar{x} \end{aligned} \tag{3.34}$$

where

$$\begin{aligned} x &= \left[\theta_r \quad \omega_r \quad i_q \quad T_L\right]^T \\ y &= i_q \\ u &= \left[i_d \quad v_q\right]^T \end{aligned} \tag{3.35}$$

$$A = \begin{bmatrix} 0 & 1 & 0 & 0 \\ 0\lambda & -\frac{B}{J} & \frac{3}{2}\frac{p^2}{J}_{PM} & -\frac{p}{J} \\ 0 & -\frac{\lambda_{PM}}{L_q} & -\frac{R_S}{L_q} & 0 \\ 0 & 0 & 0 & 0 \end{bmatrix} \tag{3.36}$$

$$C = \left[0 \quad 0 \quad 1 \quad 0\right]$$

$$g\left(\bar{x}\right) = \begin{bmatrix} 0 & 0 \\ \frac{3}{2}\frac{p^2}{J}\left(L_d - L_q\right)i_q & 0 \\ -\frac{L_d}{L_q}\omega_r & \frac{1}{L_q} \\ 0 & 0 \end{bmatrix} \tag{3.37}$$

Remark: *The main reason for developing the NSDO (3.34)-(3.37) stems from the presumption that the current i_q is the main contribution to the electromagnetic torque T_e, given by*

$$T_e = \frac{3}{2}p\left[\lambda_{PM} + \left(L_d - L_q\right)i_d\right]i_q = k_t i_q$$

$$k_t = \frac{3}{2}p\left(\lambda_{PM} + \left(L_d - L_q\right)i_d\right) \quad \textit{for IPMSM}$$

$$k_t = \frac{3}{2}p\lambda_{PM} \quad \textit{for SPMSM}$$

Considering the motion equation (3.26) for ω_r=const. and substituting the electromagnetic torque T_e depending on i_q

$$\omega_r = \frac{p}{B}k_t i_q - \frac{p}{B}T_L = k_i k_b i_q - k_b T_L, \quad k_b = \frac{p}{B}$$

the connection between the rotor speed ω_r, the loading torque T_L and the q axis current i_q is obtained, therefore the state vector is $x = \left[\theta_r \quad \omega_r \quad i_q \quad T_L\right]^T$

As a result of these facts, the four estimated state variables influence each other, and, because position/speed encoders are not used, the observer correction is chosen to be the error between the measured i_q and the estimated $\hat{i}_q$ current.

The nonlinear state and disturbance observer, Luenberger type, based on the model (3.34) is

$$\begin{aligned}\dot{\hat{\bar{x}}} &= A\hat{\bar{x}} + g\left(\hat{\bar{x}}\right)\bar{u} + L\left(y - C\hat{y}\right)\\ \hat{\bar{y}} &= C\hat{\bar{x}}\end{aligned} \tag{3.38}$$

with

$$\begin{aligned}\hat{\bar{x}} &= \left[\hat{\theta}_r \quad \hat{\omega}_r \quad \hat{i}_q \quad \hat{T}_L\right]^T\\ \hat{y} &= \hat{i}_q\\ L &= \left[L_1 \quad L_2 \quad L_3 \quad L_4\right]^T\end{aligned} \tag{3.39}$$

$$g\left(\hat{\bar{x}}\right) = \begin{bmatrix} 0 & 0 \\ \frac{3}{2}\frac{p^2}{J}\left(L_d - L_q\right)\hat{i}_q & 0 \\ -\frac{L_d}{L_q}\hat{\omega}_r & \frac{1}{L_q} \\ 0 & 0 \end{bmatrix} \tag{3.40}$$

Note that the equation (3.32) is not used and thus the *d* axis current i_d is not included in the state variable $\bar{x}$, the main reason being that the used control strategy is FOC with $i_d^*=0$ (MTPA conditions for SPMSM). In this case, the v_d component is not required, but, because i_d component is needed in (3.30)-(3.31), i_d is used as input variable $u = \left[i_d \quad v_q\right]^T$, instead of the usual $u = \left[v_d \quad v_q\right]^T$.

The detailed NSDO model (3.38) becomes

$$\begin{bmatrix}\hat{\theta}_r \\ \hat{\omega}_r \\ \hat{i}_q \\ \hat{T}_L\end{bmatrix}^{\bullet} = \begin{bmatrix} 0 & 1 & 0 & 0 \\ 0 & -\frac{B}{J} & \frac{3}{2}\frac{p^2}{J}\lambda_{PM} & -\frac{p}{J} \\ 0 & -\frac{\lambda_{PM}}{L_q} & -\frac{R_s}{L_q} & 0 \\ 0 & 0 & 0 & 0 \end{bmatrix}\begin{bmatrix}\hat{\theta}_r \\ \hat{\omega}_r \\ \hat{i}_q \\ \hat{T}_L\end{bmatrix} + \begin{bmatrix} 0 & 0 \\ \frac{3}{2}\frac{p^2}{J}\left(L_d - L_q\right)\hat{i}_q & 0 \\ -\frac{L_d}{L_q}\hat{\omega}_r & \frac{1}{L_q} \\ 0 & 0 \end{bmatrix}\begin{bmatrix} i_d \\ v_q \end{bmatrix} + \begin{bmatrix} L_1 \\ L_2 \\ L_3 \\ L_4 \end{bmatrix}\left(i_q - \hat{i}_q\right) \tag{3.41}$$

Where *L* is the Luenberger gain matrix designed by using the pole placement method, presented in what follows.

The characteristic polynomial $\Delta(s)$ has the expression

$$\Delta(s) = det\left(sI - A_o\right) = det\begin{bmatrix} s & -1 & L_1 & 0 \\ 0\lambda & \frac{B}{J} & s + L_2 - \frac{3}{2}\frac{p^2}{J} & _{PM} \quad \frac{p}{J} \\ 0 & \frac{\lambda_{PM}}{L_q} & s + L_3 + \frac{R_s}{L_q} & 0 \\ 0 & 0 & L_4 & s \end{bmatrix} \tag{3.42}$$

$$with\ \ A_o = A - L \cdot C = \begin{bmatrix} 0 & 1 & -L_1 & 0 \\ 0\lambda & -\frac{B}{J} & \frac{3}{2}\frac{p^2}{J}\,\lambda_{PM} - L_2 & -\frac{p}{J} \\ 0 & -\frac{\lambda_{PM}}{L_q} & -\frac{R_S}{L_q} - L_3 & 0 \\ 0 & 0 & -L_4 & 0 \end{bmatrix}$$

The important conclusion that the *proposed observer has one pole placed in origin* results from (3.42).

The poles of the system are chosen to be real negatives, with *one pole being zero*

$$P = \begin{bmatrix} 0 & -200 & -300 & -400 \end{bmatrix}$$

After selecting the desired poles P, the Luenberger gains are obtained by using the MATLAB function *place*

$$L = place\left(A', C', P\right)' = \begin{bmatrix} -100 & -27600 & 720 & 4000 \end{bmatrix}$$

where the superscript ‘ represents the matrix transpose.

3.3.2. Simulation results

A sensorless standard FOC strategy for SMPMS including the proposed NSDO (3.41) is implemented as presented in Figs. 3.16 and 3.17 using MATLAB®/Simulink®, with a sampling time of 100 μs.

The PMSM parameters are presented in Table 3.1.

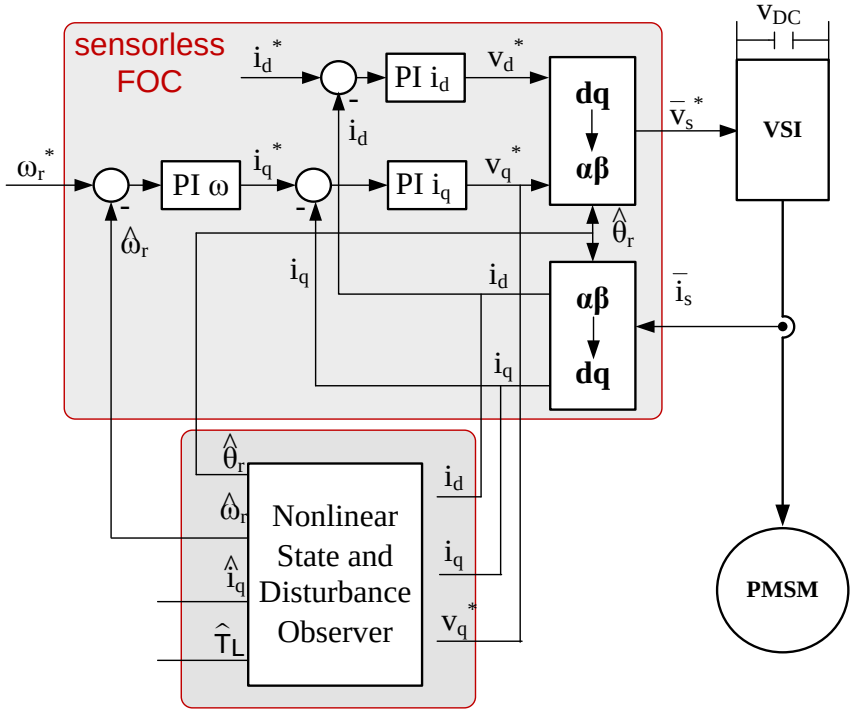

Fig.3.16. PMSM Sensorless Control using Nonlinear State and Disturbance Observer

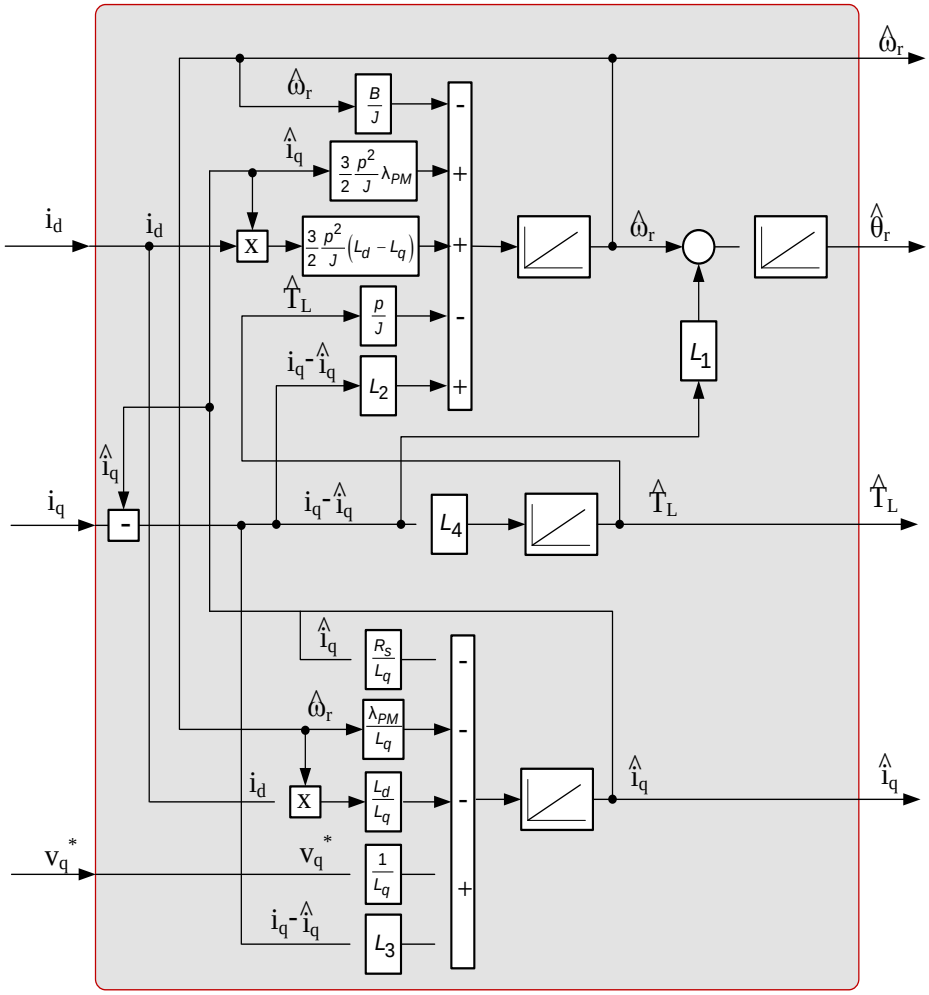

Fig. 3.17. Proposed Nonlinear State and Disturbance Observer

In order to prove the observer's performance at low speeds, three scenarios were created.

The first scenario considers the PMSM working at **zero speed** for an applied and removed load of 1.5 Nm. The results are presented in Fig. 3.18. As can be seen from the comparison between the measured values and the estimated values, the resemblance is very good. The SPMSM manages to maintain synchronism even for a sudden load of 1.5 Nm (more than half the rated torque).

The second scenario is for constant **low speed,** ω_r=10 rad/s, for an applied and removed load of 1 Nm. The results are presented in Fig. 3.19. This was created for low speed operation with a step load. The simulation results prove good dynamic performance for sudden load torque.

The third scenario is for **reversal speed,** ω_r=±30 rad/s, for a constant load of 1 Nm. The results are presented in Fig. 3.20. This scenario is for medium-low speed operation with reversal for a constant load torque applied from the start. The system proves to be robust to speed changes, and even reversal.

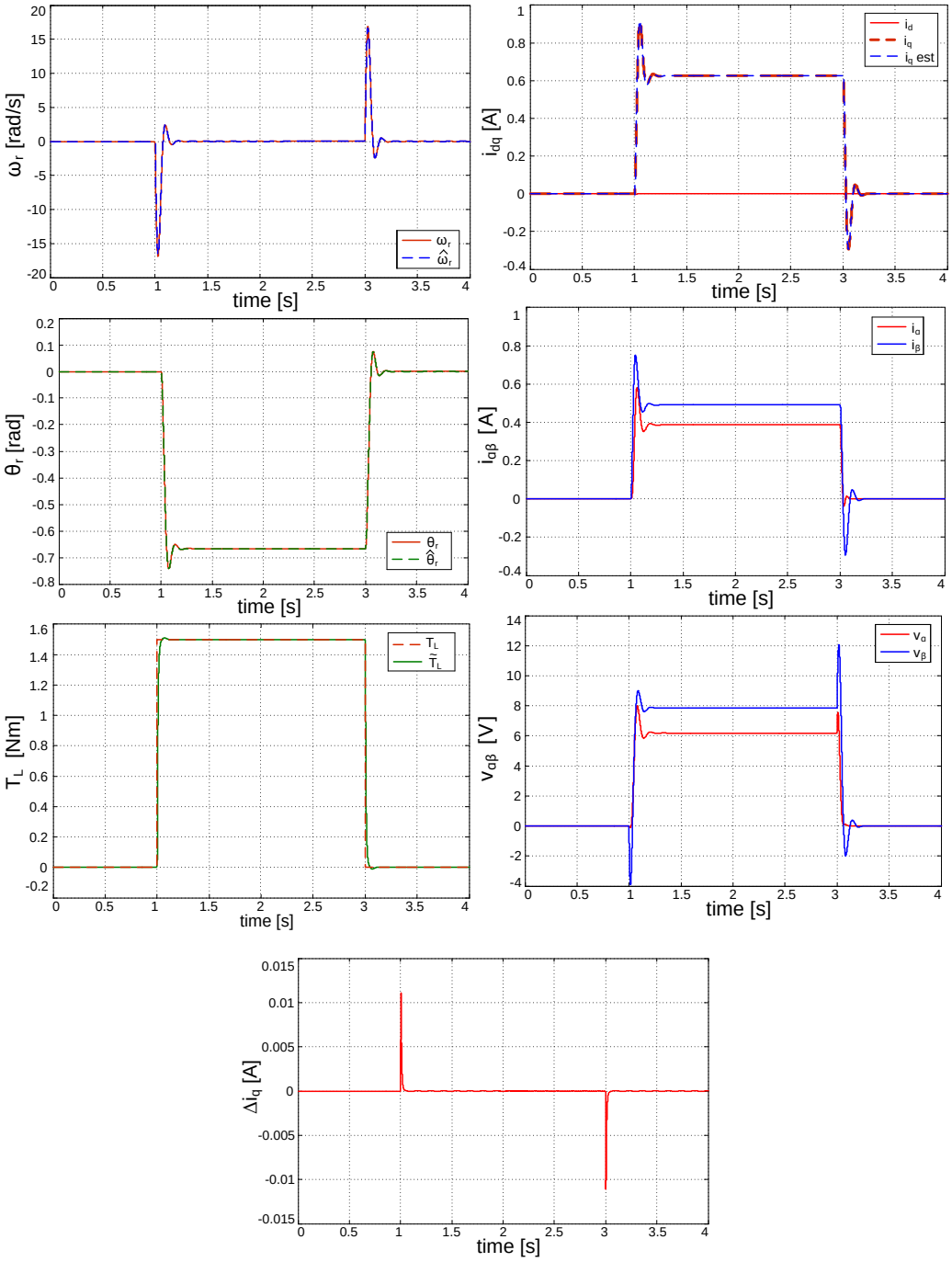

Fig. 3.18. Simulation results for *zero speed*, with a load T_L=1.5 Nm applied and removed: rotor speed variation, electric rotor position variation, load torque variation, *dq* currents variation, *αβ* current variations, *αβ* voltage variations

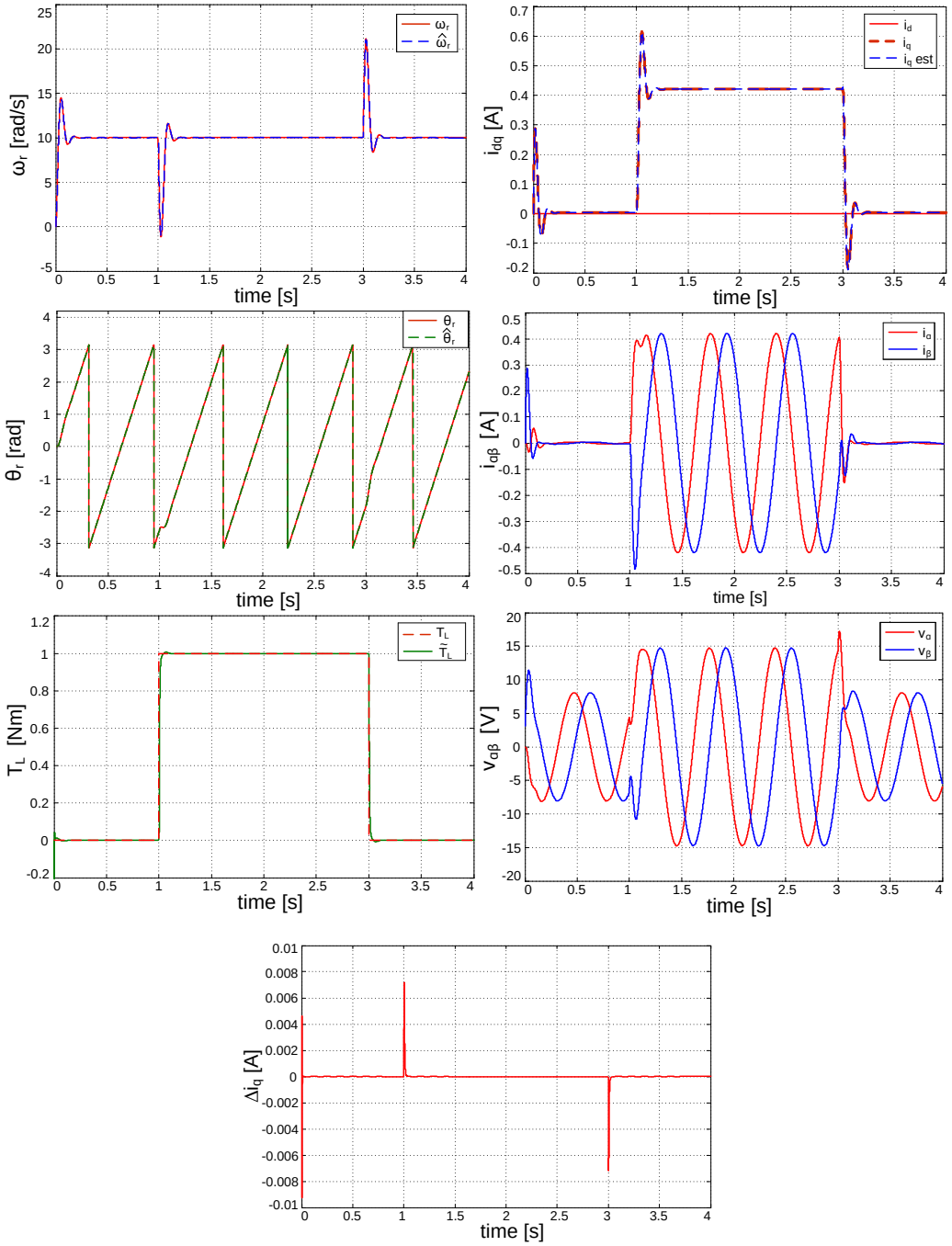

Fig. 3.19. Simulation results for *low speed* of 10 rad/s, with a load T_L=1 Nm applied and removed: rotor speed variation, electric rotor position variation, load torque variation, *dq* currents variation, *αβ* current variations, *αβ* voltage variations

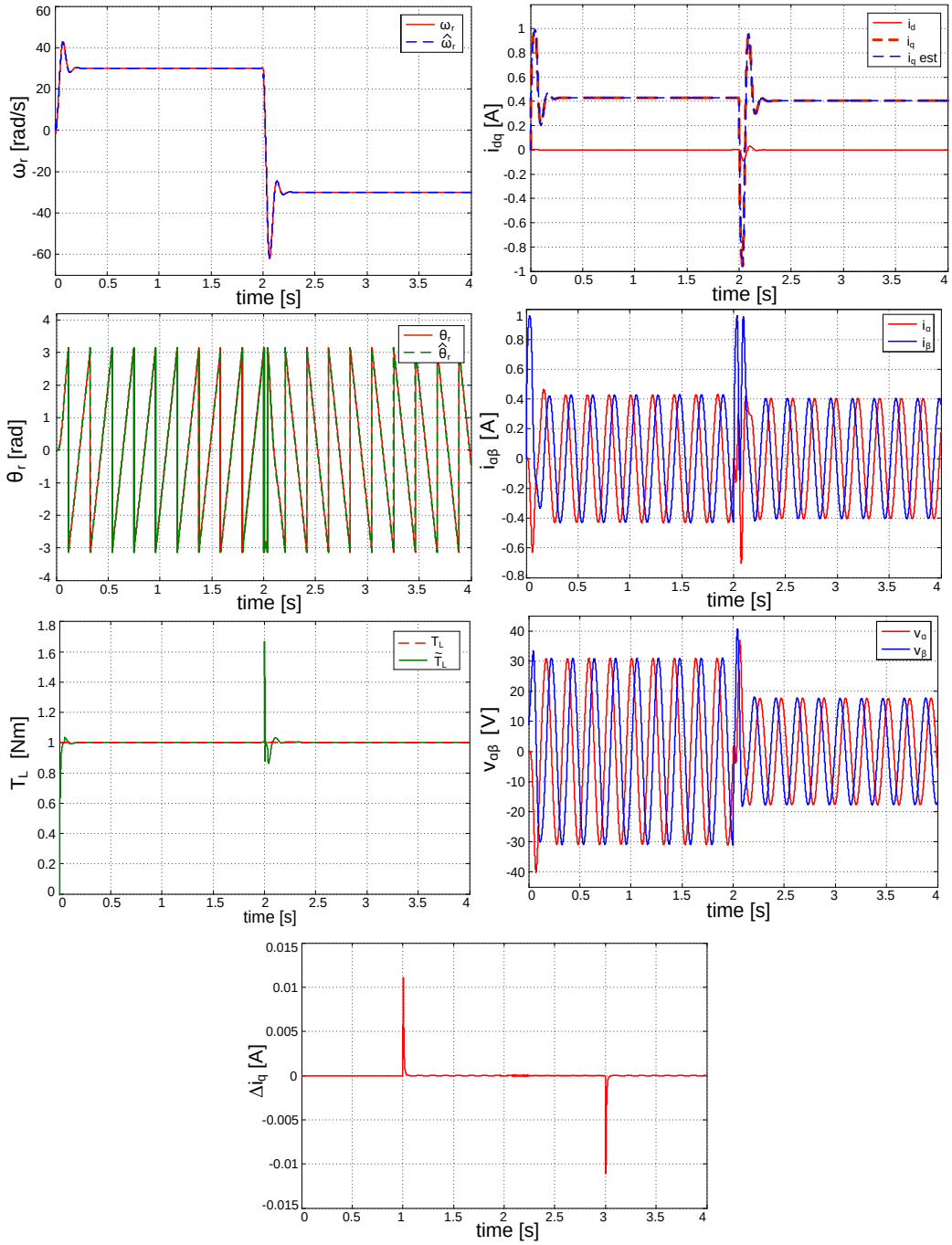

Fig. 3.20. Simulation results for *speed reversal* of ±30 rad/s, at constant T_L=1 Nm load: rotor speed variation, electric rotor position variation, load torque variation, *dq* currents variation, *αβ* current variations, *αβ* voltage variations, *q* axis current correction

Robustness for parameter variations - case study

To test the robustness performance of the proposed NSDO, extensive simulations with parameter variations were performed for low speed operation, 10 rad/s, at rated torque loading, i.e., 2.4 Nm:

i) The *stator resistance* R_s is varied considering an increasing of 5%. The simulation results in Fig. 3.21 show the disturbances introduced by the variation of stator resistance caused by temperature rising, seen especially in the equivalent load torque variation that influences the rotor position estimation. The i_q current is not disrupted by the resistance variation. The results prove that the NSDO is susceptible to resistance variations and therefore to reduce this influence, R_s real-time identification is required.

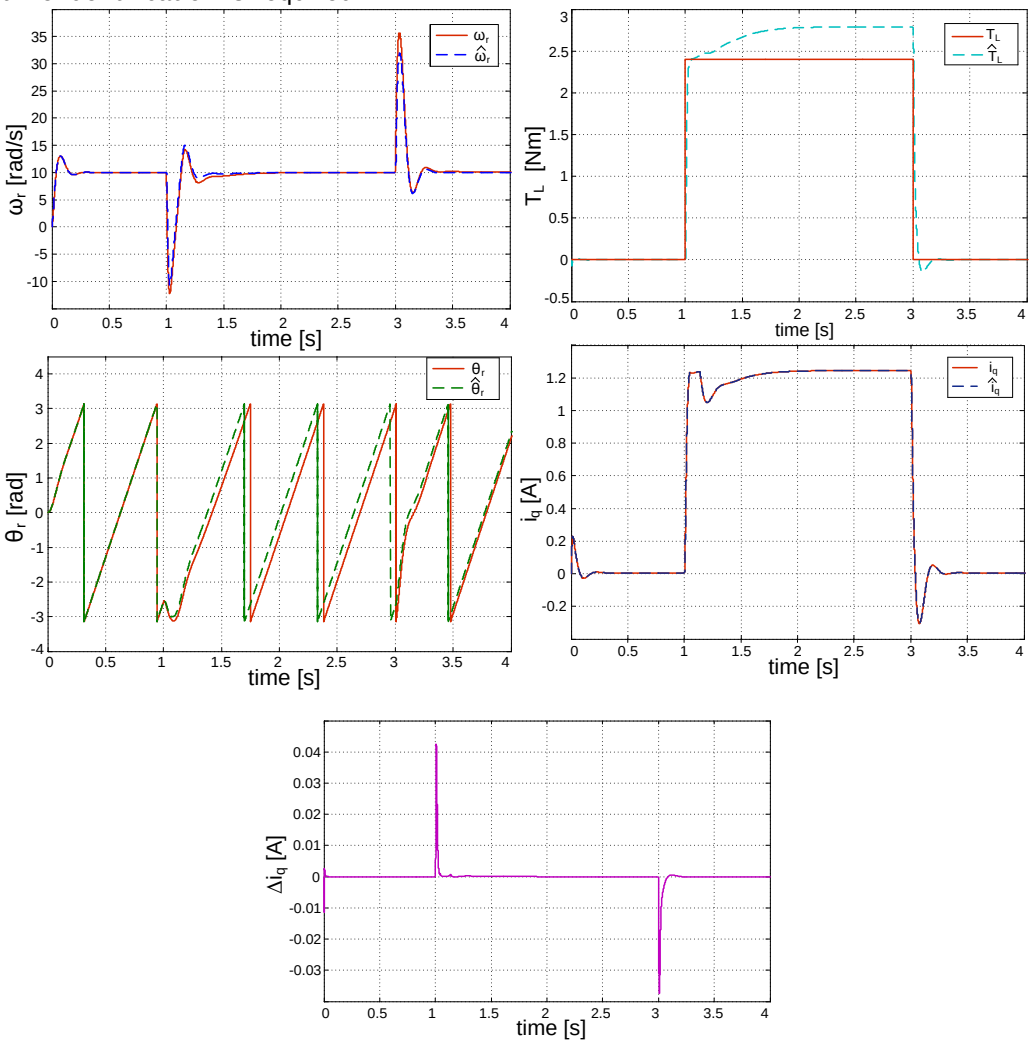

Fig. 3.21. Simulation results for *low speed* operation with rated torque loading for a 5% *increase of stator resistance*: electric speed variation, rotor position variation, load torque variation, i_q current variation and the *q* axis current correction

ii) The *phase inductance* L_s (in this case for SPMSM L_d=L_q=L_s) is modified considering a decrease of 30%. The NSDO is robust to inductance changes, even grater that 30%, as seen in Fig. 3.22.

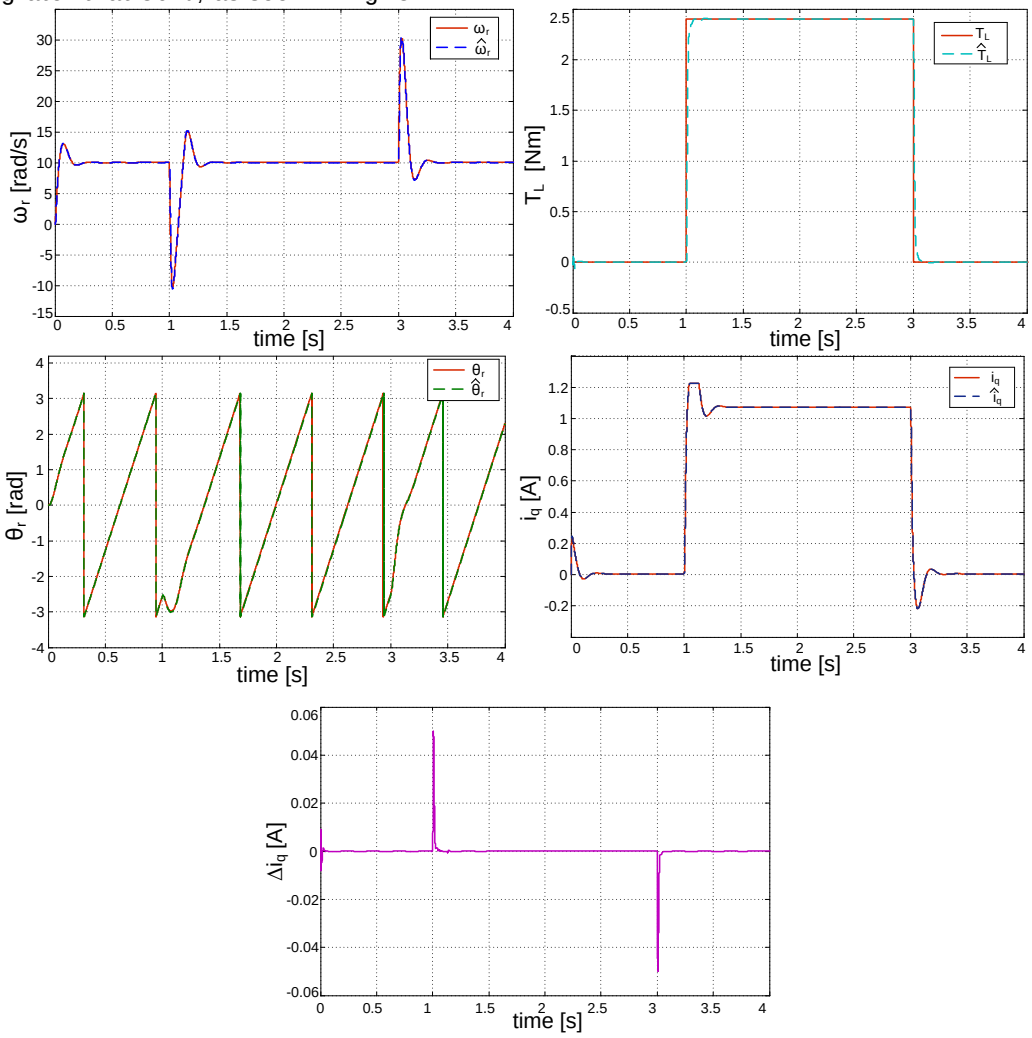

Fig. 3.22. Simulation results for *low speed* operation with rated torque loading for a 30% decrease of stator inductance: electric speed variation, rotor position variation, load torque variation, i_q current variation and the *q* axis current correction

iii) The *inertia J* is increased with 300% and the simulation results presented in Fig. 3.23. The conclusion is that the observer is robust to large range inertia variations. On the other hand, the inertia variation affects the speed response because, the PI speed controller is tuned mainly taking into account the inertia.

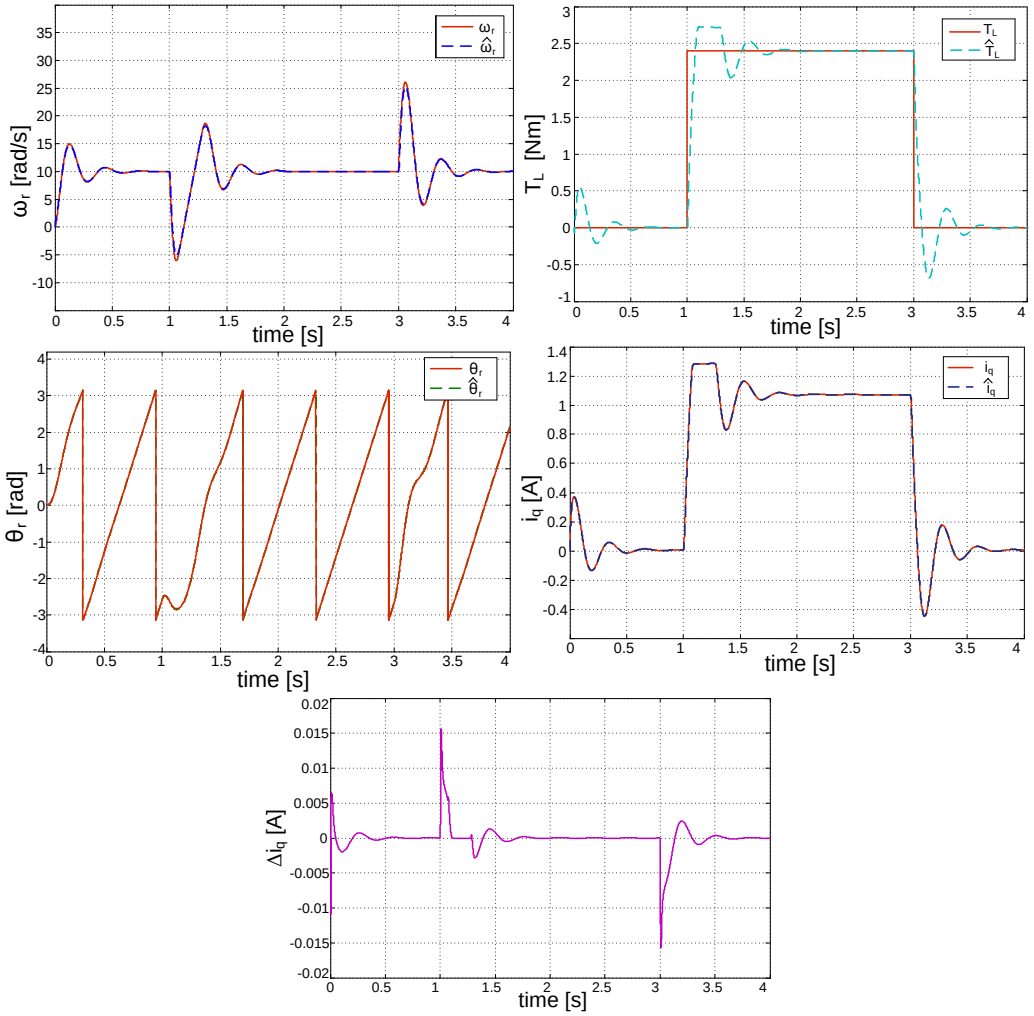

Fig. 3.23. Simulation results for *low speed* operation with rated torque loading for a 300% increase of inertia: electric speed variation, rotor position variation, load torque variation, i_q current variation and the *q* axis current correction

iv) The *PM flux linkage* λ_{PM} variation and *incorrect initial rotor position* at startup are also tested for NSDO. In these cases the observer presents instability and when the loading torque is applied, the system becomes unstable. This means that the NSDO is sensitive to PM flux linkage variation and an incorrect initial rotor position. There are *two solutions proposed to correct these disadvantages*:

- PM flux linkage λ_{PM} depends on the rotor temperature that can be estimated by measuring the stator temperature variation, with a PT1 thermal model [And1999] (pp. 39-41). Using the same stator temperature transducer, the stator resistance R_s can also be estimated.
- Initial rotor position can be estimated at standstill using: signal injection methods [Pii2008a], [And2008], [Foo2010] or [Zhu2011] and current slope method introduced by [Che2010].

3.3.3. Conclusions

The proposed NSDO is based on an extended Luenberger observer with the input vector $u = \begin{bmatrix} i_d & v_q \end{bmatrix}^T$; the i_q error for observer correction term and it has one pole placed in origin.

The NSDO has an implementation of medium complexity, and presents good simulation results for the toughest case scenarios like zero speed operation with step rated torque loading and for low speed reversal with step loading and unloading.

The conclusions of the case study made to test the robustness for parameters variation are:

i) the NSDO is robust to phase inductance and inertia variations, and sensitive to variations of stator resistance, mainly to PM flux linkage and initial rotor position;

ii) to improve the NSDO robustness, the PM flux, stator resistance and initial rotor position identification must be identified in real-time by some known methods.

4 V/f Control Strategy with two Stabilizing Feedback Corrections for PMSM Drives

This chapter contains major contributions and develops stabilizing measures needed for improving stable sensorless V/f control strategy, for large speed range, developed in the author publications [And2012], [Com2013] and [Aga2013].

First an overview of the existing stable V/f control of PMSM is presented.

4.1. Stable V/f Control Overview

Scalar V/f control is an inherent motion sensorless control method, using two (even one) current sensors, with simple implementation that leads to short sampling rate. Usually, V/f control methods do not use rotation operators, nor control loops for speed, currents, torque or flux. They are recommended for variable speed drives from medium to very high-speed (nx100 krpm), in industrial applications like fans, pumps, turbo blowers, compressors, micro gas-turbine generators [Zha2006], [Mor2006], [Mon2010]. Because scalar V/f is a simple and low cost control strategy, it becomes an attractive solution applied to PMSM drives for heating, ventilating and air conditioning (HVAC) applications [Per2002].

One of the reference studies for the stability of sensorless V/f control for PMSM drives is [Per2003]. Wide speed range operation is achieved by introducing a stabilizing loop for the applied frequency proportional to the active power variation. The proposed sensorless V/f control uses two current sensor measurements and fulfils the required performance for applications like pumps and fans.

Efficiency optimization techniques such as maximum torque per ampere (MTPA), flux weakening (FW) and maximum torque per voltage (MTPV) are included in scalar V/f control in [Cac2010], [Con2010], and later in [Con2013]. The control algorithm is based on the frequency stabilizing loop of [Per2003] and on the voltage amplitude correction based on a power factor angle reference selected using a switch to comply with the necessary MTPA, FW and MTPV conditions. The proposed effective energy saving scalar control technique for IPMSM drives has a wide speed range operation, needs a low cost control unit and uses a single current sensor measurement.

In order to improve efficiency performance of the scalar V/f control for PMSM drives, besides the compensated load angle component added to stabilize the drive based on the solution firstly introduced by [Per2003], a new requirement to regulate the imaginary power under MTPA constraint is introduced in [Sue2011]. Using MTPA conditions, minimum copper loss control strategy for sensorless V/f control with experimental results are shown in [Sue2012].

Starting from this recent state of the art in V/f control with stabilizing loops, the author develops and improves the V/f control strategy with theoretical, simulation and experimental results, published in [And2012], [Com2013] and [Aga2013].

In an attempt to obtain a stable sensorless V/f control with a simple implementation, that requires reduced computation time, in [And2012] are employed two stabilizing feedback corrections to the V/f control strategy. The first

correction is a voltage vector speed correction that uses the active power variation, based on the solution from [Per2003], and improved later in [Aga2013], which is active only in transient states. The second correction is for voltage amplitude and is based on unity power factor regulation loop which employs reactive power. The proposed solution is competitive for very-high variable speed PMSM drives like fans, pumps, micro gas-turbine generators, etc.

A completion of [And2012] with experimental results is developed in [Com2013]. Here an experimental comparison with sensored FOC is made for proving the dynamic performance of the drive.

The novelty of the solution presented in [Aga2013] is accomplished after a better evaluation of the performances introduced in [And2012] and [Com2013]. In order to operate at low speed, the stable sensorless V/f control is improved by adding another component proportional to the active power for the voltage amplitude correction. For SPMSM operation under MTPA condition is necessary to maintain i_d=0, therefore i_d regulation loop is needed, which outputs the reference power factor angle. The introduced solution estimates i_d from internal reactive power expression, thereby no coordinate transform is used. The proposed V/f control strategy is experimentally compared with sensorless vector control based on active flux (AF) observer for rotor position and speed estimation, proving very good performance in terms of fast reference tracking and step load torque response.

4.2. Stable V/f Control System with Unity Power Factor

In this section is developed a stable V/f control strategy for PMSM drives with two stabilizing feedback corrections [And2012] applied to the basic V/f control:

- a voltage vector speed correction using active power variation;
- a voltage amplitude correction based on power factor regulation loop.

The proposed V/f control structure is shown in Fig. 4.1, with the following components: the framed basic open-loop V/f control method, the inverter block INV, the PMSM, active/reactive power computation block, the high pass filter HPF to extract the active power variation, the low pass filter LPF for power factor angle reference φ^*, the PI regulator of power factor angle for voltage amplitude correction ΔV, the switch to select power factor angle φ^* for motor/generator modes using active power P sign information.

In order to develop any control structure, the process model is needed. Therefore, for convenience, the PMSM mathematical model in dq rotor reference frame is repeated here

$$v_d = R_s i_d + \frac{d\lambda_d}{dt} - \omega_r \lambda_q \tag{4.1}$$

$$v_q = R_s i_q + \frac{d\lambda_q}{dt} + \omega_r \lambda_d \tag{4.2}$$

$$\lambda_d = L_d i_d + \lambda_{PM} \; ; \; \lambda_q = L_q i_q \tag{4.3}$$

$$T_e = \frac{3}{2} p \left[\lambda_{PM} i_q + \left(L_d - L_q \right) i_q i_d \right] \tag{4.4}$$

$$J \frac{d\omega_m}{dt} = T_e - T_L - B\omega_m \; , \; \omega_m = \frac{\omega_r}{p} \tag{4.5}$$

where (v_d, v_q), (i_d, i_q) are the stator voltage and current components, R_s is the stator resistance, L_d, L_q are dq axis inductances, ω_r, θ_r are the electrical rotor speed

and position, ω_m is the mechanical rotor speed, λ_{PM} is the PM flux, T_e is the electromagnetic torque, T_L is the load torque, J is the motor inertia, B is the viscous friction coefficient and p is the number of pole pairs.

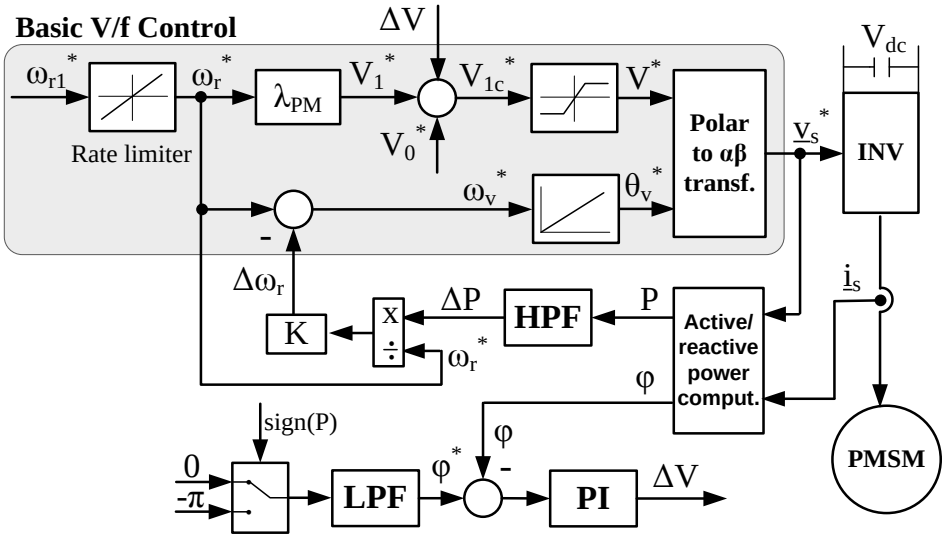

Fig. 4.1. Proposed stable V/f control structure for PMSM drives with two stabilizing feedback corrections.

The electromagnetic torque (4.4) has two components: the magnetic torque $1.5p\lambda_{PM}i_q$, and the reluctance torque driven by the difference between L_d and L_q. For SPMSM, the magnetic torque is available only because $L_d=L_q=L_s$, and therefore the reluctance torque is equal to zero.

4.2.1. Basic Open-loop V/f Control Method

A *basic open-loop V/f control method* (Fig. 4.1–upper part) is highlighted by the following elements.

The angular acceleration is fixed using a rate limiter in order to apply to the voltage vector a smooth electric speed variation ω_r^* to obtain dynamic synchronization. *In steady state the rotor speed is the same with the voltage vector speed.* Under no load condition, $\underline{i}_s=0$, equations (4.2) and (4.3) become:

$$V_1^* = \lambda_{PM} \cdot \omega_r^* \tag{4.6}$$

An offset voltage V_0^* offset is added for a correct start-up to obtain a minimum current (torque) at zero speed.

A polar $\underline{v}_s^*(V^*,\theta_v^*)$ to αβ stator reference $\underline{v}_s^*(v_\alpha^*,v_\beta^*)$ transformation is needed to generate the voltage vector reference $\underline{v}_s^*$ for the voltage source inverter (VSI) command. The voltage vector position θ_v^* is obtained by integrating the stator voltage vector speed ω_v^*

4.2.2. Voltage Vector Speed Correction $\Delta\omega_r$

The voltage vector speed correction $\Delta\omega_r$ is added in order to compensate the basic V/f control method instability, oscillatory responses, even loss of synchronism [Per2003], when the speed or load torque reference changes.

In the steady state condition the voltage vector angle in dq reference frame is constant, $\theta_{vd}=const.$, resulting the *synchronism condition* $\omega_v=\omega_r$. Because in transient state $\omega_v\neq\omega_r$, the voltage vector speed $\omega_v=d\theta_v/dt$ in αβ stator reference frame (Fig. 4.2) is given by:

$$\omega_v = \omega_r + \omega_{vd} \tag{4.7}$$

where ω_{vd} is the voltage vector speed in *dq* reference frame.

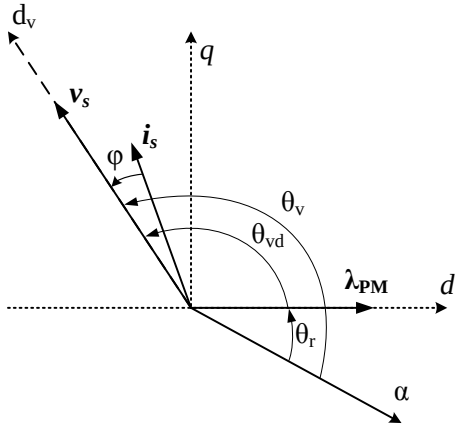

Fig. 4.2. Correlation between d_vq_v frame, *dq* frame and stator αβ frame

The principle of the voltage vector speed correction $\Delta\omega_r$ is to intervene in transient state when the rotor speed ω_r tends to oscillate around ω_r^* with a rotor speed variation $\Delta\omega_r$, the stator voltage speed reference ω_v^* will be modified with the same variation *in order to maintain the synchronism*:

$$\omega_v^* = \omega_r^* - \Delta\omega_r \tag{4.8}$$

For example, at the beginning of transient state after loading, the rotor speed ω_r decreases with $\Delta\omega_r = \omega_r^* - \omega_r$ and also ω_v must be decreased with $\Delta\omega_r$ to maintain the synchronism, because the voltage correction is not so fast.

Taking into account that the proposed V/f control is a sensorless control method (without rotor position/speed sensor), the speed variation $\Delta\omega_r$ cannot be directly measured, thus $\Delta\omega_r$ will be estimated.

In steady state, the relation between the active power *P*, the mechanical rotor speed ω_m and the electromagnetic torque T_e is

$$P = T_e \cdot \omega_m = \tfrac{3}{2}\left(\lambda_d i_q - \lambda_q i_d\right)\cdot\omega_r = \tfrac{3}{2}\left(v_d i_d + v_q i_q\right) \tag{4.9}$$

Equation 4.9 is valid in any rotor or stator frame.

Because ω_r cannot be measured, the active power is computed using the measured currents i_α, i_β and the reference voltages v_α^*, v_β^*, neglecting voltage drops on the nonlinear inverter model:

$$P = \tfrac{3}{2}\left(v_\alpha^* i_\alpha + v_\beta^* i_\beta\right) \tag{4.10}$$

From (4.5) and (4.9) it can be concluded the proportional relation between the variations of the rotor speed, the electromagnetic torque and active power variations: $\Delta\omega_r = k\Delta T_e = k\frac{\Delta P}{\omega_r}$.

The ΔP variation is extracted from P by using a high-pass filter (HPF) with the transfer function

$$H(s) = T \cdot s \,/\, (T \cdot s + 1) \tag{4.11}$$

where the time constant T is experimentally chosen depending on rotor speed oscillations.

In conclusion, the estimation of the rotor speed variation $\Delta\omega_r$ is given by:

$$\Delta\omega_r = K \,/\, \omega_r^* \cdot \Delta P \tag{4.12}$$

where $K > 0$ is a gain experimentally obtained. Note that the speed correction $\Delta\omega_r$ occurs only in transient state.

This voltage vector speed correction is introduced by [Per2003] using small-signal analysis. The novelty of the proposed structure for $\Delta\omega_r$ correction is the physical explanations taking into account, and the straightforward way to express the mathematical relations described by (4.12) in a complete different way.

4.2.3. Voltage Amplitude Correction ΔV

In the scalar V/f control, the voltage vector reference frame $d_v q_v$ is naturally used (Fig. 4.2), with the real d_v axis oriented along the voltage vector $\underline{v}_s = Ve^{j\theta v}$. In this new reference frame, the current vector $\underline{i}_s = Ie^{j\varphi}$ is controlled by the voltage amplitude V, where φ is the angle between the voltage and current vectors, i.e.,, the power factor angle.

In current-vector control methods of PMSMs, the current vector reference $\underline{i}_s^*$ is provided in dq rotor reference frame to obtain the required electromagnetic torque T_e^*. There are optimization criteria to generate $\underline{i}_s^*$ in vector control [Mor1990], [Mor1990a] which can be transposed to find optimal power factor angle reference φ^*:

- unity power factor ($cos\ \varphi=1$) control method;
- maximum torque per ampere (MTPA) control method;
- constant flux-linkage control method;
- flux weakening, maximum torque per voltage [Con2010].

The unity power factor control method is selected by employing a power factor angle control loop with $\varphi^*=0$, that modifies the voltage amplitude to obtain unity power factor. For this reason, the controller output of the power factor angle is the voltage amplitude correction ΔV of the voltage vector. By modifying the voltage vector amplitude, the current vector that imposes the electromagnetic torque is modified.

The feedback angle φ can be calculated using different methods based on:

i) zero-crossing or the peak values detection of the phase voltage and current in a half period, with sensibility to noises in current waveforms,
ii) average computation using the phase voltage and current in a half period [Mat2009], [Mat2009a], both methods using *one current sensor*, and
iii) instantaneous φ estimation, employing the instantaneous active and/or reactive power that uses *two current sensors*.

The 3rd method is selected for φ estimation by computing the instantaneous reactive power Q (4.13) and the active power P (4.10) by using the reference voltages v_α^*, v_β^* and the measured currents i_α, i_β:

$$Q = 3 / 2\left(v_\beta^* i_\alpha - v_\alpha^* i_\beta\right) \tag{4.13}$$

The power factor angle φ can be estimated in three different ways:

1) $$\sin\varphi = 2Q / \left(3IV^*\right) \tag{4.14}$$

2) $$\cos\varphi = 2P / \left(3IV^*\right) \tag{4.15}$$

where

$$I = \sqrt{i_\alpha^2 + i_\beta^2} \tag{4.16}$$

I is the stator current amplitude and V^* is the reference stator voltage amplitude.

3) $$\varphi = atan2\left(Q, P\right) \tag{4.17}$$

For power factor angle φ estimation is recommended (4.14), that has monotony within [-π/2,π/2] or better (4.17) with extended monotony within [-π,π), both centered in 0, the target of the power factor loop $\varphi^*=0$. To reduce computational effort in (4.14), the approximation $\varphi \approx \sin\varphi$ is used.

For the power factor angle control loop, a proportional-integral (PI) controller with $H(s)=k_p[1+1/(T_i s)]$ is chosen, with the time constant T_i designed close to the electrical time constant L_q / R_s. The trial and error is employed for controller fine tuning.

4.2.4. Motor / Generator Operating Mode Selection

In the motor mode (MM), the rotor speed ω_r and the electromagnetic torque T_e have the same sign: $\omega_r T_e>0$, while in the generator mode (GM) ω_r and T_e have opposite sign: $\omega_r T_e<0$.

In Fig. 4.3, for $\omega_r>0$, the vectors associated to MM are illustrated in red color ($\varphi>0$), while for GM, green color is used ($\varphi<0$). For the same electromagnetic torque absolute value, the relation between φ_M and φ_G is given by:

$$\varphi_G = \varphi_M - \pi \tag{4.18}$$

The selection of the motor/generator operating mode is given by the $sign(T_e)=sign(P)$ for $\omega_r>0$.

For unity power factor $\varphi_M=0$ and $\varphi_G=-\pi$, from (4.18). Thus, in Fig. 4.1, the reference angle φ^* is changed from 0 to -π by $sign(P)$ to select the specific operating mode.

The proposed *V/f sensorless control* structure for PMSM (Fig. 4.1) mainly employs in implementation the following elements: PI controller, HPF (4.11), LPF, active power (4.10) and reactive power (4.13) computations with *atan2* table for φ estimation (4.17) and polar to *αβ* operator with sin-cos table. Therefore, low computation effort is required.

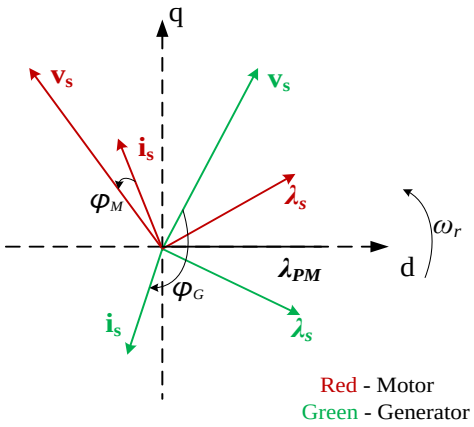

Fig. 4.3. Motor/generator operating mode: $\underline{v}_s$, $\underline{i}_s$ and $\underline{\lambda}_s$ vectors.

4.2.5. Simulation Results using IPMSM

To validate the performances of the proposed V/f control system, extensive simulations were performed using the MATLAB®/Simulink® package with h=100 μs sampling rate, that is commonly used in industrial drives.

First, an IPMSM is tested with the parameters presented in Table 4.1 and with the control system parameters from Fig. 4.1 presented in Table 4.2.

Four different scenarios were created to test dynamic performances of the proposed solution by simulation results, being the first step before the experimental testing.

Table 4.1. IPMSM Parameters for validation by simulation of the proposed V/f Control

Rated electrical speed (ω_r)	600 rad/s
Rated torque (T_{en})	12 Nm
Number of pole pairs (p)	4
Stator resistance (R_s)	0.6 Ω
d-axis inductance (L_d)	4.1 mH
q-axis inductance (L_q)	8.2 mH
Permanent magnet flux (λ_{PM})	0.2 Wb
Motor inertia (J)	0.005 kgm^2
Viscous friction coefficient (B)	0.0015 Nms/rad

Table 4.2. Control System Parameters for the proposed V/f Control

Maximum voltage (V^*)	120 V
Initial voltage (V_0^*)	2 V
Speed correction gain (K)	20 Nms/rad
HPF time constant (T)	10 ms
PI proportional constant (k_p)	0.5 V/rad
PI time constant (T_i)	20 ms
LPF time constant (T_f)	10 ms

Scenario no. 1 (Fig. 4.4) illustrates the transient responses for *startup in fast ramp reference speed* with the acceleration $\varepsilon_r^* = 1000$ rad/s^2 and speed ω_r^* from 0 to 300 rad/s, with a low load torque $T_{L0} = 0.5$ Nm. At $t_1 = 1$ s, a *step rated load torque* $T_{L1} = 12$ Nm is applied, and at $t_2 = 4.5$ s the *load torque is reduced* to T_{L0}.

The speed ω_r succeeds the reference speed ω_r^*, having an undershoot and overshoot of 70 rad/s at step rated load torque applied / removed and good quick torque response. The electromagnetic torque T_e is proportional with i_q current, and $i_d<0$ for motor mode (MM), like in vector control. The braking generator mode (GM) takes place at 0.35 s and 4.5 s for $T_e<0$, when the reference angle φ^* steps from 0 to -π rad. In this time interval, the calculated angle φ oscillates from -π to π because of the discontinuity of the *atan*2 function. The speed correction follows the torque variation and the voltage correction is in accordance with desired theoretical variations. In steady state, the power factor regulation loop leads φ to 0.

The current components variations, presented in Fig. 4.5, are highlighted in the conditions of scenario 1, but without switching to braking generator mode (GM). Note that when $T_e<0$, the i_q and i_d responses are oscillatory and i_d has twice bigger overshoot comparing with the case when GM is activated.

Scenario no. 2 (Fig. 4.6) illustrates the transient responses for *ramp speed variations* ω_r^* with 100 rad/s steps, increasing up to 300 rad/s and decreasing down to 5 rad/s for a constant load torque $T_L=2$ Nm. The purpose of this simulation is to present reference tracking ability of the control system.

The speed response ω_r matches the speed reference ω_r^* with small overshoots. The i_d current is negative during this experiment, with a fast torque response. At startup and during decreasing speed, $T_e<0$ for a short time, while the operating mode changes to breaking generator mode (GM) as seen in the power

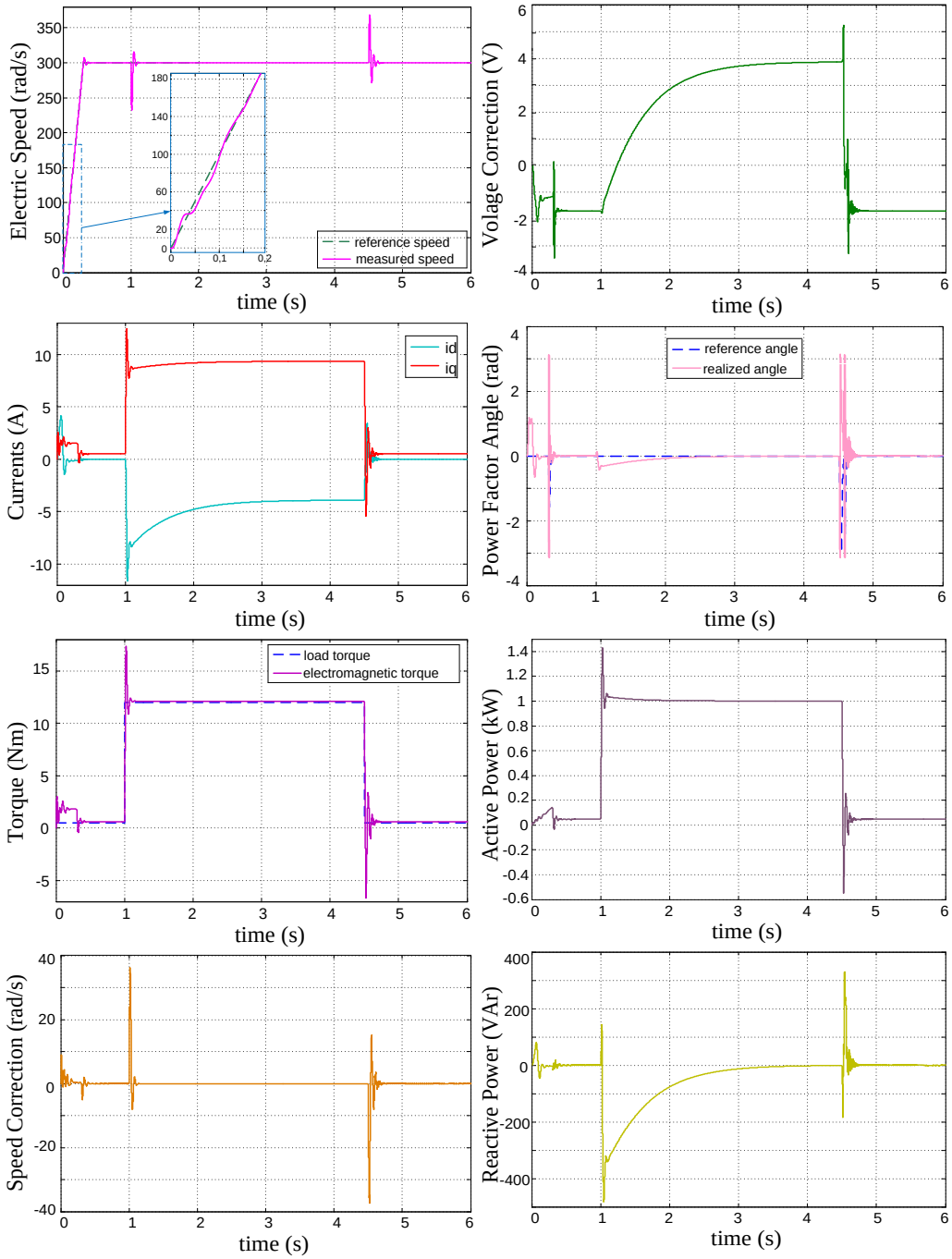

Fig. 4.4. Transient responses for ramp startup to 300 rad/s, followed by a step rated load torque T_L=12 Nm applied and removed: estimated speed, i_d, i_q currents, torque, speed correction, voltage correction, power factor angle, active power variation and reactive power variation.

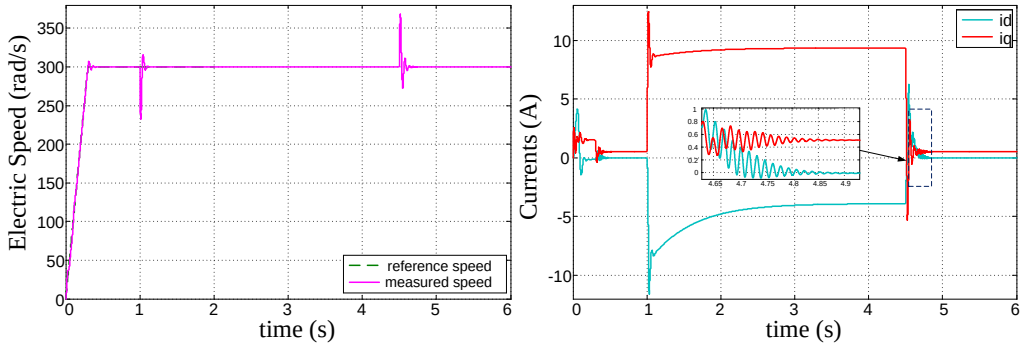

Fig. 4.5. Transient responses for ramp startup to 300 rad/s, followed by a step rated load torque T_L=12 Nm applied and removed: estimated speed, i_d, i_q currents without activating the braking generator mode (GM).

factor angle variations. The speed correction is active only in the transient state, and together with the voltage correction help to stabilize the system.

Scenario no. 3 (Fig. 4.7) illustrates the transient responses for *slow ramp reference load torque* from 0.5 to 12.5 Nm in 1.2 s, followed by a step load reduced to 1 Nm.

During the period of 1.2 s, when the ramp load is applied, the HPF generates a small speed correction of $\Delta\omega_r \approx 0.5$ rad/s because the active power P is in transient state (see Fig. 4.1). When the load is reduced and T_e<0, the operating mode is switched to GM, which is shown in the power factor angle variation.

Scenario no. 4 (Fig. 4.8) is a dynamic robustness study for a sinusoidal reference load torque. At t=1 s a sinusoidal load torque of 1 Nm and 50 Hz, superimposed to T_L^*=10 Nm, is applied and removed after 3 s. The disturbance effects (ripples) are shown in speed and currents variation, but the control system proves to be stable.

In conclusion, the extensive simulation results prove that the proposed V/f control structure with two stabilizing feedback corrections presents good dynamic stability (comparable with vector control), for fast ramp reference speed and step load rated torque. Note that i_d<0, like in vector control, excepting small time periods especially for MM to GM changeover and back.

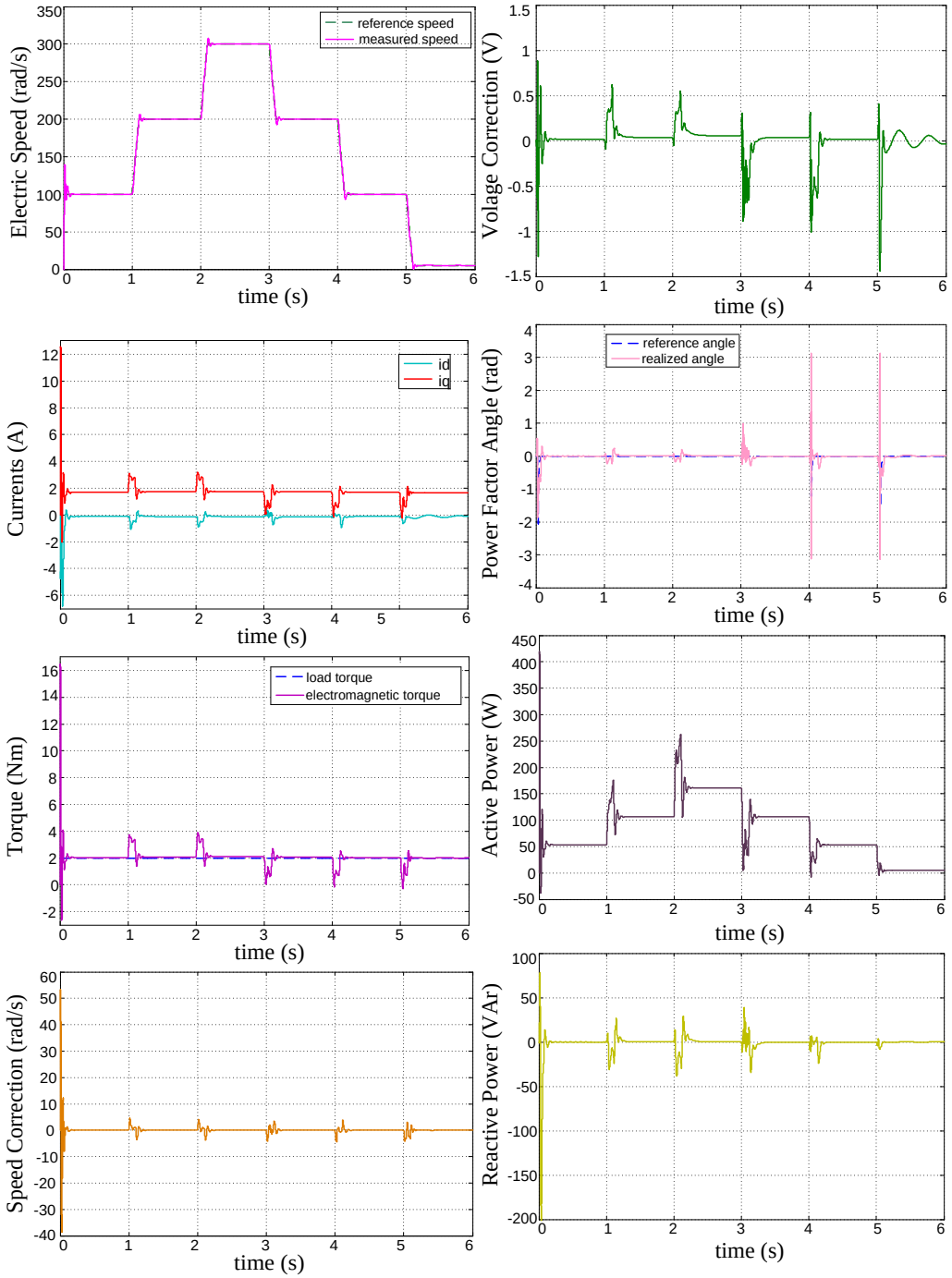

Fig. 4.6. Transient responses for cascade ramp speed increased to 300 rad/s, decreased to 5 rad/s with T_L=2 Nm: estimated speed, i_d, i_q currents, torque, speed correction, voltage correction, power factor angle, active power variation and reactive power variation.

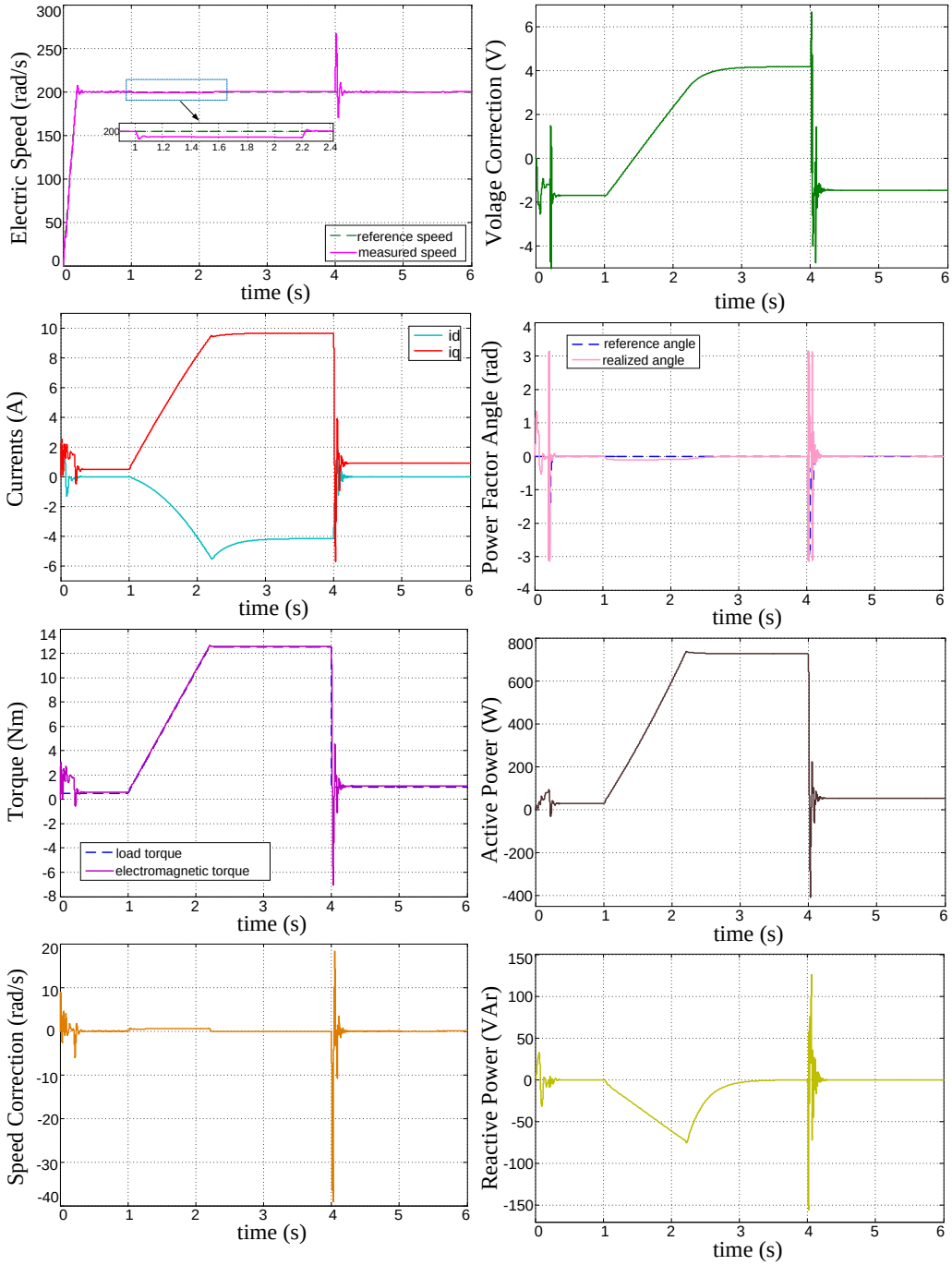

Fig. 4.7. Transient responses at 200 rad/s for slow ramp of load torque from 0.5 to 12 Nm followed by step discharge of 0.5 Nm: estimated speed, i_d, i_q currents, torque, speed correction, voltage correction, power factor angle, active power variation and reactive power variation.

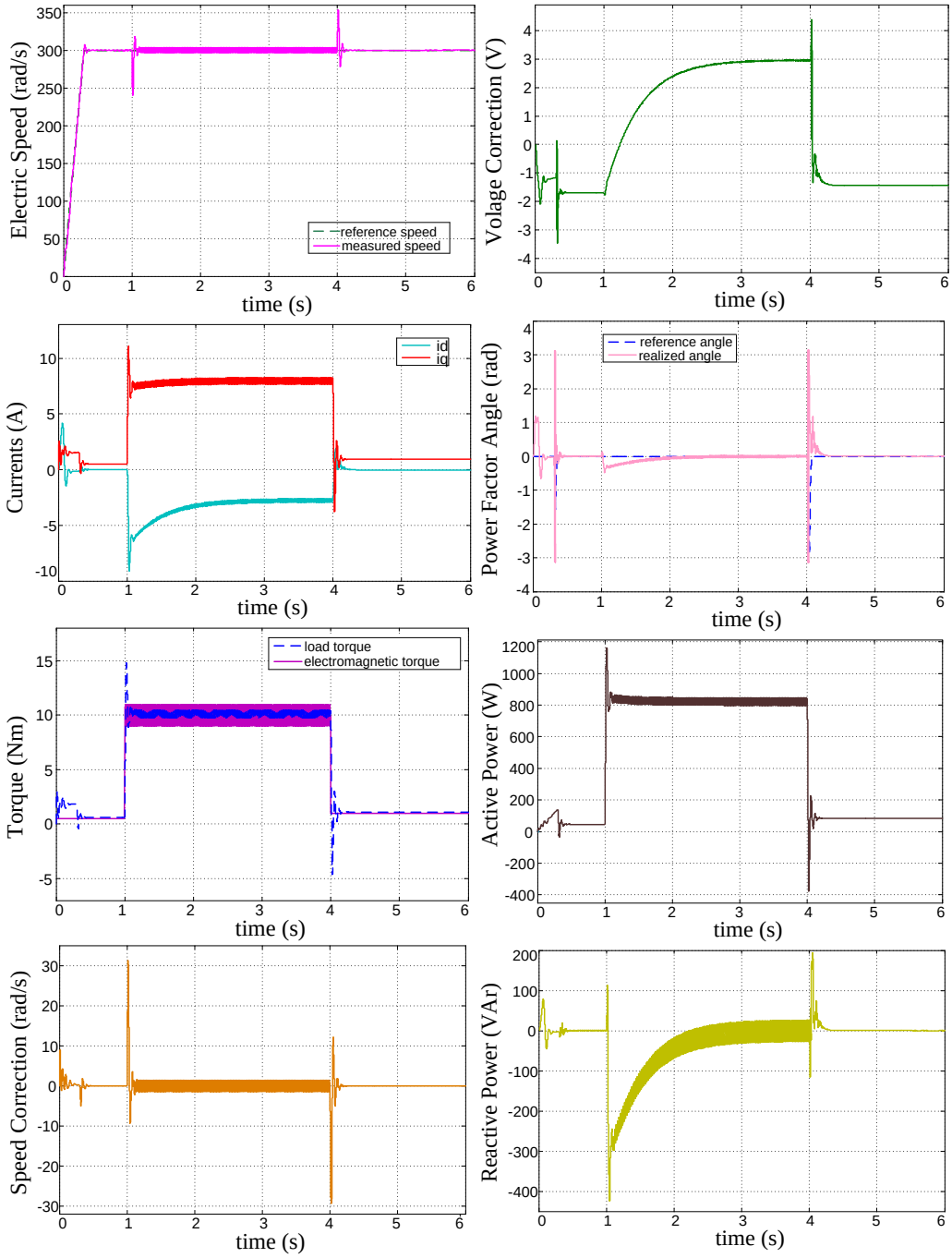

Fig. 4.8. Transient responses at 300 rad/s for sinusoidal load torque superimposed to a load torque T_L^*=10 Nm followed by step discharge until 1 Nm: estimated speed, i_d, i_q currents, torque, speed correction, voltage correction, power factor angle, active power variation and reactive power variation.

4.2.6. Comparison between Experimental and Simulation Results using SPMSM

After validating the proposed stable V/f control by means of simulation results, the control structure was implemented on the dSPACE 1103 real-time platform. The experimental test stand consists of a SPMSM, *the second type of PMSM taken into consideration in the thesis*, mechanically coupled with an induction machine (load), two Danfoss VLT 5000 voltage source inverters (VSI), three current sensors (only two are used), and an incremental encoder used only for comparison.

The parameters of the experimentally tested SPMSM are given in Table 4.3.

Table 4.3. SPMSM Parameters for experimental validation of proposed V/f Control

Rated mechanical speed (n_{rn})	1500 rpm
Rated power (P_n)	400 W
Rated phase voltage (V)	220 V
Rated current (I)	0.8 A
Number of pole pairs (p)	2
Stator resistance (R_s)	16.5 Ω
Stator phase inductance (L_s)	0.09 H
Permanent magnet flux (λ_{PM})	0.75 Wb
Motor inertia (J)	0.0025 kgm^2
Viscous friction coefficient (B)	0.003 Nms/rad

In subsections 2.2.1 and 2.2.2 are presented the *dq* axis inductances identification and the iron loss resistance estimation used for the PMSM simulation modeling. The improved PMSM simulation model is then compared with experimental results for rated speed and rated torque load operation.

The rotor speed ω_r profiles at 1500 rpm and 750 rpm are presented in Fig. 4.9, including speed variation due to rated torque loading and unloading. The comparison between simulation and experimental results is for an acceleration of 9000 rpm/s^2 from zero to 1500 rpm rated speed, with rated torque of 2.5 Nm loading and unloading; deceleration at half rated speed 750 rpm with rated torque 2.5 Nm loading and unloading; and finally deceleration down to zero speed.

The torque responses obtained by simulation and experimental results, with good dynamic performance, are compared in Fig. 4.10 with a very good agreement, thus induce the validation of the improved SPMSM simulation model.

The magnetizing *d* axis current is compared in Fig. 4.11, mentioning that for experiments, it is obtained using position information from the encoder, which is used only as a witness, in order to survey the actual behavior of the machine.

The power factor angle variation is compared in Fig. 4.12, with the note that in either simulation or experiment, unity power factor is intended.

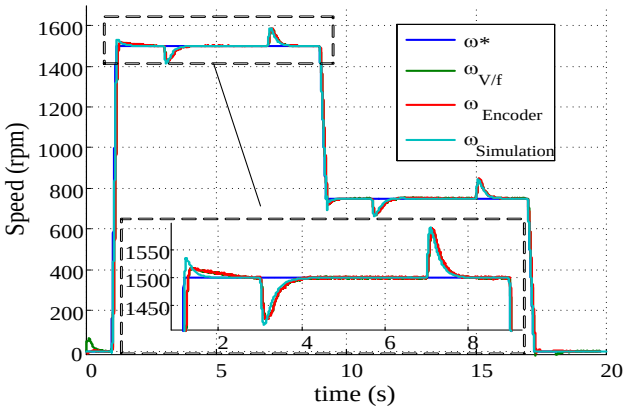

Fig. 4.9. Compared simulation and experimental results for rotor speed ω_r, including speed variation due to rated torque loading and unloading

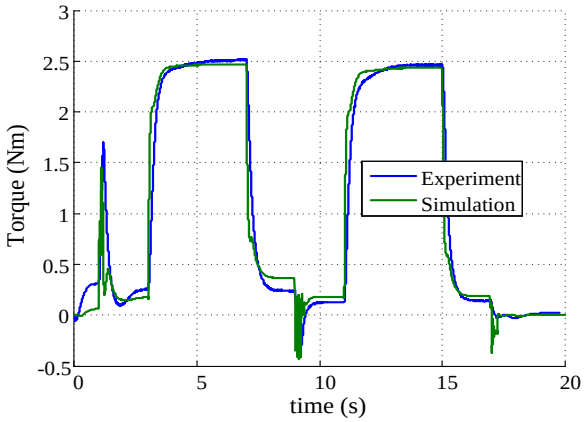

Fig. 4.10. Compared simulation and experimental results for electromagnetic torque variation

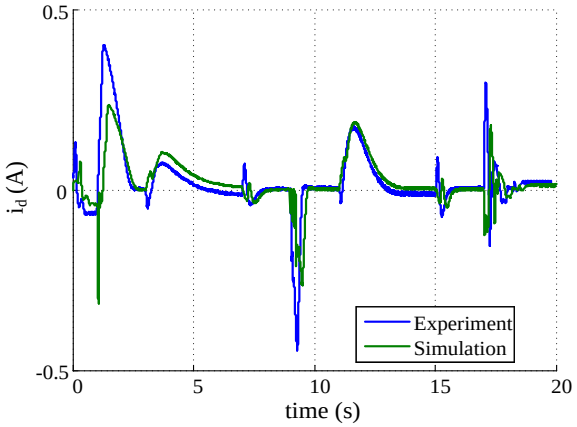

Fig. 4.11. Compared simulation and experimental results for *d* axis magnetizing current variation

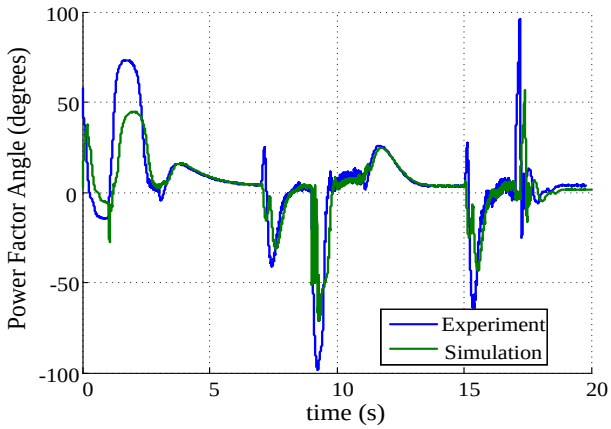

Fig. 4.12. Compared simulation and experimental results for power factor angle variation

4.2.7. Conclusions

In this section is developed a stable V/f control structure for unity power factor operation, having good performance and low computation effort.

The proposed solution, inherent for motion sensorless control of PMSM drives, employs two stabilizing feedback corrections: i) a voltage vector speed correction using active power variation working in transitory state, and ii) a voltage amplitude correction based on unity power factor regulation loop using reactive power, with motor/generator operating mode selected by the active power sign.

Simulation and experimental results validate the proposed solution with good performances in static and dynamic regimes, for fast speed variations and step rated load torque, for both IPMSM and SPMSM.

The main contributions regarding the proposed stable V/f control with two stabilizing corrections are the following:

- Novel straightforward way to obtain the voltage vector speed correction structure based on physical insightful;
- Voltage amplitude correction employing unity power factor regulation loop;
- Motor/generator operating mode selected by active power sign that modifies the power factor angle reference in accordance;
- Estimation of the instantaneous power factor angle using active/reactive power;
- Good simulation and experimental results regarding the dynamic performances of the proposed system in large speed range, *with step load torque reference*.

The proposed V/f control structure is suitable for wide speed range operation, with step rated load torque, recommended for (very) high-speed PMSM drives in applications like fans, pumps, micro gas turbine generators, where computation time is quite critical.

4.3. Experimental Comparison between Stable V/f Control and Sensored Field Oriented Control

This paragraph is a completion of section 4.2 and is based on the author paper [Com2013].

After testing of the stable V/f control with two stabilizing feedback corrections by means of simulations and experiments, were obtained the promising results presented above.

In order to compare the performance of the proposed sensorless V/f control with the performance of the standard vector control, a standard Field Oriented Control (FOC) strategy with *measured position* from an encoder is used.

4.3.1. FOC Strategy Implementation

The standard FOC strategy with $i_d^*=0$ for SPMSM implementation is presented in Fig. 4.13, where the main blocks are: PIω is the speed controller, PIi_d and PIi_q are the current controllers, all tuned by using Kessler methods [Pre2011], Appendix B, SVM is the space vector modulation block, VSI is the voltage source inverter, PMSM mechanical coupled with the load, two rotor *dq* to stator *abc* coordinate transforms (and reverse), rotor position and rotor speed processing block from incremental encoder.

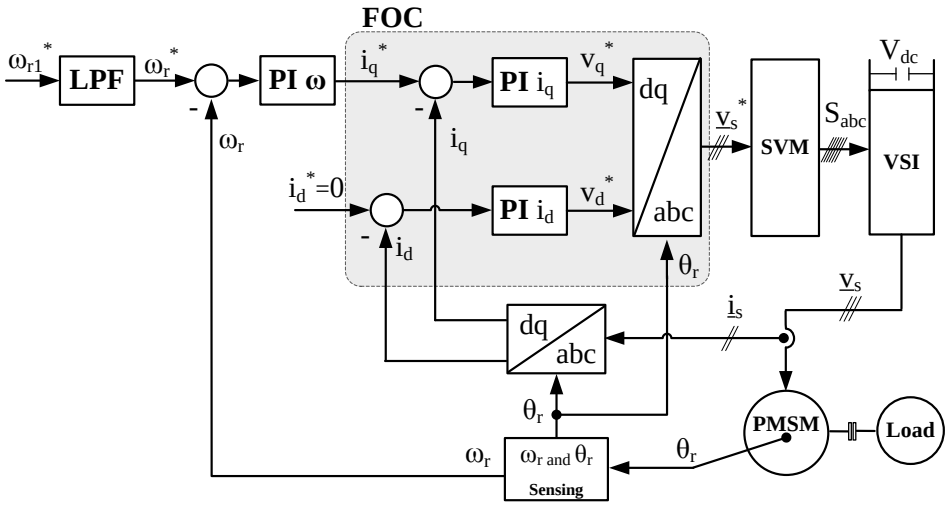

Fig. 4.13. FOC strategy implementation for PMSM drive

4.3.2. Experimental Results Comparison

The sensorless stable V/f control with two stabilizing loops (Fig. 4.1) and the standard FOC strategy, Fig. 4.13, are implemented using MATLAB®/Simulink® on the real-time platform dSPACE 1103. The experimental test stand hardware is presented in section 4.2.6 and the SPMSM parameters are expressed in Table 4.3.

The rotor speed ω_r profiles at 1500 rpm and 750 rpm are presented in Fig. 4.14, including speed variation due to rated torque loading and unloading. The

experimental scenario from section 4.2.6 is maintained. A compromise between good speed reference tracking capability and good disturbance rejection must be taken into account for the FOC speed controller tuning. Even if the V/f control presents less speed overshoot, the FOC strategy is capable to handle higher acceleration demands.

Similar profiles of the electromagnetic torque for sensorless stable V/f control and sensored FOC are seen in Fig. 4.15. In both cases, the developed torque is estimated based on the i_q current obtained with position information from the encoder, not used in control

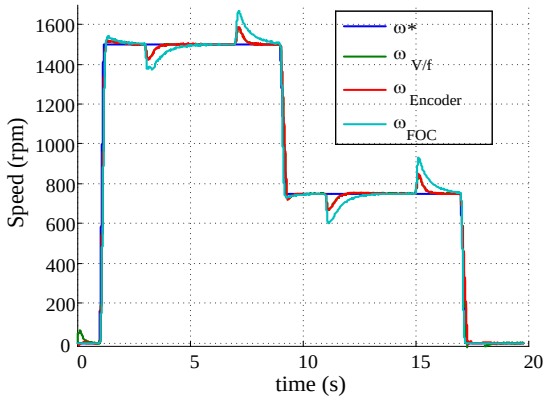

Fig. 4.14. Experimental results for rotor speed variation ω_r - comparison between sensorless V/f control and sensored FOC

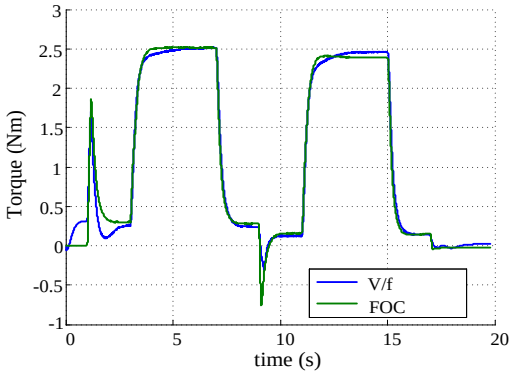

Fig. 4.15. Experimental results for electromagnetic torque - comparison between sensorless V/f control and sensored FOC

The magnetizing *d* axis current is illustrated in Fig. 4.16. While FOC succeeds in maintaining i_d=0 during the entire test, V/f control presents i_d variation in transient state but in time settling somewhere close to zero for steady state operation. This fact is expected because a constant power factor regulation is adopted for V/f control.

The power factor angle variation is presented in Fig. 4.17. From extensive experiments it has been observed that under rated load operation, sensorless stable V/f control and sensored FOC settle to a very low value of φ: 6.6 degrees for FOC

and respectively 3.5 degrees for V/f control during steady state. Therefore an optimal $\varphi^*=3.5$ degrees will be used.

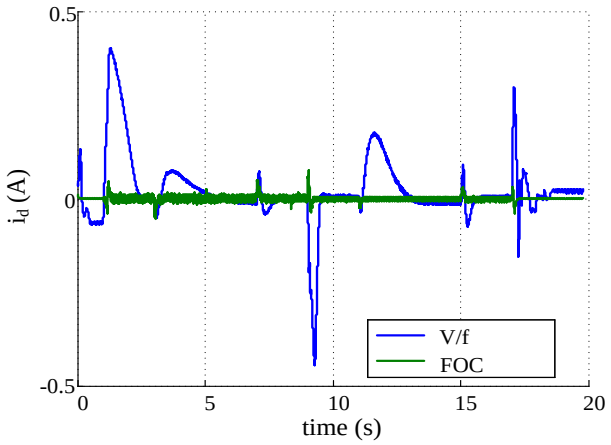

Fig. 4.16. Experimental results for *d* axis current i_d - comparison between sensorless V/f control and sensored FOC

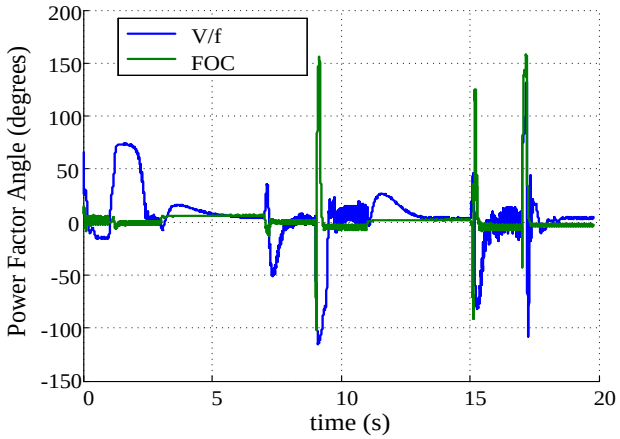

Fig. 4.17. Experimental results for power factor angle variation - comparison between sensorless V/f control and sensored FOC

4.3.3. Conclusions

The simplest sensored vector control structure for PMSM, i.e., standard FOC with $i_d^*=0$ (Fig. 4.13), mainly contains: 3 PI regulators (2 *dq* current regulators, 1 rotor speed PI regulator), LPF for speed reference, emf compensation block, 2 abc↔dq coordinate transforms with sin-cos look-up table and position incremental encoder. Comparatively with FOC, the proposed inherent sensorless V/f control structure requires rather *less computation effort*, mainly containing: rate limiter, 1 PI regulator for power factor angle, 1 HPF for active power extraction, 1 LPF for power factor angle reference, atan2 function for power factor angle computation and

sin, cos functions for polar to $\alpha\beta$ coordinate transform using look-up tables and does not use position incremental encoder.

The proposed stable V/f control strategy proves *good dynamic performance in terms of fast reference tracking and prompt disturbance rejection for step rated load torque*. An optimal constant power factor angle reference of 3.5 degrees is experimentally chosen.

Evaluation of experimental results between the proposed stable V/f control and the standard FOC using position encoder prove appropriate dynamic performances.

4.4. Enhanced V/f Control System

This section is based on the author publication [Aga2012] and is a completion of sections 4.2 and 4.3. In section 4.2 simulation and experimental results were presented for stable sensorless V/f control in order to test its performance. In section 4.3 the proposed stable sensorless V/f control is experimentally compared with standard sensored FOC strategy, to underline its dynamic performances and low implementation effort needed.

In this section, the stable sensorless V/f control with two stabilizing loops (Fig. 4.1) is enhanced with: i) a supplementary voltage amplitude correction proportional to the active power ΔV_p, needed for low speed operation, and ii) an addition for the power factor angle reference φ^* based on i_d current loop.

A performance comparison based on experimental results between the enhanced V/f control and sensorless FOC based on active flux is performed.

4.4.1. Proposed Enhanced V/f Control System

a) Voltage amplitude additional correction using active power

From extensive simulations and experiments, for low speed operation of the SPMSM (Table 4.3), it was noticed that the voltage amplitude correction loop is too slow. For sudden heavy loading it is necessary for another component for the voltage amplitude correction to step in and help the SPMSM not lose synchronism.

The power-factor angle control loop uses a PI regulator (4.19), with the integral time constant designed close to the electrical time constant $T_i^{\varphi} = 0.005$ s $\approx L_s/R_s$. The proportional term $k_p^{\varphi} = 0.2$ V/rad is chosen to obtain a desired bandwidth and to avoid chattering.

$$\Delta V_{\varphi} = k_p^{\varphi}\left(1+\frac{1}{sT_i^{\varphi}}\right)\left(\varphi^* - \hat{\varphi}\right) \tag{4.19}$$

The additional component ΔV_p for low speed operation is chosen to be proportional to the active power P and is functional only for low speeds:

$$\Delta V_P = k_P \cdot P \,,\; k_P = 0.3 \tag{4.20}$$

The proportional gain k_P was obtained experimentally by trial and error.

b) Power factor angle reference based on i_d current loop

In order to operate under MTPA conditions, an i_d current closed loop that maintains i_d=0 is proposed for SPMSM. This loop will continuously modify the power factor angle reference φ^* such that the stator current has only the torque component.

The current control loop requires i_d feedback, but to avoid coordinate transforms that need rotor position information - not available, the proposed solution is to estimate i_d current using the internal reactive power Q expression for SPMSM [Anc2010], [Sue2011]:

$$\hat{i}_d = \frac{2Q}{3\omega_v^*\lambda_{PM}} - \frac{L_s I_s^2}{\lambda_{PM}}, \quad I_s^2 = i_\alpha^2 + i_\beta^2 \qquad (4.21)$$

The enhanced stable sensorless V/f control with two stabilizing corrections implementation is presented in Fig. 4.18.

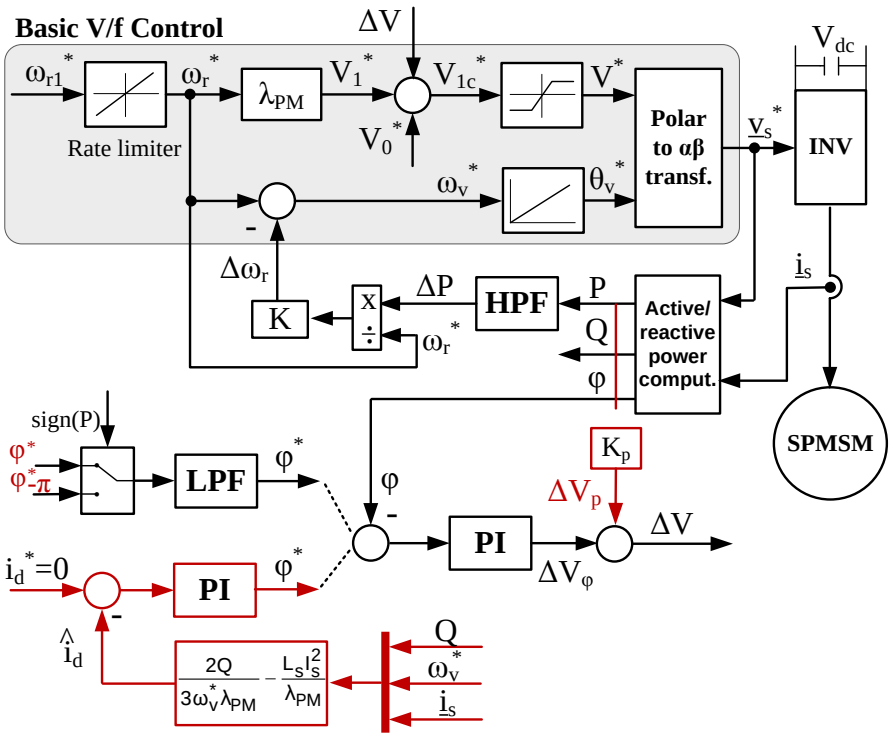

Fig. 4.18. Enhanced sensorless V/f control with two stabilizing corrections with i_d current control loop for φ^* reference and additional voltage amplitude correction ΔV_p for SPMSM drives

4.4.2. Simulations and Experimental Results at Unity Power Factor for enhanced Sensorless V/f Control

The enhanced V/f control from Fig. 4.18 is implemented using MATLAB®/Simulink® software and real-time platform dSPACE 1103. The

experimental test stand hardware is presented in section 4.2.6 and the SPMSM parameters are expressed in Table 4.3.

To validate the performance of the enhanced sensorless V/f control system with fixed φ^* given through LPF way, both simulations and experiments are performed. It is known that in order to obtain the MTPA below the rated speed, a variable power factor angle must be prescribed depending on speed and loading conditions. However, the addition of such part for referencing φ^* will increase the complexity and computational effort. Therefore, a unity power factor is firstly investigated as a compromise that is worth adopting when simplicity and low cost implementation are required.

The simulation test scenario employing unity power factor contains a fast acceleration to the rated speed, loading and unloading with the rated torque, reversing to the negative rated speed, loading again and unloading again in rated conditions and braking down to zero speed.

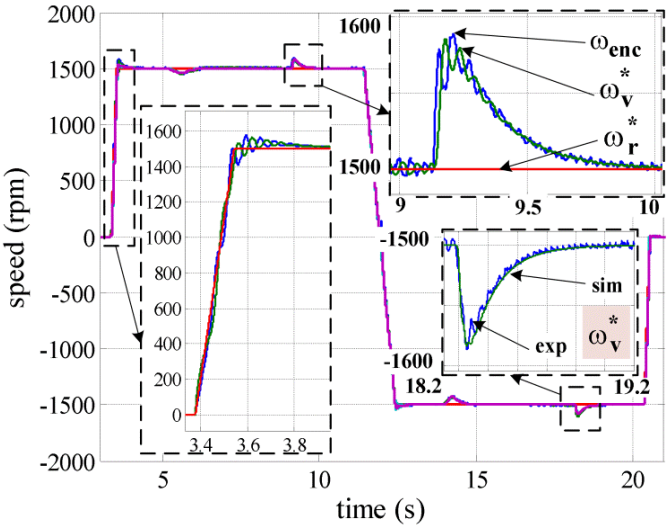

Fig. 4.19. Comparison between experimental (exp) and simulation (sim) results of speed responses at unity power factor: *left zoom*: acceleration to rated speed; *top right zoom*: comparison between measured speed (ω_{enc}), corrected stator voltage vector speed (ω_v^*) and reference speed (ω_r^*); *bottom right:* corrected stator voltage vector speed (ω_v^*)

The reference rotor speed has a slope of 300 Hz/s (9000 rpm/s), and no load acceleration to the rated speed (1500 rpm) is done in 166 ms. Referring to Fig. 4.19, there are three zoomed regions: acceleration, unloading at positive and negative rated speed. In the top right region, when the machine is unloaded, the corrected reference speed ω_v^* follows the rotor real speed ω_{enc} (measured with an encoder - as a witness) in a successful attempt to maintain the synchronization between the stator rotating magnetic field and the rotor, while the uncorrected reference speed ω_r^* is unaware of the rotor speed disturbance. The unloading action is shown here because it is more violent in term of torque disturbance than the loading action by the given load. The bottom left zoomed region shows the good agreement between simulation and experiments in term of corrected reference speed ω_v^*.

Comparison between experimental and simulation results for the speed profile in Fig. 4.19 is presented in Fig. 4.20. In the. Fig. 4.20*a* is shown the rated

torque loading and unloading. The i_d current, Fig. 4.26*b*, settles to a negative value for motor mode (MM) under load, because the power factor angle is kept constant around zero, Fig. 4.26*c*. The voltage vector speed correction $\Delta\omega_r$, Fig. 4.26*d*, proportional to the active power variation extracted with the high pass filter, is active only in transient states, and together with the voltage amplitude correction helps to stabilize the system. The agreement between experimental and simulation results looks quite satisfactory. On the other hand, although the proposed control is stable and improves the drive dynamics it does not guarantee yet the zero i_d (MTPA) operation, because there is only φ^* feedback loop.

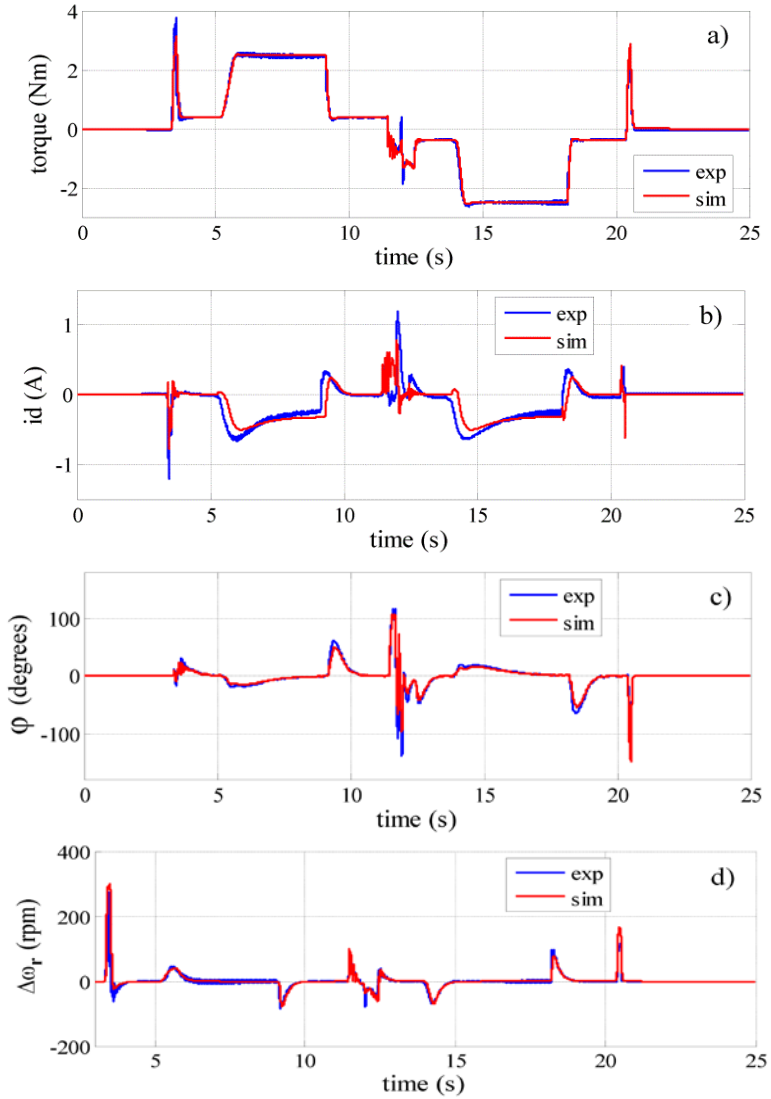

Fig. 4.20. Comparison between experimental (exp) and simulation (sim) results for the speed profile shown in Fig. 4.19 for: a) electromagnetic torque T_e, b) *d* axis current i_d, c) power factor angle φ, and d) voltage vector speed correction $\Delta\omega_r$

4.4.3. Experimental Results at Different Constant Power Factor Angles for enhanced V/f Control

In order to investigate the drive dynamics, experiments at different power factor angle references are performed, while attempting to maintain the same timing in terms of acceleration, deceleration and loading, for different φ^*.

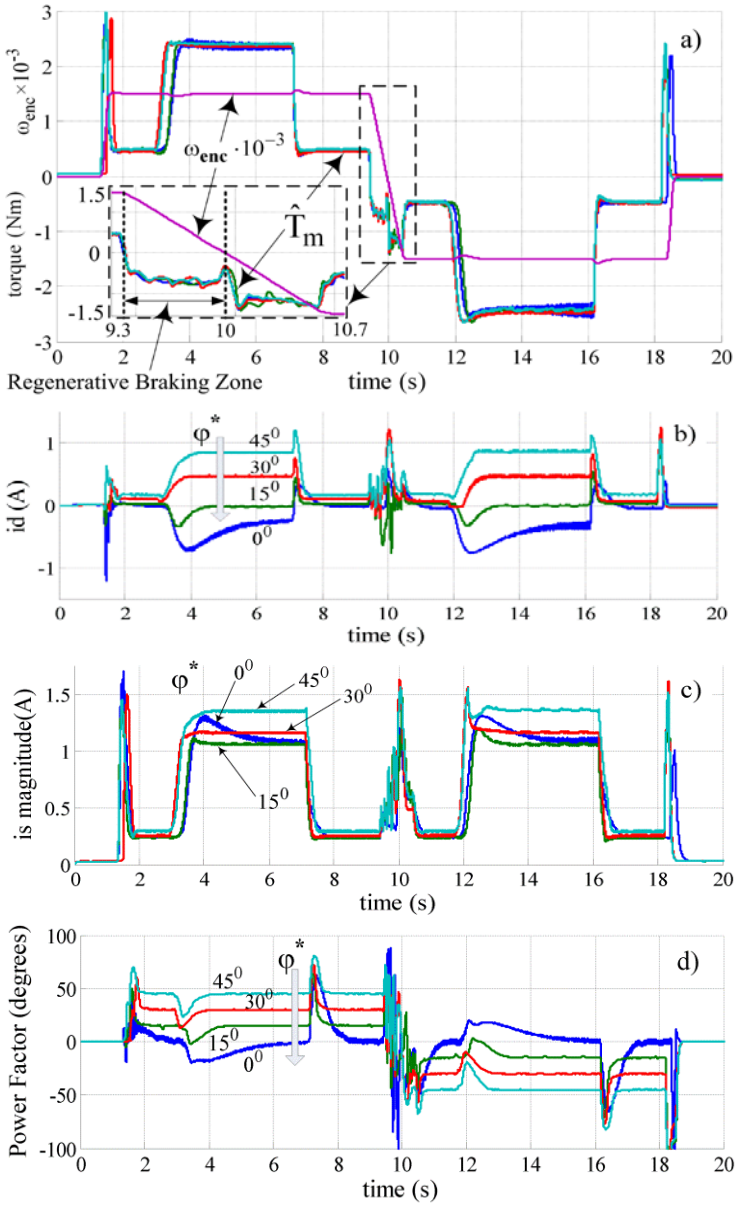

Fig. 4.21. Experimental results for different power factor angle references (0-45 degrees): a) electromagnetic torque T_e, b) magnetizing d axis current i_d, c) stator current amplitude I_s, and d) power factor angle φ

The experimental results are shown in Fig. 4.21, for the same speed profile illustrated in Fig. 4.19, showing transient responses of electromagnetic torque, i_d current, stator current amplitude I_s, and power factor angle φ.

In Fig. 4.21*a* (zoom) regenerative braking is obtained during deceleration at positive speed.It is obvious from the electromagnetic torque response, Fig. 4.21*a*, that for various power factor angle references ($\varphi^* = 0^0$, 15^0, 30^0 and 45^0, Fig. 4.21*d*) the system response to transients is stable. In general $i_d \neq 0$, but the stator current amplitude is lowest near $\varphi^* = 15^0$, Fig. 4.21*c*, where i_d approaches zero as expected, Fig. 4.21*b*.

4.5. Experimental Comparison between Enhanced V/f Control with i_d Loop and Sensorless Vector Control Based on Active Flux

A brief introduction for sensorless vector control based on active flux (AF) is presented used for comparison with the enhanced V/f control with stabilizing feedback corrections in terms of complexity and dynamic performances.

4.5.1. Sensorless Vector Control Based on Active Flux

For a simple and fair comparison, the sensorless vector control based on active flux vector introduced in [Pai2009] is implemented with the control structure presented in Fig. 4.22, is implemented. This structure contains mainly FOC strategy and the active flux based observer (AFO) for rotor position and speed estimation.

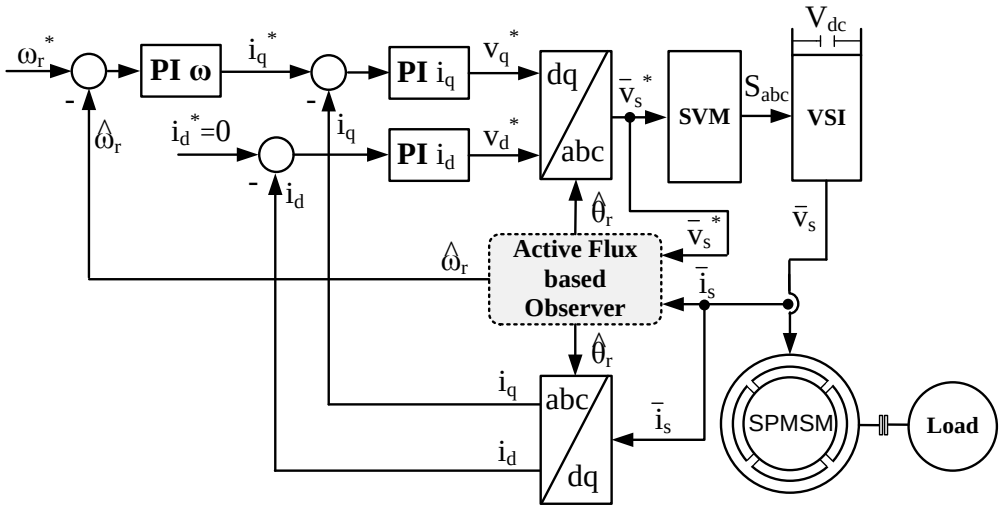

Fig. 4.22. Sensorless FOC structure for SPMSM based on Active Flux based Observer

The active flux vector $\bar{\lambda}_{act}$, obtained by subtracting the term $L_q \cdot \bar{i}_S$ from the stator flux vector, is given by:

$$\bar{\lambda}_{act} = \int \left(\bar{V}_S - R_S \cdot \bar{i}_S + \bar{V}_{comp} \right) dt - L_q \cdot \bar{i}_S \qquad (4.22)$$

where V_{comp} represents a compensation voltage that handles the drift problem of a pure integrator [Aga2011].

The stator flux vector could be estimated using a pure integrator. A well-known solution to mitigate the drift problem is to replace the pure integrator from (4.22) with a low-pass filter $H(s) = 1/(s+2\cdot\pi\cdot f_0)$, where f_0 is the cutoff frequency. Firstly, this simple technique was tested, but due to severe errors in phase angle and amplitude errors for stator frequencies around f_0 (0.5-2Hz, practical values), the drive failed to run at the minimum stator flux frequency of 3 Hz achieved with the proposed V/f control

Consequently, the stator flux vector is estimated by using the feedback voltage compensation vector $\overline{V}_{comp}$ from (4.22).

The active flux based observer (AFO), presented in Fig. 4.23, comprises both the voltage model $\overline{\lambda}_{su}$ (4.23) and the current model $\overline{\lambda}_{si}$ (4.24) in stator reference frame for stator flux estimation, with a PI compensator that handles the stator flux error from both models and operates at the voltage model level [Bol2008][Pai2009].

$$\overline{\lambda}_{su} = \int \left(\overline{V}_S - R_S \cdot \overline{i}_S + \overline{V}_{comp} \right) dt \tag{4.23}$$

$$\overline{\lambda}_{si} = \left(\lambda_{PM} + L_d I_d + jL_q I_q \right) \cdot e^{j\hat{\theta}_r} \tag{4.24}$$

$$\overline{V}_{comp} = \left(K_p + \frac{K_i}{s} \right) \cdot \left(\overline{\lambda}_{si} - \overline{\lambda}_{su} \right) \tag{4.25}$$

where $\overline{\lambda}_{su}$ is the stator flux vector in stator coordinates obtained from the voltage model, $\overline{\lambda}_{si}$ is the stator flux vector in stator coordinates obtained from the current model, and k_p and k_i are the proportional and the integral gains of the PI compensator that outputs $\overline{V}_{comp}$.

At low speeds, the current model acts as a reference model correcting the voltage model output, which, without the compensation loop, progressively drifts away due to offsets and quantization errors. The components of the active flux vector (AF) in stator reference are computed based on (4.22).

The main AF propriety is that the AF angle is equal at any time with the rotor position angle ($\theta_{\lambda_{act}} = \theta_r$). Therefore, if the AF vector is correctly estimated, then from the AF components, the estimated rotor position $\hat{\theta}_r$ (4.25) and rotor speed $\hat{\omega}_r$ (4.24) [Pai2009] are extracted with good accuracy.

$$\hat{\theta}_r = a\tan 2\left(\lambda_{act\beta}, \lambda_{act\alpha} \right) \tag{4.25}$$

$$\hat{\omega}_r = \frac{\hat{\lambda}_{act\alpha-1}\hat{\lambda}_{act\beta} - \hat{\lambda}_{act\beta-1}\hat{\lambda}_{act\alpha}}{h\left(\hat{\lambda}_{act\alpha}^{\,2} + \hat{\lambda}_{act\beta}^{\,2} \right)} \tag{4.24}$$

where h is the sample time and the subscript "-1" refers to one period delayed signal.

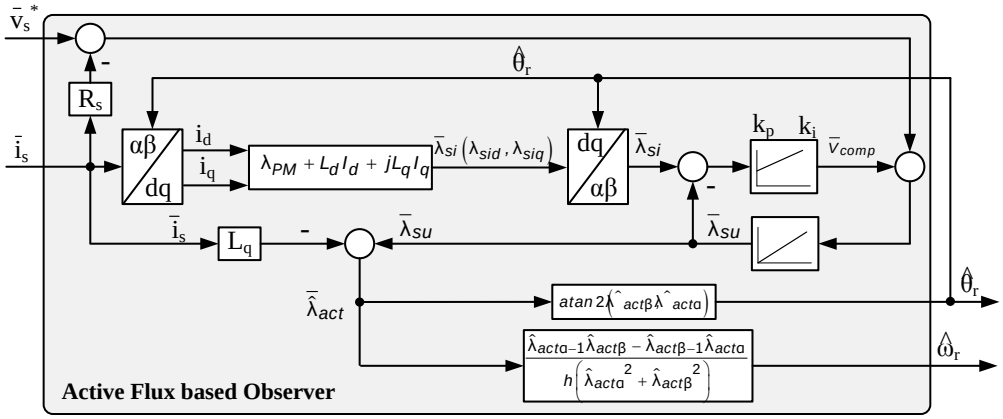

Fig. 4.23. Active Flux based Observer for rotor position and speed estimation

4.5.2. Experimental Comparison Results

The proposed enhanced V/f control with two stabilizing correction with power factor angle reference given by i_d current loop, Fig. 4.18, and the sensorless vector control based on active flux, Fig. 4.22 and Fig. 4.23, are implemented using MATLAB®/Simulink® on the real-time platform dSPACE 1103. The experimental test stand hardware is presented in section 4.2.6 and the SPMSM parameters are expressed in Table 4.3.

The experimental comparison has the purpose to prove the good dynamics and rotor position/speed estimation for the proposed enhanced V/f control, as well as to test the proposed solution for power factor angle reference based on i_d current control loop. Experimental results for low and high speed are presented as follows.

a) Low speed operation

Experimental results are firstly obtained for low speeds. A comparison between the proposed enhanced V/f control and sensorless FOC based on AFO for 3Hz (90 rpm) is shown in Fig. 4.24.

Referring to Fig. 4.18, at low speed operation the total compensation voltage ΔV is negative, mitigating the stator voltage amplitude to a few volts. This negative value is mainly the contribution of power factor angle loop ΔV_φ. After loading the machine the negative power factor angle loop output ΔV_φ becomes smaller, and the voltage vector amplitude increases. In this case, the main contribution to the voltage vector amplitude is ΔV_P which is proportional to the estimated active power P. Without this new contribution the drive could not run safely at 3 Hz.

The rotor speed response under load torque disturbances are illustrated in Fig. 4.24*a* and is important to note the smaller ripples in the measured speed obtained with the enhanced V/f control. In Fig. 4.24*b* is presented the loading torque variation, with the mention that for enhanced V/f control, the loading torque is not suddenly applied. Fig. 4.24*c* illustrates the estimated i_d current based on (4.21) for the proposed V/f control strategy and based on AFO estimated reference

frame. Both control strategies estimate a power factor angle close to zero (Fig. 4.24*d*).

At this low frequency, the performance of the proposed V/f control is considered satisfactory.

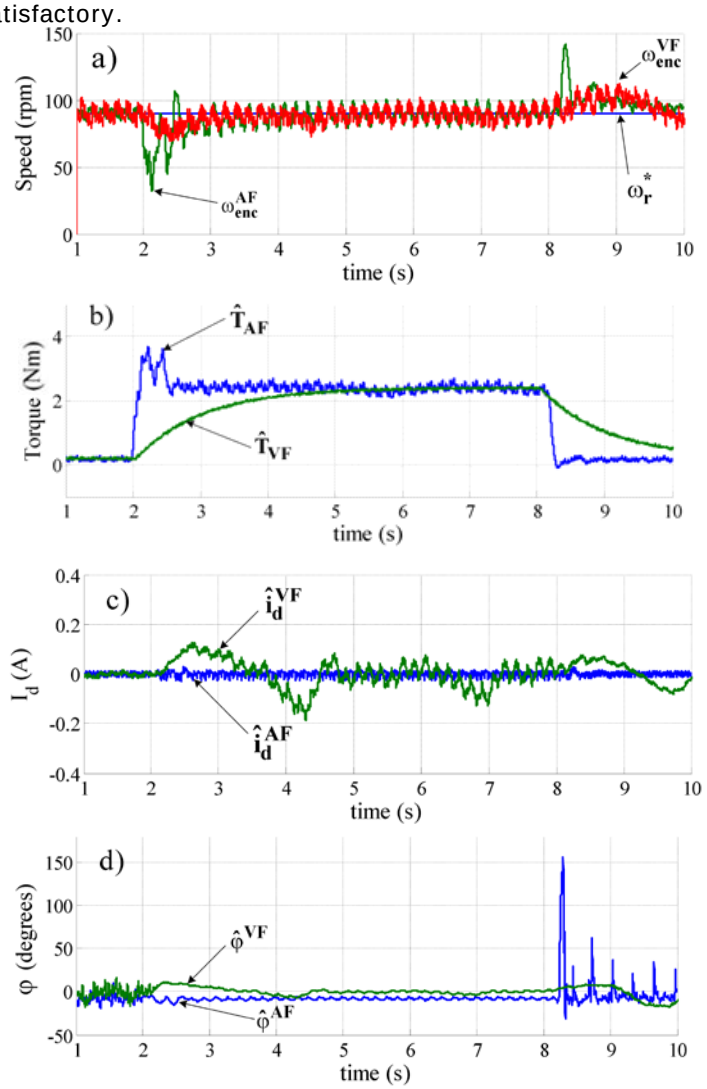

Fig. 4.24. Comparative experimental results at low speed 3Hz (90 rpm) between the proposed enhanced V/f control (VF) and sensorless vector control based on AF (AF): a) measured rotor speed, b) torque, c) i_d current, d) power factor angle

b) High speed operation

As presented in Fig. 4.25, the performance based on experimental results of proposed enhanced V/f control will notably increases as the frequency rises, with considerable merits over the AFO based sensorless vector control.

In order to further highlight the i_d control loop action during *operation at high speed*, including speed reversal operation (Fig. 4.25*a*) and for loading and

unloading torque (Fig. 4.25*c*), the experimental stator current component i_d is shown in Fig. 4.25*d* for $i_d^*=0$ (MTPA).

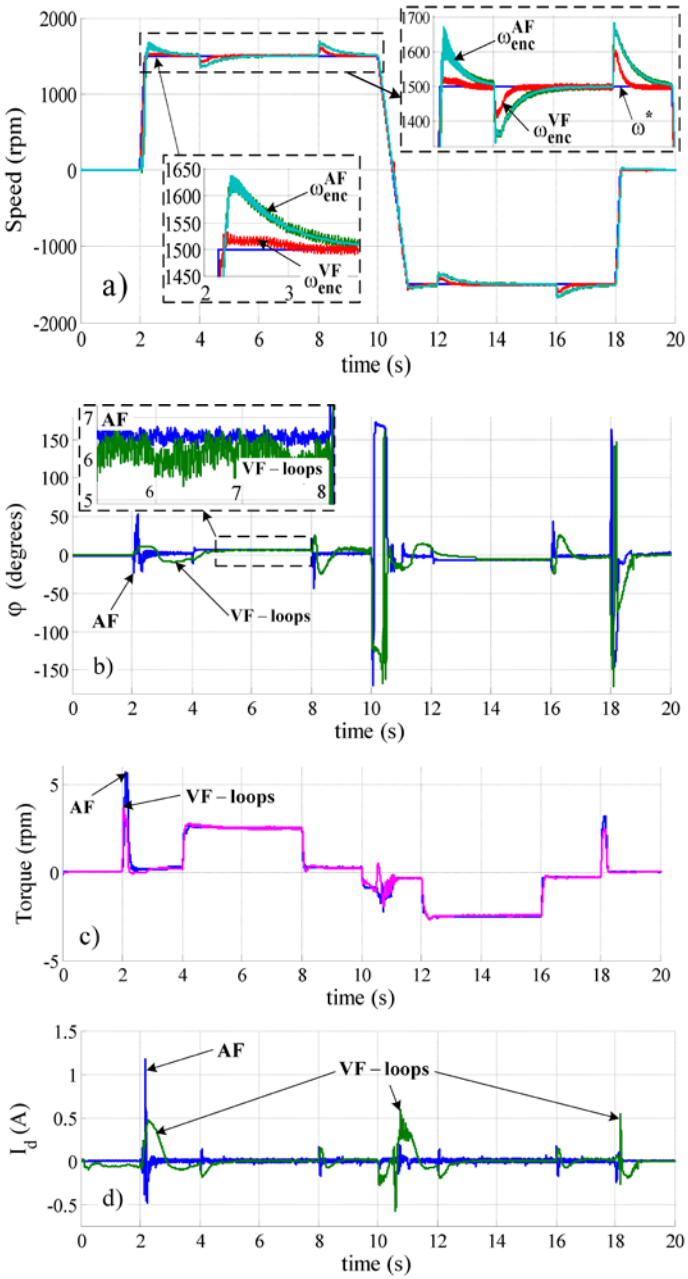

Fig. 4.25. Comparative experimental results at high speed between the proposed enhanced V/f control (VF) and sensorless vector control based on active flux (AF): a) measured rotor speed, b) power factor angle with *id*-loop active, c) torque, d) i_d estimated with (4.21) and calculated based on measured currents

The speed response illustrated in Fig. 4.25*a* shows that for good tuning the proposed enhanced V/f control strategy can reach the reference speed as quick as the sensorless vector control based on AF, moreover with about 1% overshoot. Furthermore, during loading and unloading, the rotor speed variation from the enhanced V/f control (measured with the encoder, as a witness) presents half the variation of the rotor speed obtained using sensorless vector control based on AF, proving superior load torque rejection.

Both strategies seem to identify almost the same (0.3 degrees error) power factor angle that provides MTPA during steady states (Fig. 4.25*b*), with i_d=0 control realized. The power factor angle varies (Fig. 4.5*b*) as expected. Larger current transients are noticed during start-up under sensorless vector control (Fig. 4.25*c* and *d*), but once it has caught the *d*-axis position, the MTPA operation is preserved during rated transients (speed, load), yielding very good performance for both sensorless vector control based on AF and the proposed enhanced V/f strategy.

4.5.3. Conclusions

The proposed V/f control strategy proves very good performance in terms of fast reference tracking and prompt disturbance rejection. Compared experimental results comparison between the proposed enhanced V/f control and sensorless vector control based on AF show superior dynamics of the enhanced V/f control in speed tracking and load transients.

For the power-factor angle reference an optimized reference (MTPA with i_d=0 for SPMSM) based on i_d current regulation loop is proposed, which shows fast and stable responses to speed and load torque transients. This way also, full speed / torque range control for maximum torque per current (MTPA) is implicitly performed.

In summary, the proposed enhanced V/f control structure with two stabilizing feedback corrections presents good dynamic stability (comparable with a medium complexity sensorless vector control), for fast ramp reference speed and full load rated torque disturbances.

Flux weakening was not attempted due to the low stator inductance (L_s) for the given SPMSM.

5 Integrated Starter-Alternator Control System for Automotive

In this chapter is developed a control system for an Integrated Starter-Alternator (ISA) used in hybrid electric vehicles (HEVs), based on the author publication [And2013].

ISA is an electric machine mounted between the internal combustion engine (ICE) and transmission to work as a starter motor, engine balancer and assist traction motor [Wik2014].

5.1. Introduction

Hybrid and electric vehicles are developed in order to reduce pollution, especially in city areas, and to increase energetic efficiency. The electric vehicles (EV) have relative short autonomy per battery charge, and therefore hybrid electric vehicles (HEV) are more suitable. For high electric power demand, the battery DC bus has increased from 14 V to 42 V. A solution for cost reduction is to substitute the starter and alternator machines with a single integrated starter-alternator (ISA) that can work in both motor and generator mode. Studies to determine the best topology and control strategy of the ISA are made in [Wil2007].

One choice for ISA in automotive industry is the induction machine (IM). In [Jai2006] is presented a topology for integrated starter generator (ISG) with IM using direct torque control (DTC) on 42 V bus. Other studies [Mud2003], [Mud2004], [Xu2012] employ IM for ISA driven by a direct rotor flux oriented control (DFOC) connected to the 42 V bus, with the advantage of predicting ISA regulated DC voltage developed during load dump and sudden speed change.

The PM-assisted reluctance synchronous machines (PM-RSM) prove to have high peak tangential force densities, moderate saturation level, 90% efficiency for high speed (over 2000 rpm) and the advantage that the PM does not demagnetize at peak torque [Bol2004]. Direct torque and flux control with space vector modulation (DTFC-SVM) strategy is used for an experimental PM-RSM sensorless control in [Bol2006] proving effectiveness for low to high speed.

Another recently prototype for ISA is the permanent magnet synchronous motor (PMSM) [Fag2008]. In [Alb2010] a PMSM with fractional-slot winding prototype is built and tested, and the results show high torque and satisfactory flux-weakening operating region. Segmented PMSM prototype is studied in [Zhu2012], with reduced cogging torque and high starting torque performances. Furthermore, design improvements for IPM machines are made in [Mir2013].

The biaxial excitation generator for automobiles (BEGA) used for ISA in HEVs is proposed and is validated by experimental results in [Bol2010]. A sensorless control strategy for BEGA based on the active-flux is applied in [Cor2011] in wide speed range.

This chapter develops the proposed control system employs a PMSM for ISA model and ICE model uses DC motor equations, for simulations only. The chosen control strategy is field oriented vector control with torque reference for motor /

generator mode selection. The operating mode is selected by a switch that allows the reference torque: an external torque for motor mode and a torque delivered by DC voltage loop to charge the battery for generator mode. The ICE is simulated by a DC motor with speed control, and the battery is managed by using the ISA active power.

The simulation results, based on real scenarios, prove the ability of the proposed ISA control system to work in motor and generator modes with smooth transition between them. The scenarios include the motor mode with starting and added mechanical torque at demand, and the generator mode to charge the battery up to 42 V, with good dynamic responses.

5.2. ISA Modeling and Control

The advantages of using ISA are the reduction of system weight and allowing new functions for *reducing fuel consumption and air pollution*:

- START / STOP function (urban driving, traffic lights);
- Regenerative braking during deceleration;
- Power boost at high loads for ICE, etc.

The main requirements imposed for ISA are to have high starting torque (for low speed operation) and to perform a smooth transition between motor and generator modes (at high speed).

An overview of ISA positioning in HEVs is presented in Fig. 5.1.The chosen topology is a parallel ISA, with the note that the major difference between the parallel ISA design and the basic parallel design is the location of the clutch [Wil2007].

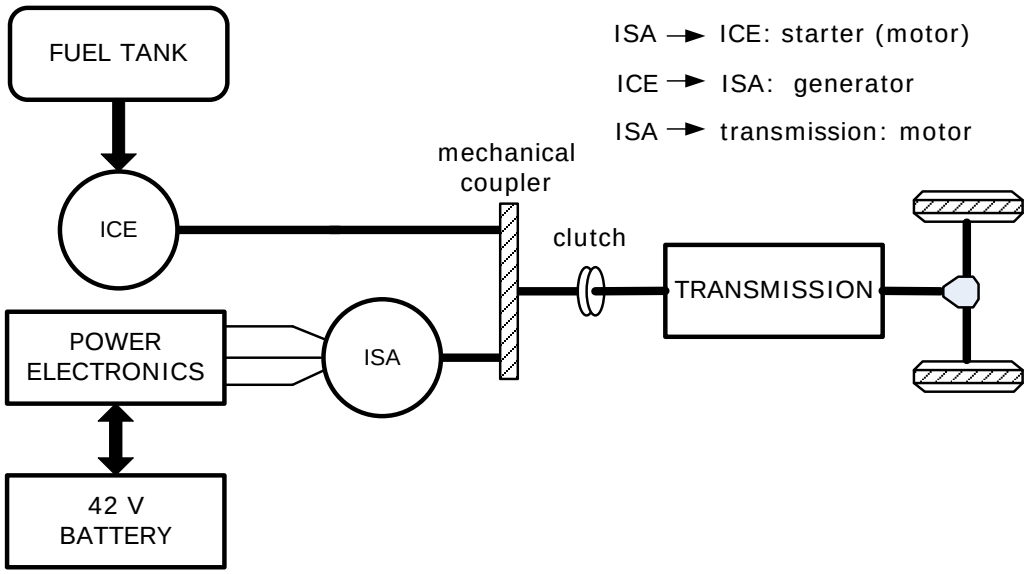

Fig. 5.1. 42 V Bus System Parallel HEV Architecture [Wil2007]

5.2.1. ISA Model using PMSM

For ISA a PMSM is chose with the *dq* rotor reference frame given by the equations:

$$v_d = R_s i_d + \frac{d\lambda_d}{dt} - \omega_r \lambda_q \quad (5.1)$$

$$v_q = R_s i_q + \frac{d\lambda_q}{dt} + \omega_r \lambda_d \quad (5.2)$$

$$\lambda_d = L_d i_d + \lambda_{PM} \; ; \; \lambda_q = L_q i_q \quad (5.3)$$

$$T_e = \frac{3}{2} p \left[\lambda_{PM} i_q + \left(L_d - L_q \right) i_d i_q \right] \quad (5.4)$$

$$J \frac{d\omega_m}{dt} = T_e - T_L - B\omega_m \; , \; \omega_m = \frac{\omega_r}{p} \quad (5.5)$$

$$\dot{\theta}_r = \omega_r \quad (5.6)$$

where v_d and v_q are the stator voltage vector components $\bar{v}_S \left(v_d , v_q \right)$, i_d and i_q are the stator current vector components $\bar{i}_S \left(i_d , i_q \right)$, R_s is the stator resistance, L_d and L_q are *dq* axis inductances, ω_r is the electrical rotor speed, ω_m is the mechanical rotor speed, θ_r is the rotor position, p is the number of pole pairs, λ_{PM} is the permanent magnet flux, T_e is the electromagnetic torque, J is the motor inertia, B is the viscous friction coefficient and T_L is the load torque.

5.2.2. ICE Model using DC Motor

The internal combustion engine (ICE) is modeled using the DC motor with the mathematical model:

$$v_a = R_a i_a + L_a \frac{di_a}{dt} + k_V \omega_r \quad (5.7)$$

$$T_E = k_T i_a \quad (5.8)$$

where v_a is the armature voltage, i_a is the armature current, R_a is the armature resistance, L_a is the armature inductance, k_V is the back-EMF constant, T_E is the electrical torque and k_T is the torque constant. The eq. (5.5) is added.

5.2.3. Proposed ISA Control Structure

The proposed control system is presented in Fig. 5.2, where ISA and ICE are mechanical coupled. The main part of the ISA control system containes : the field oriented control (*FOC*) with $i_d^* = 0$ with the electromagnetic torque T_e^* as control reference (Fig. 5.3), *VSI* is the voltage source inverter, *R*-V_{DC} is the PI regulator for battery DC voltage, *R*-ω is the PI speed regulator of ICE (DC motor), and *R*-i_a is the PI armature current regulator.

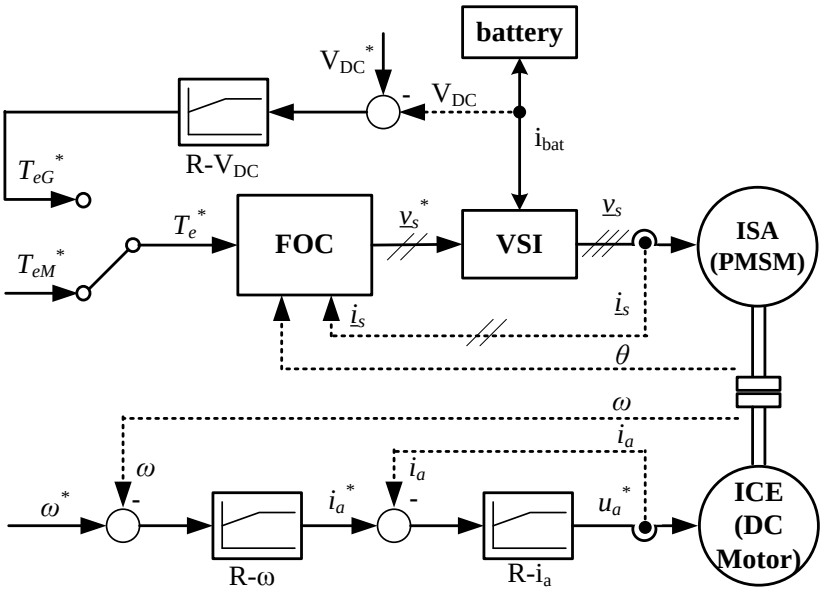

Fig. 5.2. Proposed ISA control structure

The ISA (PMSM) motor / generator mode is selected by a switch that gives to the FOC torque reference T_e^*: i) an external torque T_{eM}^* (motor mode), or ii) a torque T_{eG}^* delivered by the DC voltage loop for battery charge (generator mode). The ICE (DC motor) has a speed control loop (R-ω) with cascaded current control (R-i_a).

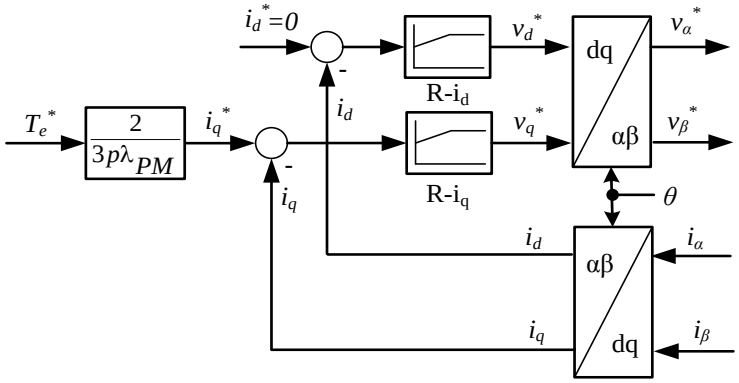

Fig. 5.3. FOC strategy with $i_d^*=0$ and torque reference as input for ISA control

The mechanical coupled model of ISA (PMSM) and ICE (DC motor) is presented in (Fig. 5.4), highlighting that the total electromagnetic torque $T_{e\Sigma}$ applied to the mechanical model (5.5) is the sum between the ICE (DC motor) torque T_E and the ISA (PMSM) torque T_e, which is positive in motor mode and negative in generator mode. The mechanical coupled model of ISA and ICE has the expression

$$\frac{J_\Sigma}{p}\frac{d\omega_r}{dt} = T_{e\Sigma} - T_L - \frac{B}{p}\omega_r \qquad (5.9)$$

where the total inertia J_Σ and the total electromagnetic torque $T_{e\Sigma}$ are given by

$$J_\Sigma = J_{ICE} + J_{ISA}$$
$$T_{e\Sigma} = T_E + T_e \quad (5.9)$$

At startup, PMSM works as motor with the maximum reference torque T_{eM} needed to power the ICE. After establishing the desired mechanical rotor speed, the PMSM switches to generator mode with the T_{eG}^* as reference torque given by R-V_{DC}. If there is a requirement for an added mechanical motor torque to ICE for faster acceleration, then ISA switches in motor mode.

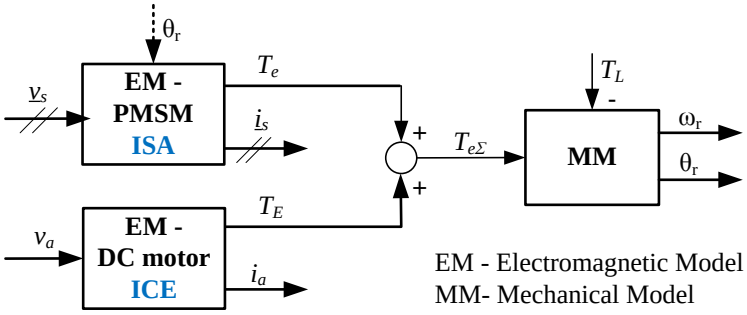

Fig. 5.4. Mechanical coupled model of ISA and ICE

The battery model [Cor2009], given in Fig. 5.5, has the parameters: V_0, R_0, R and C, and with auxiliary loads R_1 and R_2. To obtain 42 V battery, three 14 V batteries are connected in series. The chosen command variable is the battery current i_{batt} computed by using the PMSM active power P (5.10) given by the reference stator voltages v_α^*, v_β^*, and the measured stator currents i_α, i_β (Fig. 5.3). The i_{batt} flows in/out the battery for charging/ discharging, respectively, depending on the P sign.

$$P = \frac{3}{2}\left(v_\alpha^* i_\alpha + v_\beta^* i_\beta\right) \quad (5.10)$$

$$i_{batt} = \frac{P}{V_0} \quad (5.11)$$

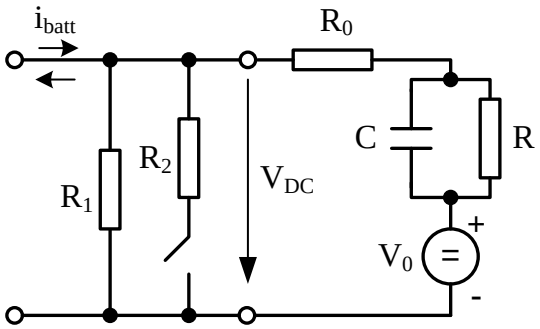

Fig. 5.5. Battery model with auxiliary loads R_1 and R_2

5.3. Simulation Results

Simulation tests are performed to prove the performance of the ISA proposed control system. Fig. 5.2 is implemented in MATLAB®/Simulink®, with a 100 μs sampling rate, considering the mechanical coupling (Fig. 5.4) and the battery model (Fig. 5.5).

The PMSM and the DC motor parameters are presented in Table 5.1 and Table 5.2, respectively. The chosen battery model parameters are presented in Table 5.3.

Table 5.1. PMSM (ISA) Parameters

Rated power (P_n)	3.3 kW
Rated torque (T_e)	19 Nm
Rated mechanical speed (ω_{rn})	157 rad/s
Number of pole pairs (p)	2
Stator resistance (R_s)	0.01 Ω
d-axis inductance (L_d)	0.5 mH
q-axis inductance (L_q)	0.5 mH
Permanent magnet flux (λ_{PM})	0.06 Wb
Equivalent inertia (J)	1 kgm^2

Table 5.2. DC Motor (ICE) Parameters

Rated power (P_n)	10 kW
Rated torque (T_E)	60 Nm
Rated mechanical speed (ω_{rn})	157 rad/s
Armature resistance (R_a)	0.4 Ω
Armature inductance (L_a)	0.02 H
Torque constant (k_T)	1.5 Nm/A
Back-EMF constant (k_V)	1.5 V/rad/s

Table 5.3. Battery Parameters

Internal resistance (R_0)	0.008 Ω
Load resistance (R_1)	5 Ω
Load resistance (R_2)	5 Ω
Resistance (R)	0.02 Ω
Capacitor (C)	50 F
Voltage source (V_0)	42 V

In order to show the performances of the proposed solution, two case scenarios are developed:

The first scenario is created to simulate the real events for ISA, and to show the performance of the proposed ISA control system in motor/generator modes: startup, cruising, acceleration with added mechanical torque, and again cruising. The imposed speed profile contains the following phases: acceleration only with ISA in motor mode until 50 rad/s; starting ICE and cruising at 50 rad/s with ISA switched in generator mode; acceleration until 100 rad/s as generator, then acceleration until 150 rad/s as motor, and finally cruising at 150 rad/s as generator. In this scenario, Fig. 5.6 shows the dynamic responses for the mechanical speed ω_{mec}, ISA torque T_e, ICE torque T_E, the ISA active power P and the DC voltage V_{DC}.

In the startup phase, i.e.,, acceleration to 50 rad/s in 2.5s, ISA operates as motor with positive maximum torque T_{eM} = 19 Nm, and ICE is not started (T_E = 0). The DC voltage drops because the current i_{batt} flows out of the battery.

When 50 rad/s is reached, ICE starts and a 50 rad/s cruising speed is regulated by ICE speed controller. ISA is switched to generator mode with the negative torque reference T_e given by the DC voltage regulation loop for battery charge, while ICE develops a positive torque T_E. In this period the DC voltage increases to the 42 V reference, i_{batt} current flows in the battery for charging.

At time 10 s, ICE accelerates with maxim torque T_E = 60 Nm until 100 rad/s (time 11 s), when ISA is switched to motor mode to obtain an added torque of T_e = 19 Nm for better acceleration. At 150 rad/s ISA is switched to generator mode and a 150 rad/s cruising speed is regulated by ICE speed controller.

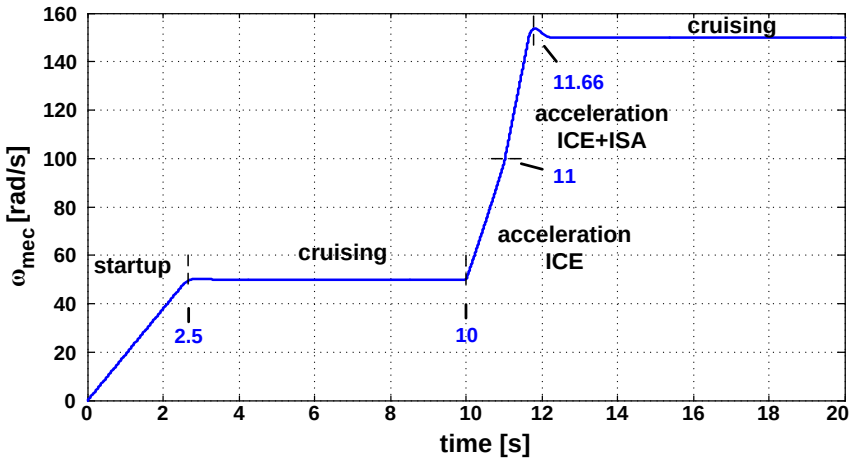

a) mechanical speed ω_{mec} variation;

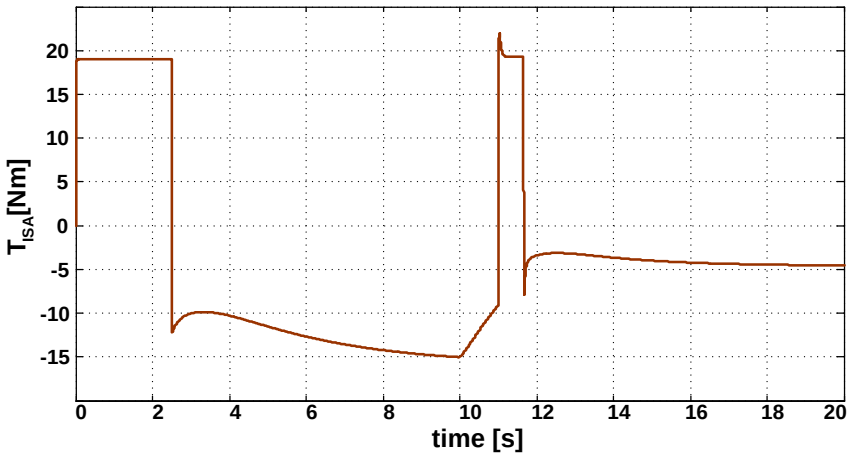

b) ISA electromagnetic torque T_{ISA} variation;

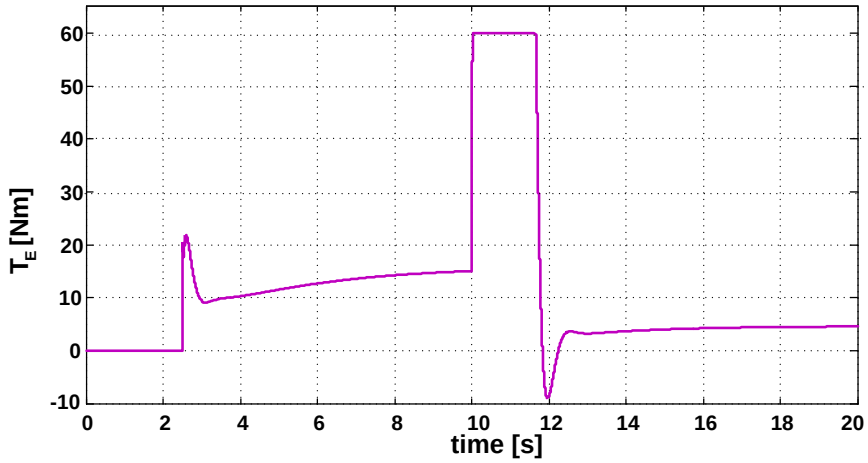

c) ICE torque T_E variation;

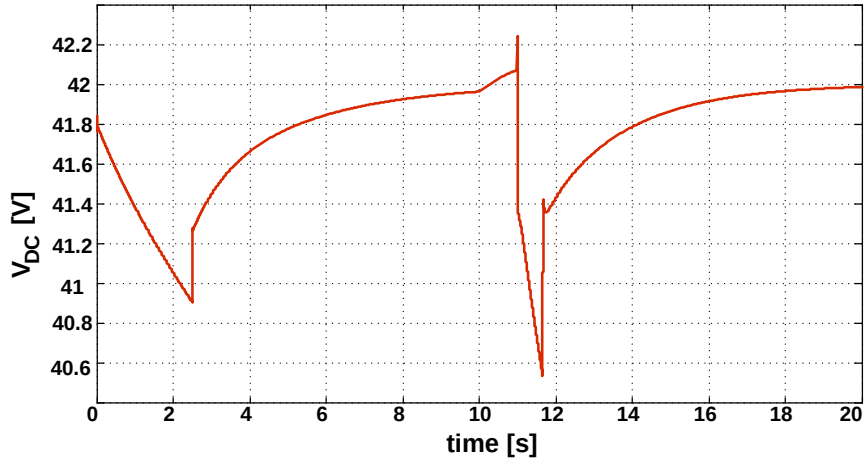

d) battery DC voltage V_{DC} variation;

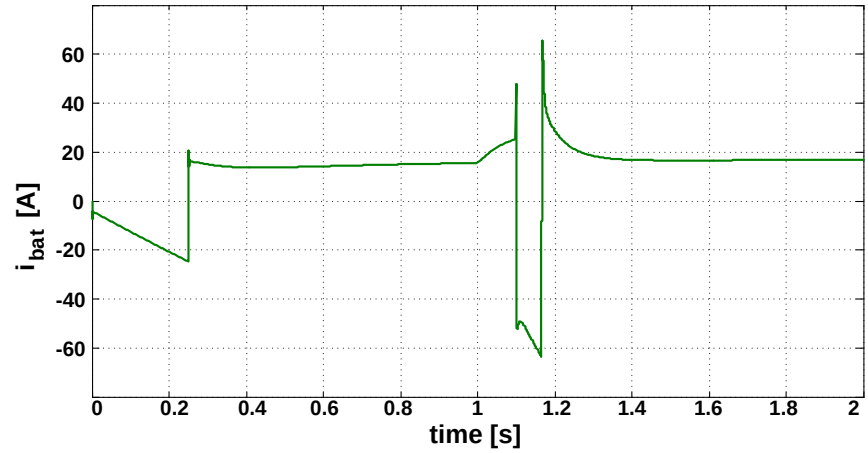

e) battery current i_{bat} variation;

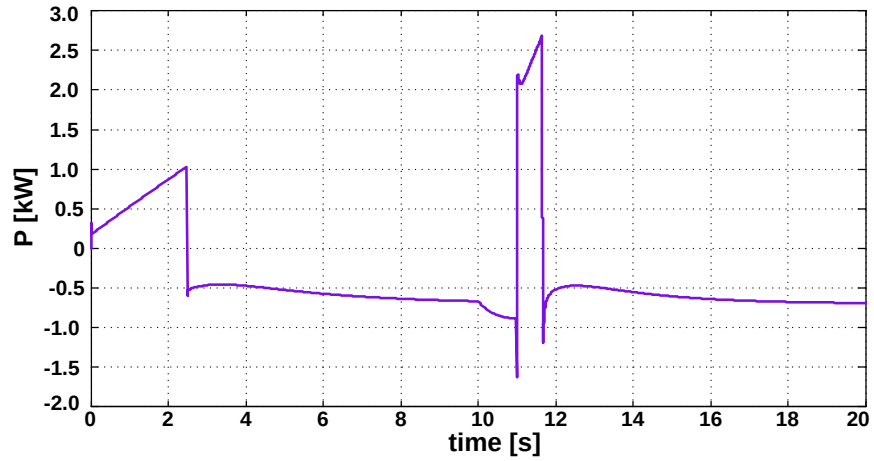

f) ISA active power *P* variation;

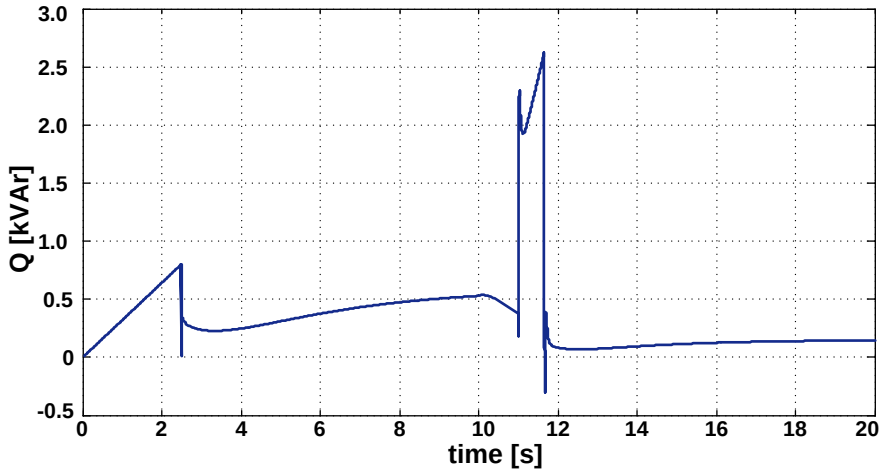

g) ISA reactive power *Q* variation;

Fig. 5.6. First scenario dynamic responses of the proposed ISA control system for motor and generator modes changing

The second scenario is created to show the performance to reject load disturbance of the DC voltage regulation loop for battery charge in ISA generator mode, with dynamic responses presented in Fig. 5.7.

At startup until 100 rad/s, ISA operates in motor mode with maximum torque T_{eM} = 19 Nm, and ICE is not started (T_E = 0). When the speed reaches 100 rad/s, ICE starts to run with 100 rad/s cruising speed regulated by ICE speed controller, and ISA is switched to generator mode.

After the DC voltage reaches steady state of 42 V, the resistance R_2 = 5 Ω is switched off at 20 s, and back on after 2 s. In the R_1 and R_2 parallel connection, if R_2 is interrupt then the load resistance increases, and thus the ISA torque T_e, the ICE torque T_E and the ISA active power *P* decrease. The simulation results from Fig. 5.6 prove good load disturbance rejection of ISA control system.

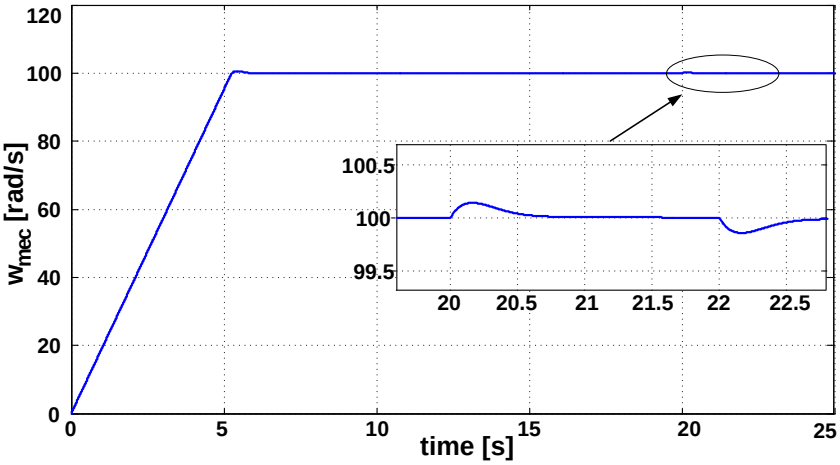

a) mechanical speed ω_{mec} variation

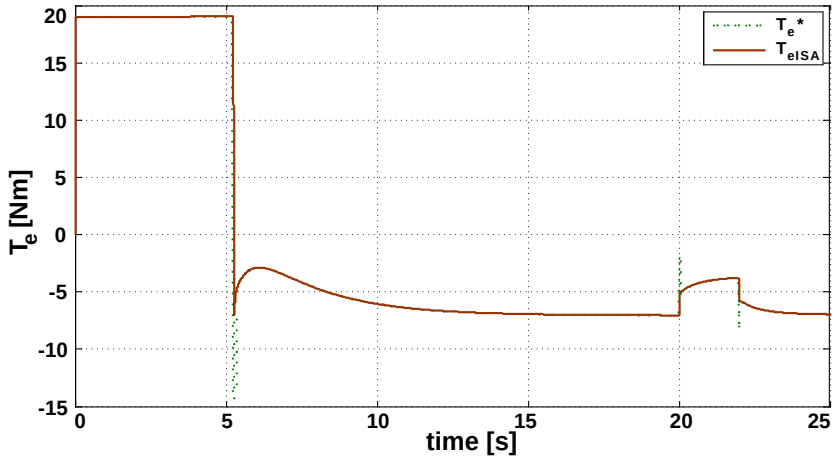

b) electromagnetic reference torque T_e^* and ISA torque T_{ISA} variation;

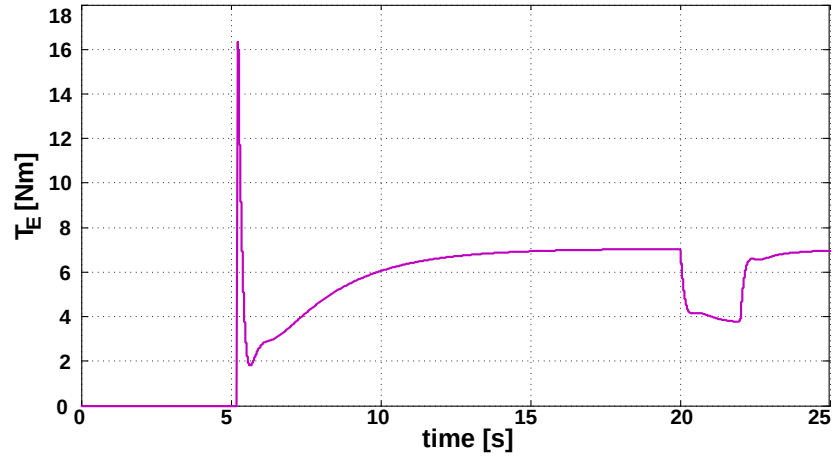

c) ICE torque T_E variation;

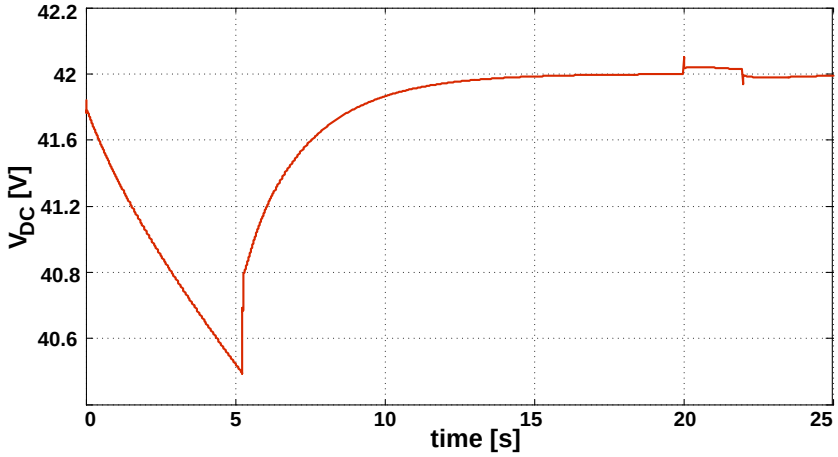

d) battery DC voltage V_{DC} variation;

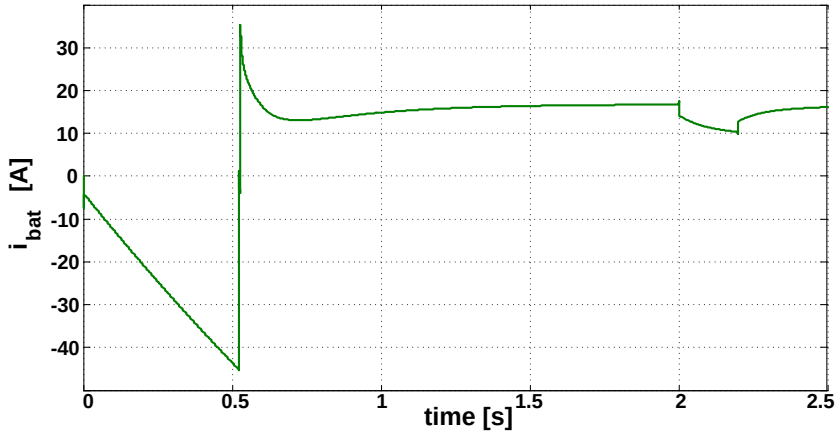

e) battery current i_{bat} variation;

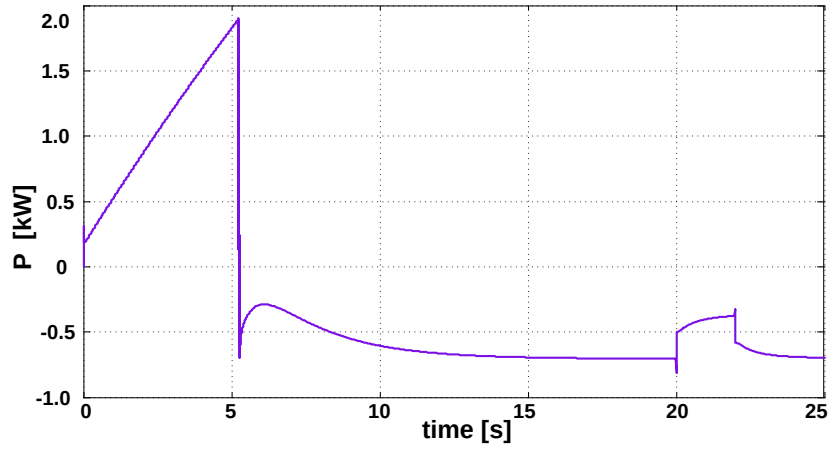

f) ISA active power P variation;

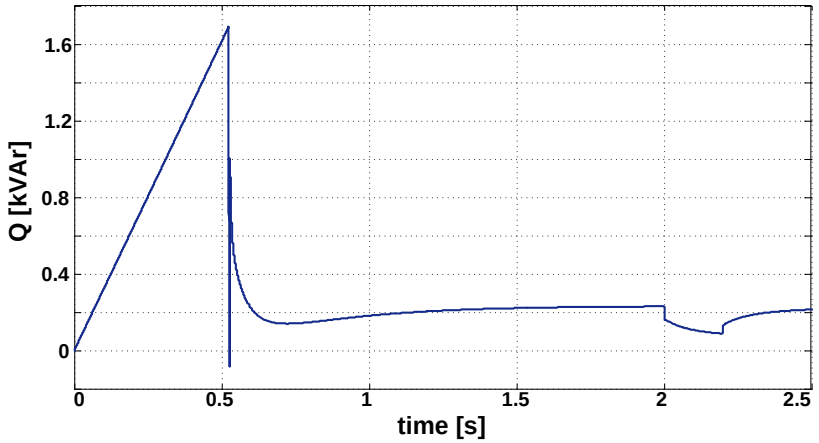

g) ISA reactive power *P* variation;

Fig. 5.7. Second scenario dynamic responses of the proposed ISA control system for R_2 load resistance switch off and switch on

5.4. Conclusion

This chapter introduces the proposed ISA control system employing a PMSM with field oriented vector control (FOC) having the electromagnetic torque as control reference, and a voltage source inverter supplied by 42 V battery. The internal combustion engine (ICE) is simulated using a DC motor with speed control.

The main contributions are the following:

- The ISA motor / generator mode is selected by a switch that gives to the FOC torque reference an external torque (motor mode), or a torque delivered by a DC voltage loop to charge the battery to 42 V (generator mode).
- The battery is managed in simulation by using the ISA active power that gives the battery current.
- The simulation test results, based on real scenarios, prove good performance of the proposed ISA control system in motor / generator mode, and with good load disturbance rejection. The scenarios include the motor mode: starting, and added mechanical torque to ICE at request, and the generator mode to regulate the battery voltage to 42 V, with good dynamic responses.

6 The Experimental Test Stand

In this chapter is presented the hardware and the software implementation of the experimental test stand.

The experimental test stand is sited at Politehnica University Timişoara, Faculty of Automation and Computers, Department of Automation and Applied Informatics, in Timişoara, Romania.

6.1. Hardware Implementation

The test stand configuration can be seen in Fig. 6.1. It contains the following components:

- ➔ SPMSM, working in motor mode;
- ➔ IM, working as generator/load;
- ➔ dSPACE:
  - DS1103 PPC Controller Board;
  - CLP1103 Connector Panel;
- ➔ 2 VSI Danfoss VLT®5000 Series;
- ➔ 3 current sensors LA 55-P;
- ➔ 1 voltage transducer LV 25-P;
- ➔ 1 incremental encoder 2RH;
- ➔ PC, with MATLAB®/Simulink®.

The PMSM is rigid coupled with the load (IM). On the shaft is mounted the incremental encoder, which transmits the position information to dSPACE platform. The VSI connected to the PMSM has a specific interface board that communicates with the dSPACE platform and allows touse the experimental algorithms implemented on dSPACE for VSI control (see Fig. 6.2).

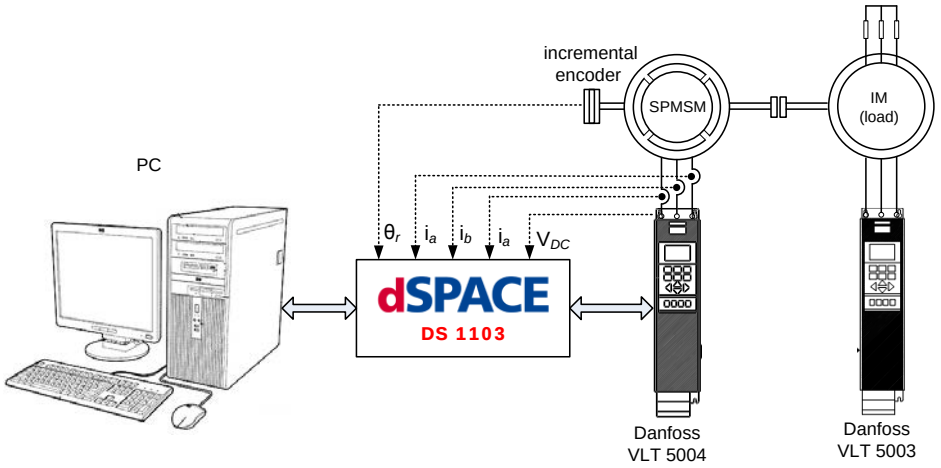

Fig. 6.1. The experimental test stand configuration

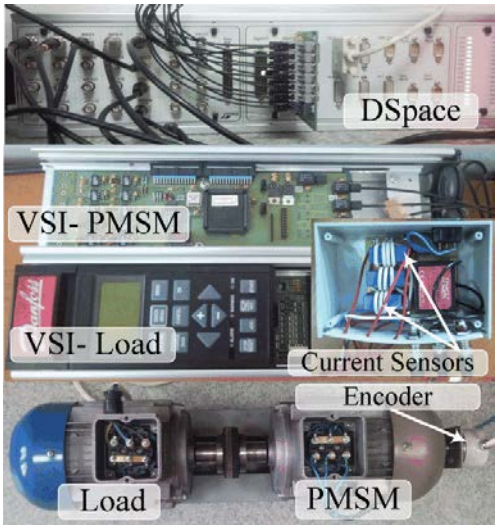

Fig. 6.2. Experimental setup components

As presented in Section 2.2, the *dq* inductances were experimentally identified for the 400 W SPMSM motor with 2 pair poles. The SPMSM parameters are listed in Table 6.1.

6.2. Software Implementation

The control algorithms are implemented using the MATLAB® R2007*a* software. In order to communicate with dSPACE platform, some libraries and interfaces are used, i.e., Real-Time Interface to Simulink (RTI1103) 5.5, MotionDesk Blockset 1.3.8, MATLAB-dSPACE Interface Libraries 4.6.3, ControlDesk to Simulink Interface 3.1.1.

The MATLAB®/Simulink® RTI scheme is presented on Fig. 6.3, in *Function-Call Subsystem* block are implemented the SW protections, the control strategy used and also the acquisition data from dSPACE platform, i.e., current sensors information, DC voltage information and position encoder information.

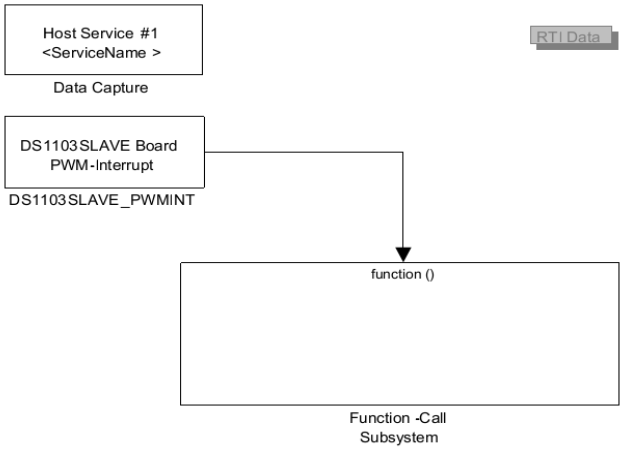

Fig. 6.3. MATLAB®/Simulink® RTI Implementation

A space vector modulation (SVM) specific program developed by Associate Professor Cristian LASCU, Ph.D., directly controls the VSI power switches with inverter dead-time compensation, presented in Appendix C.

The used experiment software is dSPACE ControlDesk® 3.1.1, which unites functionalities all covered by several specialized tools [Dsp2013]. Using ControlDesk® made it easy to change input measures or to adjust regulator constants in the Simulink model. In Fig. 6.4 are presented some of the experimental results for stable V/f control, from Section 4.3, using ControlDesk®.

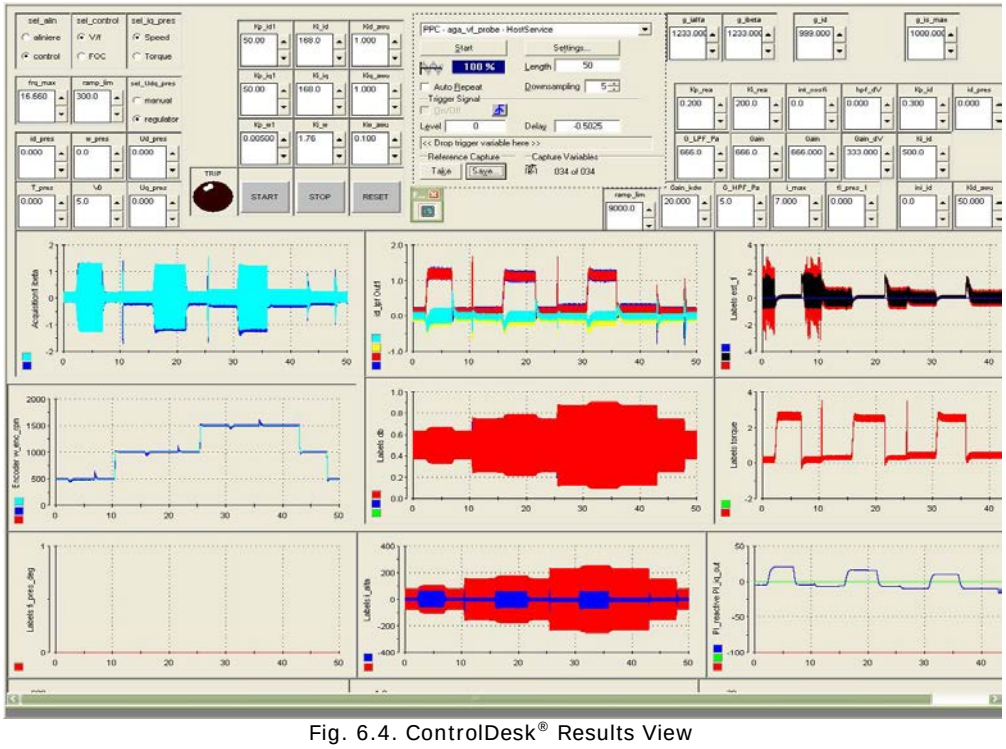

Fig. 6.4. ControlDesk® Results View

Table 6.1. SPMSM Parameters

Rated mechanical speed (n_{rn})	1500 rpm
Rated power (P_n)	400 W
Rated phase voltage (V)	220 V
Rated current (I)	0.8 A
Number of pole pairs (p)	2
Stator resistance (R_s)	16.5 Ω
Stator phase inductance (L_s)	0.09 H
Permanent magnet flux (λ_{PM})	0.75 Wb
Motor inertia (J)	0.0025 kgm^2
Viscous friction coefficient (B)	0.003 Nms/rad

6.3. Conclusion

The experimental test stand used for sensorless stable V/f control strategy, presented in Chapter 4, is introduced. The position information from the incremental encoder is used only for comparison.

The used HW and the SW components are also presented.

7 Final Conclusions and Contributions

7.1. Conclusions

The *direction* of the research study presented in this thesis is the control of PMSM drives; mainly sensorless control for applications where low cost requirements are mandatory, and ISA control for automotive industry were the demand for high efficiency and low cost production is continuously growing. In Chapter 3 are presented three categories of observers for sensorless control PMSM drives, Chapter 4 continues with sensorless control by developing the V/f control with two stabilizing feedback corrections and Chapter 5 is an introduction to automotive industry by developing an ISA control structure used in HEV topology.

The *multidisciplinary research study* of the thesis includes: control system engineering, electric drives, power electronics, electrical engineering and mechanical engineering. The arguments for including the thesis in the control system engineering field of study are presented as follows:

- Modeling of PMSM, with parameters identification;
- Development of an nonlinear state and disturbance observer;
- Implementing and developing sensorless control systems, i.e., V/f control with two stabilizing feedback corrections;
- Proposing an ISA control structure;
- Real-time implementation;
- Comparative simulation results.

The thesis is organized into 7 chapters. The first chapter is the introduction in the research field of the study, continuing with:

- *Chapter 2* presents the PMSM model with the experimental determination of the *dq* inductances and the iron loss resistance modeling.
- *Chapter 3* is the review of the studied rotor position and speed observers used for sensorless control of PMSM. The following observers are taken into account: i) *Voltage Model Flux Estimators* using Active Flux, ii) *MRAS* based observer and iii) *Nonlinear State and Disturbance Observer*.
- *Chapter 4* represents the core of the thesis, and develops the V/f control with two stabilizing feedback corrections with real-time implementation and experimental results. Comparative simulation and experimental studies, with sensored FOC and sensorless vector control using AF, were performed for large speed range and step rated torque loading.
- *Chapter 5* develops a solution for ISA control for automotive industry, taking into account the motor and generator operating modes, validated through simulation results.
- *Chapter 6* is an overview of the experimental test stand used for real-time experiments.
- *Chapter 7* presents the final conclusions and the author contributions to this thesis.

The research results related to the PhD thesis are presented in 4 publications:

(i) three are proceedings papers, presented at international conferences indexed in the IEEE, Scopus and INSPEC databases; and

(ii) one article published in an UK journal indexed in the ISI Web of Knowledge, with an impact factor IF=1.562.

7.2. Contributions

Next, the author contributions to the research field of study are presented following the outline of the thesis.

1) Improvement of PMSM simulation model by experimental determination of *dq* inductances and iron loss resistance estimation.

2) Comparative study with good simulation results, in large speed range, for two rotor position observer topologies: 3 topologies of modified equivalent integrators, and MRAS based observer using emf observer for position estimation and sliding mode observer for speed estimation.

3) Development of an extended nonlinear state Luenberger observer, i.e., nonlinear state and disturbance observer (NSDO), for rotor position and speed with extended load torque estimations, having the following particularities:

i) *Structure characteristics*: the input vector $\underline{u}=[i_d\ v_q]^T$, the compensation using only the estimation error of the i_q current and the placement of one pole in the origin;

ii) *NSDO performances*: very good simulation results of the sensorless vector controlled (sensorless FOC strategy) NSDO, with fast response for step rated torque loading/unloading at low speed, including zero speed, and reversal;

iii) *NSDO robustness study* with good results for parameter variations, highlighting that the parameters R_s, λ_{PM} and θ_i must be real-time identified.

4) Development of the V/f control with two stabilizing feedback corrections, with the following contributions:

i) The *stator voltage amplitude correction* given by the power factor angle regulation loop, with φ estimated from active and reactive power, using measured stator currents and reference stator voltages;

ii) The *additional voltage amplitude correction* ΔV_p for low speed operation, proportional to the active power variation;

iii) *Power factor angle reference based on id current loop*, for SPMSM control only;

iv) *Comparison with sensored FOC and sensorless vector control based on AF*, with close experimental results.

5) Development of an ISA control system used in HEV topology, having the particularities:

i) The torque reference for ISA motor and generator modes operation is given by a switch. For motor mode is selected an external torque and for generator mode the reference is the torque delivered by the DC voltage regulator.

ii) The battery is managed using the ISA active power.

iii) The simulation test results, based on real scenarios, prove good performance of the proposed ISA control system in motor / generator mode, and with good load disturbance rejection.

Appendix A

The Park transformation

The direct transform (from *abc* to *dq*) is

$$\begin{bmatrix} f_d \\ f_q \\ f_0 \end{bmatrix} = \frac{2}{3} \begin{bmatrix} cos(-\theta_r) & cos\left(-\theta_r + \frac{2\pi}{3}\right) & cos\left(-\theta_r - \frac{2\pi}{3}\right) \\ sin(-\theta_r) & sin\left(-\theta_r + \frac{2\pi}{3}\right) & sin\left(-\theta_r - \frac{2\pi}{3}\right) \\ \frac{1}{2} & \frac{1}{2} & \frac{1}{2} \end{bmatrix} \begin{bmatrix} f_a \\ f_b \\ f_c \end{bmatrix}$$

The inverse transform (from *dq* to *abc*) is

$$\begin{bmatrix} f_a \\ f_b \\ f_c \end{bmatrix} = \begin{bmatrix} cos(\theta_r) & -sin(\theta_r) & 1 \\ cos\left(\theta_r - \frac{2\pi}{3}\right) & -sin\left(\theta_r - \frac{2\pi}{3}\right) & 1 \\ cos\left(\theta_r + \frac{2\pi}{3}\right) & -sin\left(\theta_r + \frac{2\pi}{3}\right) & 1 \end{bmatrix} \begin{bmatrix} f_d \\ f_q \\ f_0 \end{bmatrix}$$

The Clarke transformation

The direct transform (from *abc* to *αβ*) is

$$\begin{bmatrix} f_\alpha \\ f_\beta \\ f_0 \end{bmatrix} = \begin{bmatrix} \frac{2}{3} & -\frac{1}{3} & -\frac{1}{3} \\ 0 & \frac{1}{\sqrt{3}} & -\frac{1}{\sqrt{3}} \\ \frac{1}{3} & \frac{1}{3} & \frac{1}{3} \end{bmatrix} \begin{bmatrix} f_a \\ f_b \\ f_c \end{bmatrix}$$

The inverse transform (from *αβ* to *abc*) is

$$\begin{bmatrix} f_a \\ f_b \\ f_c \end{bmatrix} = \begin{bmatrix} 1 & 0 & 1 \\ -\frac{1}{2} & \frac{\sqrt{3}}{2} & 1 \\ -\frac{1}{2} & -\frac{\sqrt{3}}{2} & 1 \end{bmatrix} \begin{bmatrix} f_\alpha \\ f_\beta \\ f_0 \end{bmatrix}$$

Appendix B
Kessler Modulus and Symmetrical Criterions

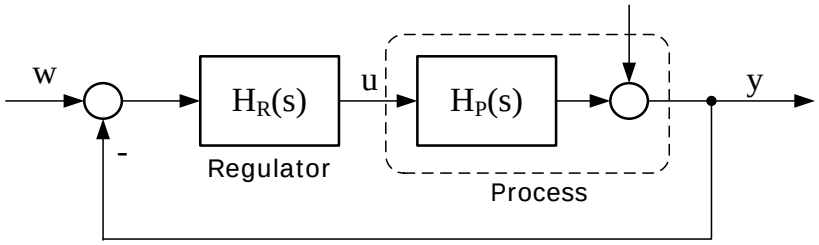

w - command signal v - disturbance signal

u - input signal y – output signal

Kessler Modulus Criterion

Nr.	Process transfer function $H_P(s)$	Regulator	
		RG-Type	Transfer function $H_R(s)$
1.	$H_P(s) = \frac{K_p}{1+sT_\Sigma}$	I	$H_R(s) = \frac{K_r}{s}$
2.	$H_P(s) = \frac{K_p}{(1+sT)(1+sT_\Sigma)}$	PI	$H_R(s) = \frac{K_r}{s}(1+sT_r)$
3.	$H_P(s) = \frac{K_p}{(1+sT_1)(1+sT_2)(1+sT_\Sigma)}$	PID	$H_R(s) = \frac{K_r}{s}(1+sT_{r1})(1+sT_{r2})$ $T_{r1} = T_1; T_{r2} = T_2$

Kessler Symmetrical Optimum Criterion

Nr.	Process transfer function $H_P(s)$	Regulator	
		RG-Type	Transfer function $H_R(s)$
1.	$H_P(s) = \frac{K_p}{s(1+sT_\Sigma)}$	PI	$H_R(s) = \frac{K_r}{s}(1+sT_r)$
2.	$H_P(s) = \frac{K_p}{s(1+sT_1)(1+sT_\Sigma)}$	PID	$H_R(s) = \frac{K_r}{s}(1+sT_{r1})(1+sT_{r2})$ $T_{r1} = T_1; T_{r2} = T_2$

The references used are [Pre2005] and [Pre1982].

Appendix C
Space Vector Modulation (SVM) for PMSM

Author: Associate Professor **Cristian LASCU**, Ph.D, 2005
INPUT: V_{dc}, $V_{s\alpha}$, $V_{s\beta}$, I_{sa}, I_{sb}, I_{sc}, k
OUTPUT: D_a, D_b, D_c, V_α, V_β

```
#include <math.h>
#include "tmwtypes.h"
# define h 0.000125
#define pi 3.1415926

#define R3 1.732051

// SVM parameters
const float tdead = 1.5e-6;     // dead time    [s]
const float zone = 0.1;         // linear zone  [A]
const float Dmax = 0.98;        // max duty cycle
const float Dmin = 0.02;        // min duty cycle

// Saturation function
float sat(real_T x, real_T z)
{
        if (x>z) return 1.0;
        else if (x<-z) return -1.0;
        else return x/z;
}

// Space Vector Modulation

void SVM(real_T *u, real_T *i, real_T *d, real_T *y, const real_T *k)
{
        struct Vector{float alfa,beta;} Us;
        float K=(*k)*tdead/h;
        float Umax=R3/u[0];
        float Da,Db,Dc;
        float T1,T2;
        int sector;
        Us.alfa = R3*Umax*u[1];
        Us.beta = Umax*u[2];
        if (Us.beta>0)
        if (Us.alfa>Us.beta)
```

```
{
        sector=0;
        T1=0.5*(Us.alfa-Us.beta);
        T2=Us.beta;
}
else if (-Us.alfa<Us.beta)
{
        sector=1;
        T1=0.5*(Us.alfa+Us.beta);
        T2=0.5*(Us.beta-Us.alfa);
}
else
{
        sector=2;
        T1=Us.beta;
        T2=-0.5*(Us.alfa+Us.beta);
}
else if (Us.alfa<Us.beta)
{
        sector=3;
        T1=0.5*(Us.beta-Us.alfa);
        T2=-Us.beta;
}
else if (-Us.alfa>Us.beta)
{
        sector=4;
        T1=-0.5*(Us.alfa+Us.beta);
        T2=0.5*(Us.alfa-Us.beta);
}
else
{
        sector=5;
        T1=-Us.beta;
        T2=0.5*(Us.alfa+Us.beta);
}
if (T1>1.0) T1=1.0,T2=0.0;
else if (T2>1.0) T2=1.0,T1=0.0;
else if (T1+T2>1.0) if (T1>T2) T2=1.0-T1;
else T1=1.0-T2;

switch (sector)
{
case 0: Da=0.5*(1.0+T1+T2);
```

```
                Db=0.5*(1.0-T1+T2);
                Dc=0.5*(1.0-T1-T2);
                break;
        case 1: Da=0.5*(1.0+T1-T2);
                Db=0.5*(1.0+T1+T2);
                Dc=0.5*(1.0-T1-T2);
                break;
        case 2: Da=0.5*(1.0-T1-T2);
                Db=0.5*(1.0+T1+T2);
                Dc=0.5*(1.0-T1+T2);
                break;
        case 3: Da=0.5*(1.0-T1-T2);
                Db=0.5*(1.0+T1-T2);
                Dc=0.5*(1.0+T1+T2);
                break;
        case 4: Da=0.5*(1.0-T1+T2);
                Db=0.5*(1.0-T1-T2);
                Dc=0.5*(1.0+T1+T2);
                break;
        case 5: Da=0.5*(1.0+T1+T2);
                Db=0.5*(1.0-T1-T2);
                Dc=0.5*(1.0+T1-T2);
                break;
        default:
        Da=0.0;Db=0.0;Dc=0.0;
        }
        // Stator voltage
        y[0] = u[0]*(2.0*Da-Db-Dc)/3.0;
        y[1] = u[0]*(Db-Dc)/R3;
        // Dead-time compensation
        Da = Da + K*sat(i[0],zone);
        Db = Db + K*sat(i[1],zone);
        Dc = Dc + K*sat(i[2],zone);
        // Pulse drop
        if (Da>Dmax) Da=1.0; else if (Da<Dmin) Da=0.0;
        if (Db>Dmax) Db=1.0; else if (Db<Dmin) Db=0.0;
        if (Dc>Dmax) Dc=1.0; else if (Dc<Dmin) Dc=0.0;
        // Duty cycles output
        d[0] = Da;
        d[1] = Db;
        d[2] = Dc;
}
```

Author's Papers Related to the PhD Thesis

[1] Andreescu G.-D., **Coman C.-E.**, Moldovan A. and Boldea I., "*Stable V/f control system with unity power factor for PMSM drives*", Proc. 13th Int. Conf. Optimization of Electrical and Electronic Equipment (OPTIM 2012), Braşov, Romania, pp. 432-438, May 2012 (IEEE Xplore, Scopus).

[2] Agarlita S.-C., **Coman C.-E.**, Andreescu G.-D. and Boldea I., "*Stable V/f control system with controlled power factor angle for permanent magnet synchronous motor drives*", IET Electric Power Applications, vol. 7, no. 4, pp. 278 – 286, April 2013 (IEEE Xplore, Scopus, ISI Web of Knowledge, IF=1.562).

[3] **Coman C.-E.**, Agarlita S.-C. and Andreescu G.-D., "*V/f Control Strategy with Constant Power Factor for SPMSM Drives, with Experiments*", Proc. 8th IEEE International Symposium on Applied Computational Intelligence and Informatics (SACI 2013), Timişoara, Romania, pp. 147-151, May 2013 (IEEE Xplore, Scopus).

[4] Andreescu G.-D. and **Coman C.-E.**, "*Integrated Starter-Alternator Control System for Automotive*", Proc. 14th IEEE International Symposium on Computational Intelligence and Informatics (CINTI 2013), Budapest, Hungary, pp. 339-343, November 2013 (IEEE Xplore).

[5] **Coman C.-E.**, "*Fault Tolerant Control System of Permanent Magnet Synchronous Motor Drives for Rotor Position Sensor Faulty*", Proc. 1st Workshop - Interdisciplinary and Research Management, Politehnica University Timisoara, Timisoara, Romania, November 2011 (on CD).

[6] **Coman C.-E.**, "*V/f Control System with Two Stabilizing Feedback Corrections for PMSM Drives*", Proc. 2nd Workshop - Interdisciplinary and Research Management in Doctoral Studies, The University of Oradea, Baile Felix, Romania, June 2012 (on CD).

References

[Aga2011] Agarlita S.C., Boldea I. and Blaabjerg F., "*High frequency injection assisted "active flux" based sensorless vector control of reluctance synchronous motors, with experiments from zero speed*", Proc. IEEE Energy Conversion Congress and Exposition (ECCE 2011), Phoenix, Arizona, USA, pp. 2725-2732, September 2011.

[Aga2013] Agarlita S.-C., **Coman C.-E.**, Andreescu G.-D. and Boldea I., "*Stable V/f control system with controlled power factor angle for permanent magnet synchronous motor drives*", IET Electric Power Applications, vol. 7, no. 4, pp. 278 – 286, April 2013.

[Alb2010] Alberti L., Barcaro M., Pre M.D., Faggion A., Sgarbossa L., Bianchi N. and Bolognani S., "*IPM machine drive design and tests for an integrated starter-alternator application*," IEEE Trans. on Industry Applications, vol. 46, no. 3, pp. 993-1001, May/June 2010.

[Anc2010] Ancuţi R., Boldea I. and Andreescu G.-D., "*Sensorless V/f control of high-speed surface permanent magnet synchronous motor drives with two novel stabilising loops for fast dynamics and robustness*", IET Electric Power Applications, vol. 4, no. 3, pp. 149-157, March 2010.

[And1999] Andreescu G.-D., "Estimatoare în sisteme de conducere a acţionărilor electrice. Aplicaţii la maşini sincrone cu magneţi permanenţi", Editura Orizonturi Universitare, Timisoara, Romania, 1999.

[And2003] Andreescu G.-D., "*Sliding-mode observer for sensorless control of permanent magnet synchronous motor drives*", Journal of Control Engineering and Applied Informatics (CEAI), vol. 5, no. 1, pp. 27-34, 2003.

[And2008] Andreescu G.-D., Pitic C.I., Blaabjerg F. and Boldea I., "*Combined flux observer with signal injection enhancement for wide speed range sensorless direct torque control of IPMSM drives*", IEEE Trans. on Energy Conversion, vol. 23, no. 2, pp. 393–402, June 2008.

[And2012] Andreescu G.-D., **Coman C.-E**., Moldovan A. and Boldea I., "*Stable V/f control system with unity power factor for PMSM drives*", Proc. 13th Int. Conf. Optimization of Electrical and Electronic Equipment (OPTIM 2012), Braşov, Romania, pp. 432-438, May 2012.

[And2013] Andreescu G.-D. and **Coman C.-E.**, "*Integrated Starter-Alternator Control System for Automotive*", Proc. 14th IEEE International Symposium on Computational Intelligence and Informatics (CINTI 2013), Budapest, Hungary, pp. 339-343, November 2013.

[Bol2004] Boldea I., Tutelea L. and Pitic C.I., "*PM-assisted reluctance synchronous motor/generator (PM-RSM) for mild hybrid vehicles: electromagnetic design*", IEEE Trans. on Industry Applications, vol. 40, no. 2, pp. 492-498, March/April 2004.

[Bol2006] I. Boldea, C.I. Pitic, C. Lascu, G.-D. Andreescu, L. Tutelea, F. Blaabjerg, and P. Sandholdt, "DTFC-SVM motion-sensorless control of a pm-assisted reluctance synchronous machine as starter-alternator for hybrid electric vehicles," *IEEE Trans. on Power Electronics*, vol. 21, no. 3, pp. 711-719, May 2006.

[Bol2006a] Boldea I., "Synchronous Generators", CRC Press, Taylor & Francis Group, 2006.

[Bol2008] Boldea I., Paicu M.C. and Andreescu G.-D., "*Active flux concept for motion sensorless unified AC drives*", IEEE Trans. on Power Electronics, vol. 23, no. 5, pp. 2612–2618, September 2008.

[Bol2010] Boldea I., Corban-Schramel V., Andreescu G., Blaabjerg F. and Scridon S., *"BEGA starter/alternator—Vector control implementation and performance for wide speed range at unity power factor operation,"* IEEE Trans. on Industry Applications, vol. 46, no. 1, pp. 150-158, January/February 2010.

[Bol2011] Boldea I. and Agarlita S.C., "*The active flux concept for motion-sensorless unified ac drives: a review*", Proc. 2011 Electromotion Joint Conference Electrical Machines and Power Electronics (ACEMP 2011), Istanbul, Turkey, pp. 1-16, September 2011.

[Cac2010] Cacciato M., Consoli A., Scarcella G. and Scelba G., "*A novel efficiency optimization scalar control technique for industrial IPMSM drives*", Proc. 2010 IEEE Int. Symposium on Industrial Electronics (ISIE 2010), Bari, Italy, pp. 1181-1186, Jul. 2010.

[Che2010] Chen J.-L., Liu T.-H. and Chen C.-L., "*Design and implementation of a novel high-performance sensorless control system for interior permanent magnet synchronous motors"*, IET Electric Power Applications, vol. 4, no. 4, pp. 226-240, April 2010.

[**Com2013**] **Coman C.-E**., Agarlita S.-C. and Andreescu G.-D., "*V/f Control Strategy with Constant Power Factor for SPMSM Drives, with Experiments*", Proc. 8th IEEE International Symposium on Applied Computational Intelligence and Informatics (SACI 2013), Timişoara, Romania, pp. 147-151, May 2013.

[Con2010] Consoli A., Scarcella G., Scelba G. and Cacciato M., "*Range extended efficiency optimization technique for scalar IPMSM drives*", Proc. 14th Int. Power Electronics and Motion Control Conf. (EPE/PEMC 2010), Orhid, Macedonia, pp. S10-7-S10-14, September 2010.

[Con2013] Consoli A., Scelba G., Scarcella G. and Cacciato M., "*An effective energy-saving scalar control for industrial IPMSM drives*", IEEE Trans. on Industrial Electronics, vol. 60, no. 9, September 2013.

[Cor2009] Coroban-Schramel V., "BEGA - as a Starter/Generator with Vector Control", Ph.D. Thesis, Politehnica Publishing House, Timisoara, pp. 70-114, 2009.

[Cor2011] Corban-Schramel V., Boldea I., Andreescu G.-D. and F. Blaabjerg, *"Active-flux-based motion-sensorless vector control of biaxial excitation generator/motor for automobiles*", IEEE Trans. on Industry Applications, vol. 47, no. 2, pp. 812-819, March/April 2011.

[Dsp2013] http://www.dspace.com, December 2013.

[Fag2008] Faggion A., Sgarbossa L., Alberti L., Barcaro M., Dai Pre M. and Bolognani S., "*Effective control of an Integrated Starter-Alternator with an IPM synchronous machine*," Proc. IEEE Power Electronics Specialists Conference (PESC 2008), pp. 3924-3929, Jun. 2008.

[Foo2010] Foo G. and Rahman M.F., "*Sensorless sliding-mode MTPA control of an IPM synchronous motor drive using a sliding-mode observer and HF signal injection*", IEEE Trans. on Industrial Electronics, vol. 57, no. 4, pp. 1270–1278, April 2010.

[Gad2013] Gadoue S.M., Giaouris D. and Finch J.W., "*Stator current model reference adaptive systems speed estimator for regenerating-mode low-speed operation*

of sensorless induction motor drives", IET Electric Power Applications, vol. 7, no. 7, pp. 597-606, August 2013.

[Gie2010] Gieras J.F., "Permanent Magnet Motor Technology -Design and Applications, 3rd Edition", CRC Press, Taylor & Francis Group, 2010.

[Hu1998] Hu J. and Wu B., "*New integration algorithms for estimating motor flux over a wide speed range*", IEEE Trans. on Power Electronics, vol. 13, no. 5, pp. 969-977, September 1998.

[Hug2006] Hughes A., "Electric Motors and Drives", Third Edition, Elsevier, 2006.

[Jai2006] Jain A.K., Mathapati S., Ranganathan V.T. and Narayanan V., "*Integrated starter generator for 42-V powernet using induction machine and direct torque control technique*", IEEE Trans. on Power Electronics, vol. 21, no. 3, pp. 701-710, May 2006.

[Kha2012] Khan M.R. and Iqbal A., "*Model reference adaptive system with simple sensorless flux observer for induction motor drive*", Proc. IEEE Int. Conf. on Power Electronics, Drives and Energy Systems (PEDES 2012), Bengaluru, India, pp. 1-6, December 2012.

[Lau2005] Lau J. and Uddin M.N., "*Nonlinear adaptive position control of an interior permanent magnet synchronous motor*", Proc. IEEE Int. Conf. on Electric Machines and Drives, San Antonio, TX, USA, pp. 1689-1694, May 2005.

[Leo1997] Leonhard W., "Control of Electrical Drives. 2nd Completely Revised and Enlarged Edition", Springer, 1997.

[Lin2007] Lin C.-K., Liu T.-H. and Yang S.-H., "*Design and implementation of a nonlinear controller for an IPMSM position control system*", Proc. 33rd Annual Conf. of the IEEE Industrial Electronics Society (IECON 2007), Taipei, Taiwan, pp. 1027-1032, November 2007.

[Mat2009] Matsushita M., Kameyama H., Ikeboh Y. and Morimoto S., "*Sine-wave drive for PM motor controlling phase difference between voltage and current by detecting inverter bus current*", IEEE Trans. on Industry Applications, vol. 45, no. 4, pp. 1294-1300, July/August 2009.

[Mat2009a] Matsushita M., Kameyama H., Ikeboh Y. and Morimoto S., "*Stabilization control of sensorless sinusoidal wave drive for control of power factor of PM motor*", Proc. Int. Conf. on Electrical Machines and Systems (ICEMS 2009), Tokyo, Japan, pp. 1-5, November 2009.

[Mir2013] Mirahki H. and Moallem M., "*Design improvement of interior permanent magnet synchronous machine for integrated starter alternator application*", Proc. IEEE Int. Electric Machines & Drives Conference (IEMDC 2013), pp. 382-385, May 2013.

[Miy1990] Miyata Y. and Yamamura E., "*The model reference adaptive system in the dynamic input-output model*", Papers in Regional Science, vol. 68, no. 1, pp. 57-70, January 1990.

[Moh2000] Mohamed A. El-Sharkawi, "Elements of Electric Drives", Brooks/Cole Publishing Company, pp. 125-128, 2000.

[Mon2010] Montesinos-Miracle D., Perera P.D.C., Galceran-Arellano S., and Blaabjerg F., "*Sensorless V/f control of permanent magnet synchronous motors*", Motion Control (Book Ch. 23), F. Casolo, Ed. InTech, Croatia, pp. 439-458, 2010.

[Mor1990] Morimoto S., Takeda Y. and Hirasa T., "*Current phase control methods for permanent magnet synchronous motors*", IEEE Trans. on Power Electronics, vol. 5, no. 2, pp. 133-139, April 1990.

[Mor1990a] Morimoto S., Takeda Y., Hirasa T. and Taniguchi K., "*Expansion of operating limits for permanent magnet motor by current vector control considering inverter capacity*", IEEE Trans. on Industry Applications, vol. 26, no. 5, pp. 866-871, September/October 1990.

[Mor2006] Morimoto M., Aiba, K., Sakurai, T., Hoshino, A., and Fujiwara,, "Position sensorless starting of super high-speed PM generator for micro gas turbine," *IEEE Trans. on Industrial Electronics*, vol. 53, no. 2, pp. 415-420, Apr. 2006.

[Mud2003] Mudannayake C.P. and Rahman M.F., "*An integrated starter alternator for the 42 V PowerNet*", Proc. 5th Int. Conf. on Power Electronics and Drive Systems (PEDS 2003), vol. 1, pp. 648-653, November 2003.

[Mud2004] Mudannayake C.P. and Rahman M.F., "*A MATLAB/Simulink model for a prototype integrated starter alternator for automobiles*", Proc. 4th Int. Power Electronics and Motion Control Conf. (IPEMC 2004), vol. 3, pp. 1679-1684, August 2004.

[Pac2005] Pacas M. and Weber J., "*Predictive direct torque control for the PM synchronous machine*", IEEE Trans. on Industrial Electronics, vol. 52, no. 5, pp. 1350–1356, October 2005.

[Pai2009] Paicu M.C., Boldea I., Andreescu G.-D. and Blaabjerg F., "*Very low speed performance of active flux based sensorless control: interior permanent magnet synchronous motor vector control versus direct torque and flux control*", IET Electric Power Applications, vol. 3, no. 6, pp. 551-561, March 2009.

[Per2002] Perera P.D.C., "Sensorless control of permanent-magnet synchronous motor drives", Ph.D. Thesis, Institute of Energy Technology, Aalborg, Denmark, December 2002.

[Per2003] Perera P.D.C., Blaabjerg F., Pedersen J.K. and Thogersen P., "*A sensorless, stable V/f control method for permanent-magnet synchronous motor drives*", IEEE Trans. on Industry Applications, vol. 39, no. 3, pp. 783-791, May/June 2003.

[Pii2007] Piippo A., Suomela K., Hinkkanen M. and Luomi J., "*Sensorless PMSM drive with DC-link current measurement*", Proc. 42nd IAS Annual Meeting. IEEE Industry Applications Conference, New Orleans, Louisiana, USA, pp. 2371–2377, September 2007.

[Pii2008] Piippo A., Hinkkanen M. and Luomi J., "*Analysis of an adaptive observer for sensorless control of interior permanent-magnet synchronous motors*", IEEE Trans. on Industrial Electronics, vol. 55, no. 2, pp. 570–576, February 2008.

[Pii2008a] Piippo A., Hinkkanen M. and Luomi J., "*Signal injection in sensorless PMSM drives equipped with inverter output filter*", IEEE Trans. on Industry Applications, vol. 44, no. 5, pp. 1614–1620, September/October 2008.

[Pre1982] Preitl Ş., Dragomir T.-L. and Boraci R., "Teoria Sistemelor şi Reglaj Automat - Regulatoare Automate", Institutul Politehnica Traian Vuia, 1982.

[Pre2005] Preitl Ş. and Precup R.-E., "Elemente de Reglare Automată. Aplicaţii la sistemele de reglare automată a excitaţiei şi vitezei generatoarelor sincrone", Editura Orizonturi Universitare, Timişoara, 2005.

[Sue2011] Sue S.-M., Hung T.-W., Liaw J.-H., Li Y.-F. and Sun C.-Y., "*A new MTPA control strategy for sensorless V/f controlled PMSM drives*," Proc. 6th IEEE Conf. on Industrial Electronics and Applications (ICIEA 2011), Beijing, China, pp. 1840-1844, June 2011.

[Sue2012] Sue S.-M. and Hung T.-W., "*Minimum Copper Loss Control for Sensorless V/f Controlled IPMSM Drives*", Proc. IEEE Int. Symposium on Industrial Electronics (ISIE 2012), Hangzhou, China, pp. 708-712, May 2012.

[Sul2011] Sul S.-K., "Control of Electric Machine Drive Systems", IEEE Press, 2011.

[Vas1998] Vas P., "Sensorless vector and direct torque control", Oxford University Press, 1998.

[Wik2014] http://en.wikipedia.org/wiki/Integrated_Motor_Assist, January 2014.

[Wil2007] Wiliamson S.S., Khaligh A. and Emadi A., "*Impact of utilizing selective motor topologies and control strategies on the overall performance of integrated starter alternator (ISA) based HEVs*", Proc. IEEE Int. Electric Machines & Drives Conf. (IEMDC '07), vol. 1, pp. 134-139, May 2007.

[Xu2007] Xu Zhuang, Rahman M.F, "*Direct torque and flux regulation of an IPM synchronous motor drive using variable structure control approach*", IEEE Trans. on Power Electronics, vol. 22, no. 6, pp. 2487-2498, November 2007.

[Xu2012] Xu Zhuang, Rahman M.F., Wang G. and Xu Dianguo, "*Performance evaluation of an integrated starter-alternator with an IPM synchronous machine under sensor-less operation*", Journal of Power Electronics, vol. 12, no. 1, pp. 49-57, January 2012.

[Yon2013] Yongle M., Guiying L. and Yangsheng C., "*Sensorless IPMSM drives based on extended nonlinear state observer with parameter inaccuracy compensation*", 2013 Int. Conf. on Electrical Machines and Systems (ICEMS 2013), Busan, Korea, pp. 976-981, October 2013.

[Zha2006] Zhao L., Ham C.H., Han Q., Wu T.X., Zheng L., Sundaram K.B., Kapat J. and Chow L., "*Design of optimal digital controller for stable super-high-speed permanent-magnet synchronous motor*", IEE Proc. Electric Power Applications, vol. 153, no. 2, pp. 213-218, March 2006.

[Zha2008] Zhao K., Lin F., Han Q. and You X., "*A modified voltage model flux estimation of induction motors*", Proc. Int. Conf. on Electrical Machines and Systems, (ICEMS 2008), pp. 94-97, October 2008.

[Zhu2011] Zhu Z.Q. and Gong L.M., "*Investigation of effectiveness of sensorless operation in carrier-signal-injection-based sensorless-control methods*", IEEE Trans. on Industrial Electronics, vol. 58, no. 8, pp. 3431–3439, August 2011.